

**Design of fluorescent chemosensors for Naproxen and ATP and
subsequent immobilization in nanoparticles**

DISSERTATION

Zur Erlangung des akademischen Grades doctor rerum naturalium

(Dr. rer. nat.)

Vorgelegt dem Rat der Chemisch-Geowissenschaftlichen Fakultät der Friedrich-
Schiller-Universität Jena

von Dipl. Chem. Artur J. C. Moro

geboren am 9er Mai 1982 in Cascais, Portugal

Gutachter 1: PD Dr. Gerhard Mohr, Fraunhofer Institut Regensburg

Gutachter 2: Prof. Dr. Rainer Beckert, Friedrich-Schiller Universität

Tag der öffentlichen Verteidigung: 17.02.2010

CONTENTS

1. Fluorescence spectroscopy as a tool for medical applications	5
2. General Objectives	7
3. A fluorescence ICT-based chemosensor for Naproxen	8
3.1. State of the art – Internal Charge Transfer (ICT) based optical sensors	8
3.2. Design and evaluation of fluorescent chemosensor 2	13
3.2.1. Synthesis of 2	13
3.2.2. Anion targeted sensing – NSAIDs and other analytes	15
3.2.3. Interactions of chemosensor 2 with the analytes in aqueous solution	17
3.3. Fluorescent nanoparticles as tools for sensing in biological samples	20
3.3.1. Introduction to nanosensors	20
3.3.2. Immobilization of 2 into polyacrylamide nanoparticles (PAA-NPs)	21
3.3.3. Size characterization of PAA-NPs through Dynamic Light scattering (DLS) ..	22
3.4. Naproxen sensing with fluorescent PAA-NPs	24
3.4.1. Sensitivity studies	24
3.4.2. Selectivity studies	30
3.5. Conclusions	31
4. An ATP Fluorescent Chemosensor Based on a Zn(II)-Complexed Dipicolylamine Receptor Coupled with a Naphthalimide Chromophore	32
4.1. State of the art – Photoinduced Electron Transfer (PET) based fluorescent probes ...	32
4.2. Design of a naphthalimide-based chemosensor	37
4.2.1. THE FLUOROPHORE – Is naphthalimide the perfect system for sensor applications?	37

4.2.2. THE RECEPTOR – Different strategies for sensing of ATP and other phosphate derivatives	41
4.3. Strategy and synthetic pathway of fluorescent chemosensor 10	48
4.4. Spectroscopic characterization of 10	53
4.4.1. General studies on the fluorescence of 10 - Influence of concentration and pH .	53
4.4.2. Complexation of 10 with metal cations	56
4.4.3. Evaluation of [10-Metal] complexes for sensing ATP	61
4.5. Complex 10.Zn – a fluorescent sensor for ATP	65
4.5.1. Evaluation of 10.Zn as an ATP chemosensor	65
4.5.2. Selectivity studies on 10.Zn	70
4.6. Fluorescent silica nanoparticles for ATP sensing	75
4.6.1. Synthesis and characterization of surface functionalized silica nanoparticles – 10.Zn-NPs	75
4.6.2. Evaluation of 10.Zn-NPs as ATP fluorescent nanosensors	79
4.7. Conclusions	86
5. Summary and Outlook	87
6. Zusammenfassung und Ausblick	89
7. Experimental Section	91
8. Bibliography	104
List of publications	109
Curriculum vitae	111
Acknowledgements	112
Selbständigkeitserklärung	114

1. Fluorescent spectroscopy as a tool for medical applications

Fluorescent spectroscopy as a sensing method for relevant target molecules has been widely investigated for several decades. Most of the applications are, of course, biology or medicine, since these are scientific areas of critical importance for today's society. The development of simpler, faster and more reliable methods to be used in both therapeutic as well as diagnostics is a constant goal for scientists all over the world.

Fluorescence spectroscopy possesses many desirable characteristics as a tool for use in biology and medicine. One of the main advantages is the high sensitivity of the technique which can go down to concentrations in the pico and femtomole range, or even to the molecular level, through the use of a specific technique, the so-called near-field scanning optical microscopy (NSOM).¹ Other advantages are related to the simplicity of the methodology and to the fact that the required instruments and apparatus are relatively cheaper than other diagnostics techniques such as Magnetic Resonance Imaging (MRI) or Computer Tomography (CT). Furthermore, and as opposed to other techniques, there is also the possibility of instrumentation miniaturization that allows it to be used in a focused manner, e.g. in a very specific area of the skin for example, in Photodynamic Therapy applications for skin cancer.²

The use of fluorescent dyes as probes is of common use in the scientific community and its introduction for labelling of biomolecules such as DNA and proteins is now widespread due to various desirable features from these compounds. Perhaps the most important one relates to the fact that in many cases, the detection of an analyte using such fluorescent dyes occurs in a reversible manner, allowing for continuous monitoring of the analyte in a given sample, which is an essential aspect when studying, for example, dynamic processes in cells or other biosamples.

The ideal fluorescent probe is obtained if the molecule comprises all of the following parameters:

- 1) Water solubility – since most of the biological processes occur in aqueous environment;
- 2) High sensitivity – to get maximal signal change in the presence of the analyte;
- 3) High selectivity – to be able to distinguish only one analyte in a complex mixture;

4) Optical properties (including high quantum yields and molar extinction coefficients) in the visible or preferably in the NIR region – where one can still work with the common available light sources and have the least interference with biological samples.³

In spite of all these requirements, several fluorescent probes are already being used in biology. Some of the most commonly used fluorophores include fluorescein, rhodamines and cyanine dyes.

Nevertheless, a strong motivation, particularly driven by life sciences and medicine, is being directed towards the rational design of new sensors and probes and to develop new ways to incorporate them in biological systems, so that these sensors can be useful in practical applications in a short/medium term.

One of the main driving forces for such applications has been the outstanding advances in the so-called nanotechnologies in the past years which have allowed, amongst other advantageous progresses, the development of nanosized fluorescent materials that can penetrate into the cell for direct *in-vivo* fluorescence measurements.

Today, a significant amount of interdisciplinary groups are working towards this scientific pathway, converging chemistry and biology for the investigation of new fluorescent sensor materials to be used as common tools for faster, safer and more reliable medical diagnostics and research.

2. General Objectives

The present research is mainly directed to finding new fluorescent molecules for sensing applications, with emphasis towards biologically relevant analytes. Furthermore, the synthesized molecules should possess chemical groups for attachment onto structured matrixes, e.g. polymer nanoparticles or functionalized surfaces.

A thorough research was made on various fluorophore molecules that could be adequate for biological applications. The main conditions to be taken into account for the fluorophores were:

- Optical properties in the visible or Near-Infrared region;
- Versatile chemical properties that allowed the introduction of chemically reactive groups to be used as recognition or receptor towards a given target molecule;
- Possibility of functionalization with polymerisable groups (or groups that allowed covalent attachment).

After synthesis, the molecules were fully characterized structurally (NMR, mass spectrometry) and optically (absorption and fluorescence) and studies were performed (in solution) regarding their sensing properties based the optical response in the presence of the target analyte.

The last step of the research consisted on the synthesis/functionalization of nanoparticles using the synthesized fluorescent sensors.

The criteria for selection of the polymeric matrix for the production of fluorescent sensor nanoparticles were based on three factors: (a) the polymerisable group on the sensor molecule, (b) the chemical properties (charge, size, solubility) of the analyte and (c) the nature of the sensor-analyte interaction.

The final obtained nanomaterial was characterized regarding its size and sensing properties towards the target molecule using fluorescence spectroscopy.

The results of this research are presented and discussed within this thesis, concluded with an outlook on future possible investigations in the field.

3. A fluorescence ICT-based chemosensor for Naproxen

3.1. State of the art – Internal Charge Transfer (ICT) based optical sensors

Within fluorescence spectroscopy, one can distinguish several effects that be used for sensing purposes. In fluorescent molecules bearing a Donor (D) group and an Acceptor (A) group bridged by a conjugated system, one of the most important photophysical processes is the photoinduced Internal Charge Transfer (ICT). If either the donor or the acceptor group is somehow affected in the presence of a given analyte, one can use such a fluorescent system for the design of a sensor towards that same analyte by following changes in the fluorescence spectra of the sensor molecule.

Stilbenes are amongst the most studied fluorophore systems due to their versatile chemistry which allows for the introduction of numerous functional groups. Therefore one can modulate the strength of the donor and acceptor groups resulting in a stronger ICT as well as shift the spectral properties. Generally, the sensing mechanism with such molecules is based on changes in acceptor strength in the presence of the analyte, leading to changes in the optical properties of the sensor.

Several examples can be found in literature regarding the use of stilbenes as sensors. DiCesare and Lakowicz⁴ designed fluorescent sensors for sacharides by attaching a boronic acid at the end of the stilbene conjugated π -system (Figure 1). Through covalent bonding of the analyte to the boronic acid moiety, a significant change in the fluorescence properties was observed.

The use of heteroaromatic rings in these conjugated systems is also a valid approach in the design of new fluorescent sensor probes. Wolfbeis et al.^{5,6} reported a new pyrylium dye (the so-called “chameleon stain”) for labelling of proteins or amines that induces large spectral changes upon insertion of the amino group into the conjugated system which is typically translated into a colour change from blue to red. The methodology was applied at neutral pH in fluorimetric protein assays of blood plasma samples.

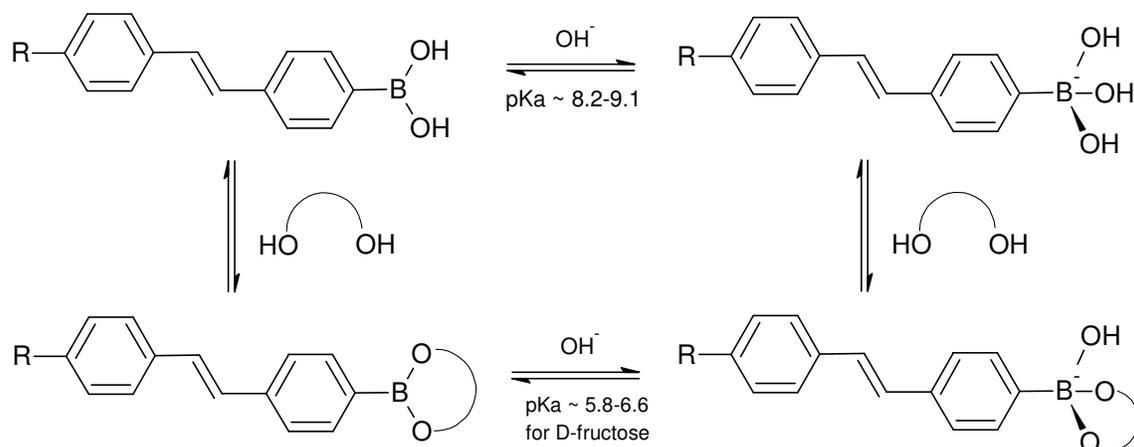


Figure 1. Equilibrium and conformation of the different forms of the boronic acid group with and without sugar.⁴

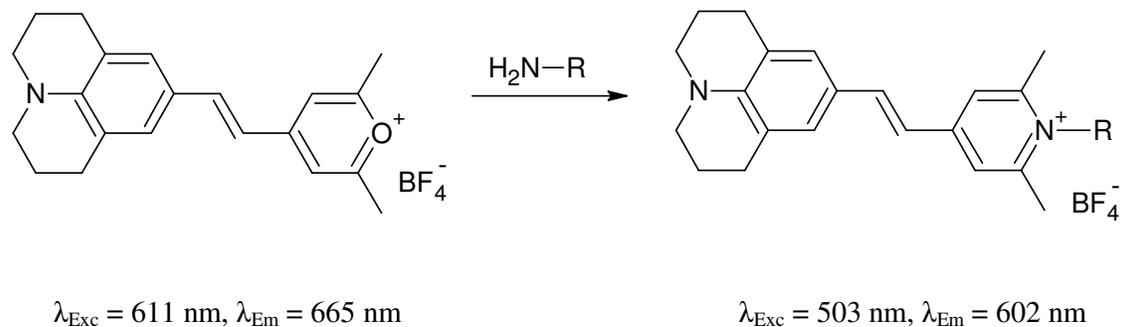


Figure 2. Reaction of the “chameleon stain” in the presence of amines.^{5, 6} The color of the dye changes from blue to red.

Mohr et al.^{7, 8} developed various derivatives of stilbene and azo dyes⁹, for sensing of aliphatic amines through reversible covalent bonding. The system was based on the reaction of amines with the trifluoroacetyl group of the sensor yielding a hemiaminal species (Figure 3). This reaction translated into a blue shift in the absorption spectra because of the decrease in the electron-withdrawing strength of the acceptor group. This means that the energy of the Lowest Unoccupied Molecular Orbital (LUMO) is higher and therefore, the energy of the first electronic transition is increased. The same system can also be used for alcohol sensing.^{10, 11, 12}

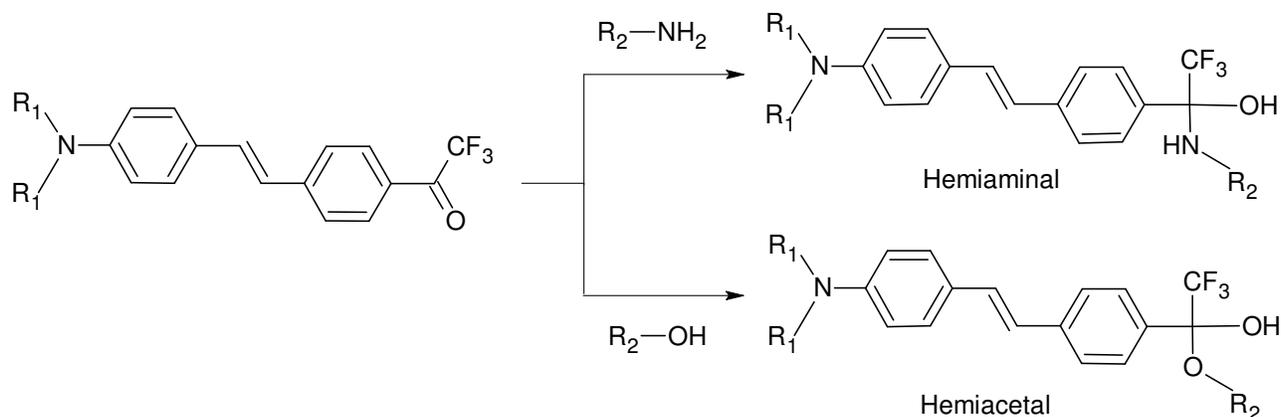
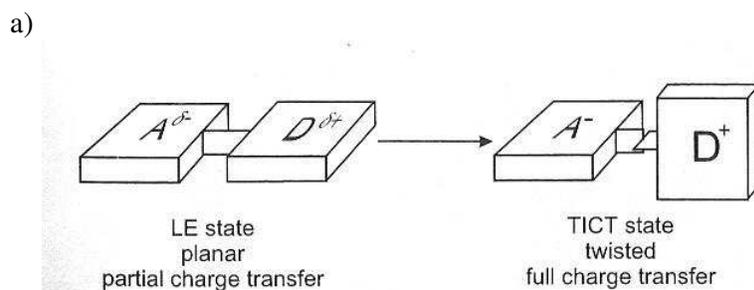


Figure 3. Reaction of the trifluoroacetyl group from a stilbene sensor with amines and alcohols to yield hemiaminals or hemiacetals, respectively.⁷⁻¹²

In some cases, a twisted internal charge transfer (TICT) is also present in these molecules in the excited state and this photophysical process dictates a significant part in the emission of stilbenes. A typical case for this TICT state can be found in stilbenes bearing dimethylaniline as the donor group.

These particular stilbenes have a planar conformation in the ground state, where the conjugated system is better stabilized. When the molecule is excited, a locally-excited state is achieved, with a partial polarization of the molecule while it remains in a planar conformation. However, when solvent relaxation takes place, a ninety degree rotation of the dimethylaniline moiety occurs, “breaking” the conjugation between donor and acceptor which results in a full charge separation (figure 4a). The charge transfer in the TICT state provokes the appearance of an emission band at longer wavelengths (figure 4b).

The importance of the formation of the TICT state in stilbenes was shown by Létard et al.¹³ (Figure 5). In this study, it was shown that the single bond twist (indicated in red) connecting the donor group (blue) and the acceptor group (yellow) was indeed essential for the emission of the molecules.



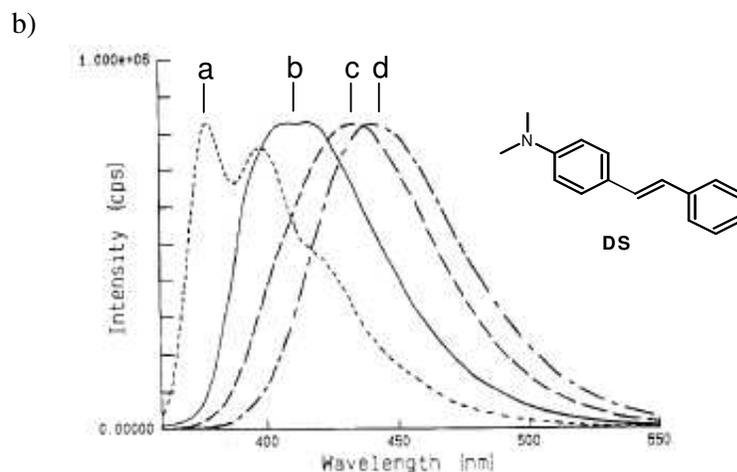


Figure 4. a) Schematic representation of the Locally Excited (LE) and the Twisted Internal Charge Transfer (TICT) states in donor-acceptor stilbenes. The figure was taken directly from reference 1. b) Normalized fluorescence spectra of dimethylaminostilbene (structure DS in the picture) in different organic solvents: a – n-hexane, b – diethyl ether, c – ethanol and d – acetonitrile. In less polar solvents, LE state is favored, while an increase in solvent polarity leads to stabilization of the TICT state. The figure was taken directly from reference 13.

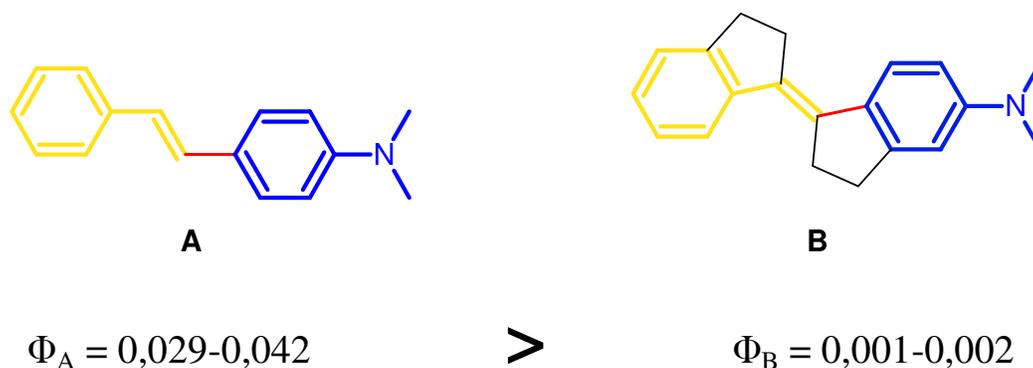


Figure 5. Structures of two stilbene derivatives bearing dimethylaniline as the donor group. The quantum yields (Φ) of the two molecules are presented.¹³

In the cases where the twisting of this single bond was prevented, non-radiative relaxation processes were favoured as the molecule returned from the excited state to the ground state, resulting in a decrease of the quantum yield.

A sub-class of heteroaromatic stilbenes which is essentially based on TICT effects and has attracted substantial focus is the styrylpyridinium system. This type of molecules presents several advantages when compared to the “normal” stilbene core, e.g. the increase of

hydrophilicity which allows for the use of these probes in water samples. This increase in water solubility is due mainly to the positive charge on the nitrogen atom. Furthermore, by increasing the donor and acceptor strength simultaneously, a shift of the optical properties towards lower energies is observed, as well as an increase in Stokes' shift.

Trupp et al.¹⁴ developed a fluorescent chemosensor for the detection of sacharides based on a styrylpyridinium dye. The sensor molecule possessed a boronic acid receptor that, upon reaction with the sacharide species, induced a strong increase in the fluorescence of the styrylpyridinium chromophore. The explanation for this lies on the formation of two covalent bonds between the boronic acid and the sacharide which results in a different environment of the nitrogen from the pyridine ring originating an increase in the fluorescence intensity at 600 nm.

Another interesting example was reported by Turkewitsch et al.¹⁵ who investigated the effect of cyclic nucleotides, namely cyclic adenosine monophosphate (cAMP) and cyclic guanosine monophosphate (cGMP), on the charge transfer mechanism of a styrylpyridinium dye. In the presence of the referred analytes, the fluorescent sensor presented a strong increase in the quantum yield. Furthermore, the sensor probe possessed a vinyl group that could be used for attachment onto polymeric matrixes. In fact, the dye was used by the same authors to develop fluorescent molecularly imprinted polymers (MIP) for the selective detection of cAMP.¹⁶

The fact that the styrylpyridinium salts present a positive charge makes them an attractive target for the design of fluorescent chemosensors towards anionic species. In case electrostatic interactions occur between the fluorescent dye and a given analyte, these interactions should be reflected in its fluorescent properties due to the sensitivity of these molecules towards their surrounding environment.

Consequently, the goal of this research was to synthesize a styrylpyridinium derivative bearing a methacrylate group as a polymerisable moiety to be used as a functional monomer in the synthesis of fluorescent nanosensors for relevant anionic species. The characterization of the synthesized chemosensor was performed both as a free molecule in solution as well as covalently attached to the nanoparticles. The results for this research are discussed in the following sections.

3.2. Design and evaluation of fluorescent chemosensor 2

3.2.1. Synthesis of 2

Taking into consideration the readiness in the reaction between benzylchloride derivatives and the nitrogen atom from pyridine rings through an S_N2 mechanism, the strategy was to synthesize first a benzylchloride possessing a methacrylate group and perform the S_N2 reaction as the second reaction step. Initially, 4-(chlorobenzyl)aniline was used as the starting material. The idea was first, to introduce the methacrylic group by reacting methacryloyl chloride with the aromatic amine. However, the strong reactivity of the amine group towards electrophiles originated that, instead of attacking the electron-deficient centre from the acyl chloride, it formed “dimers” by reacting with itself through the above mentioned S_N2 mechanism (Figure 6).

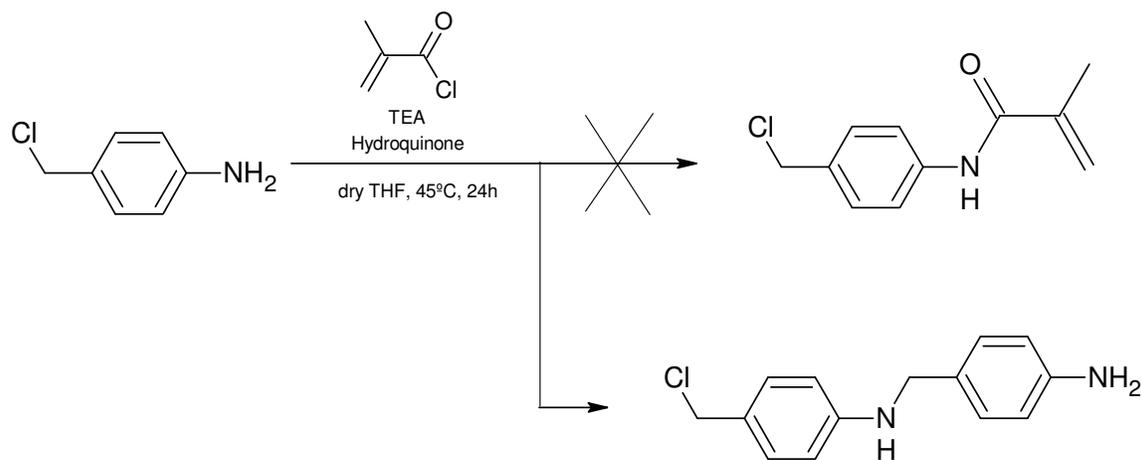


Figure 6. Formation of “dimers” resulting from the S_N2 reaction between two molecules of 4-(chlorobenzyl)aniline.

The undesired products were identified through mass spectrometry.

Thus, an alternative starting compound had to be selected which presented less nucleophilicity. This was achieved by using 4-(chloromethyl)benzyl alcohol as the starting compound. The first step, i.e. the reaction with methacryloyl chloride, was performed at 45°C

overnight and under Argon atmosphere, in the presence of triethylamine as base and hydroquinone, whose function was to stabilise the product against polymerisation. The synthesis was followed through thin layer chromatography (TLC) using pure dichloromethane as the eluent. When total consumption of the starting material was achieved, the solvents were evaporated to yield a viscous white product. After the work-up (neutralization, extraction and washing), a light brown oil was obtained, which was purified through column chromatography to yield the desired product **1**.

The second step involved the previously mentioned S_N2 reaction, with the nitrogen from the pyridine ring acting as a nucleophile towards the aliphatic carbon from the benzyl group, substituting the chlorine atom which in turn is used for the formation of the final organic salt. The scheme for the synthesis of **2** is shown in Figure 7. The full procedure is described in the experimental section.

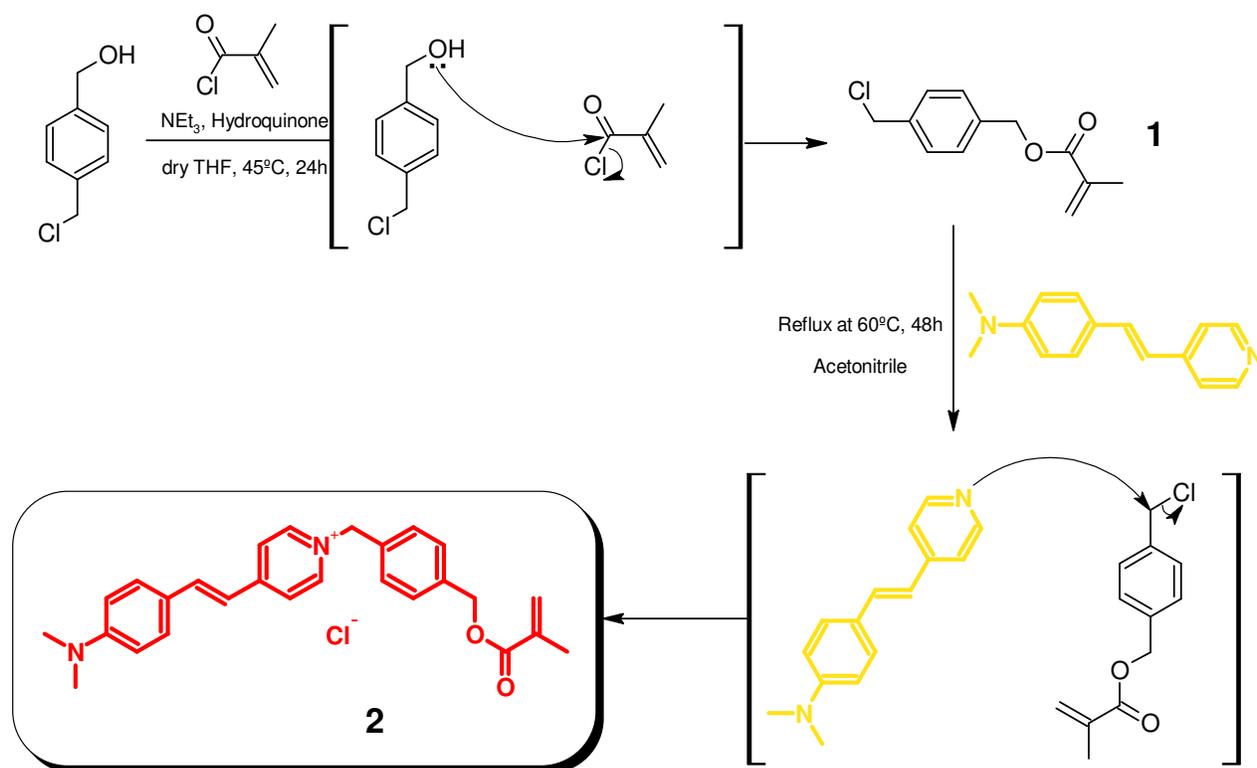


Figure 7. Synthesis of fluorescent chemosensor **2**.

3.2.2. Anion targeted sensing – NSAIDs and other analytes

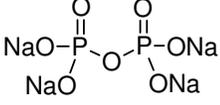
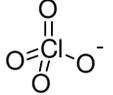
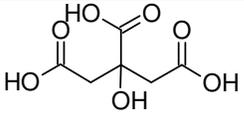
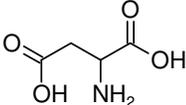
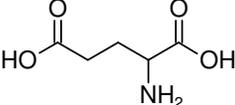
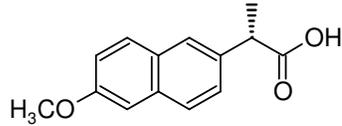
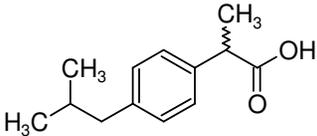
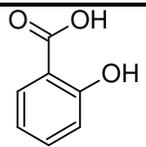
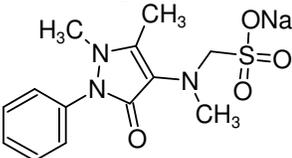
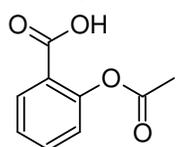
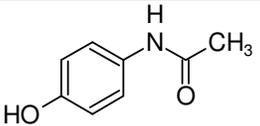
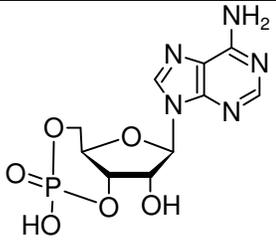
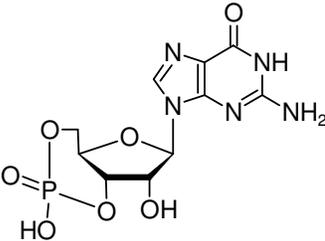
As was previously pointed out, the main objective of this work was to detect anionic species, thus taking advantage of the positive charge on the fluorescent sensor molecule.

We decided to focus on analysing pharmaceutically active compounds that present a negative charge at neutral pH, i.e. the typical pH in which they are active in the human body. Therefore, several compounds were selected in order to assess the sensitivity of the chemosensor **2**, whose structures are described in Table 1.

As it can be observed, most of the analytes belong to the class of drugs called Non-Steroid Anti-Inflammatory Drugs, NSAIDs, such as Naproxen, Ibuprofen or metamizole. NSAIDs are characterized by their analgesic, antipyretic and anti-inflammatory properties, as they act as non-selective inhibitors of the enzyme cyclooxygenase-1 (COX-1) and cyclooxygenase-2 (COX-2). These enzymes are responsible for catalyzing the formation of prostaglandins whose mission is to act as messengers in the process of inflammation, fever and pain and therefore, NSAIDs are able to prevent these processes from occurring.

Current methods for quantifying NSAIDs include sophisticated techniques such as electrophoresis¹⁷, Liquid Chromatography-Mass Spectrometry (LC-MS) combined with Solid Phase Extraction (SPE)^{18, 19}, and combination of High-Performance Liquid Chromatography with Diode-Array Detection (HPLC-DAD) and LC-MS.²⁰ The precise analysis of NSAIDs concentration is essential not only because of their wide-spread use in common medicaments but also due to their potential toxicity with high dosage or even by combining two or more of these drugs. Adverse symptoms due to high dosage are related to gastrointestinal and renal effects, which can enhance their intrinsic antiaggregation effect over platelet.²¹ Upon taking Naproxen, its levels in the plasma are increased after 30 minutes. The maximum recommended dosage of Naproxen for an adult yields a peak concentration of around 0.5 mM in plasma, approximately after 5 hours.²²

Table 1. Different molecules used in the study of selectivity of chemosensor **2** performed in solution.

Analytes		
<i>Anions</i>		
 <p>Pyrophosphate</p>	 <p>Perchlorate</p>	 <p>Citric Acid</p>
<i>Negatively Charged Amino acids</i>		
 <p>L-Aspartic Acid</p>	 <p>L-Glutamic Acid</p>	
<i>Non-Steroid Anti-Inflammatory Drugs (NSAID)</i>		
 <p>Naproxen</p>	 <p>Ibuprofen</p>	 <p>Sodium Salicylate</p>
 <p>Metamizole</p>	 <p>Acetylsalicylic Acid</p>	 <p>Tolmetin</p>
<i>Non-NSAID</i>		
 <p>Acetaminophen</p>		
<i>Nucleotides</i>		
<p>Adenosine 3':5'-cyclic monophosphate (cAMP)</p>		
<p>Guanosine 3':5'-cyclic monophosphate (cGMP)</p>		

3.2.3. Interactions of chemosensor **2** with the analytes in aqueous solution

The fluorescent chemosensor exhibits similar behaviour as the one previously reported by Turkewitsch et al.¹⁵, i.e. a broad absorbance at around 478 nm and fluorescence emission peaking at around 610 nm. Aqueous solutions of defined concentrations of the different analytes were added to a cuvette containing a solution of **2** in phosphate buffer 0.5 M with pH adjusted at 7.2. The interaction (when noticed) between the chemosensor and the analyte was detected by changes in the fluorescence intensity at the emission maximum of 610 nm.

The studied anionic species were divided into two groups: one group consisted of several drugs/active compounds (NSAIDs or non-NSAIDs) which were selected according to their structure as well as relevance in medicine; and another group that included several possible interferents with negative charge at neutral pH that are commonly found in biological systems. Figure 8 illustrates the fluorescence behavior of **2** with the different analytes.

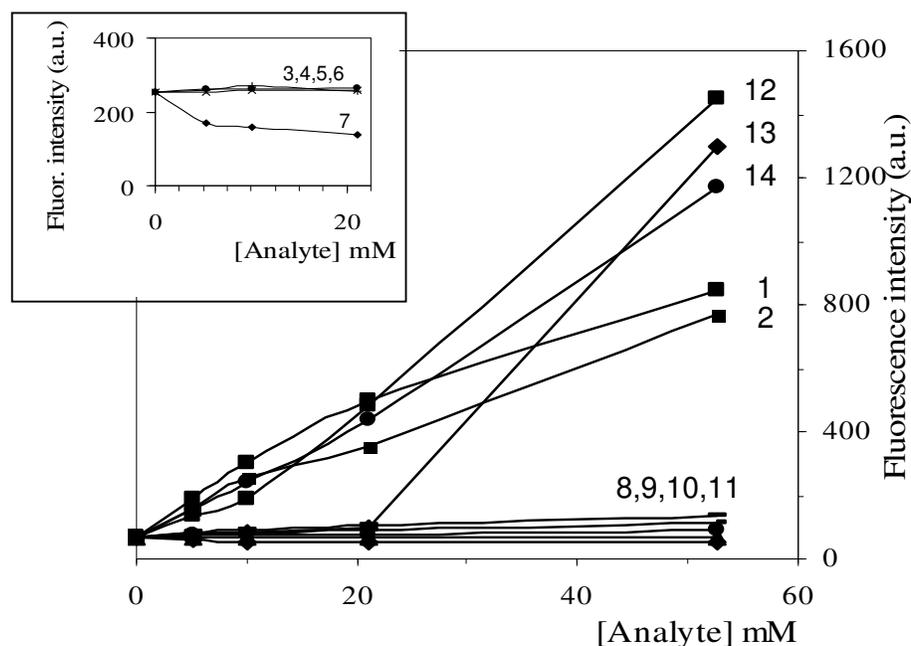


Figure 8. Variation of the fluorescence signal of **2** at 610 nm ($\lambda_{\text{exc}} = 475$ nm) with the concentration of different analytes. Tested standard solutions of 1.0, 5.3, 10.1, 21.1 and 52.6 mM. Analytes: (1) cAMP, (2) cGMP, (3) L-glutamic acid, (4) L-aspartic acid, (5) citric acid, (6) pyrophosphate, (7) perchlorate, (8) acetaminophen, (9) metamizole, (10) acetylsalicylic acid, (11) salicylate, (12) tolmetin, (13) Ibuprofen, (14) Naproxen.

The analysis of the results can be made by dividing the analytes into three categories, according to their effect in the fluorescence signal of **2** at 610 nm. In this way, there is one group of analytes that invokes an increase in the fluorescence emission of the monomer. Within this first group, we distinguished two separate subgroups of analytes, in the first subgroup are included those that show a strong increase of the fluorescence signal (between 7.5 to 15-fold for the highest concentration), in which it was observed that Naproxen shows a slightly better response than cAMP, being cGMP the one presenting the smallest response. Ibuprofen only shows response at the highest tested concentration and tolmetin was not taken into consideration, due to its absorbance at 430 nm that interferes with the absorbance of the chemosensor. In the second subgroup of analytes that show a minor increase in the fluorescence signal (less than 0.5 fold for the highest concentration), only metamizole and acetaminophen are included, the increase in fluorescence being higher in the latter. A second group is formed by two of the analytes, perchlorate and salicylate, that slightly quench the fluorescence of the dye. Finally, a third group includes analytes that induce almost no response on the fluorescence of the monomer such as the negatively charged amino acids, L-glutamic acid and L-aspartic acid, as well as pyrophosphate and citric acid.

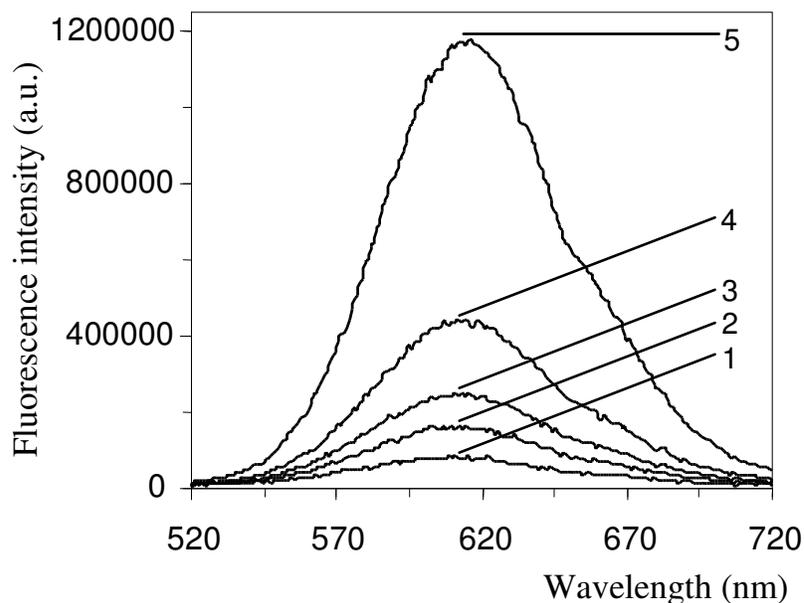


Figure 9. a) Fluorescence spectra of **2** in response to increasing concentrations of Naproxen in phosphate buffer pH 7.2: (1) 0, (2) 5.3, (3) 10.1, (4) 21.1, and (5) 52.6 mM ($\lambda_{\text{exc}} = 478$ nm).

From these results, it can be concluded that the fluorescent chemosensor **2** shows a much stronger affinity towards Naproxen than for any other of the studied drugs and also for the majority of the anionic analytes. Figure 9 describes the spectral changes of **2** upon increasing concentration of Naproxen. Apart from the significant increase in the fluorescence intensity, a concomitant slight red shift of the emission maximum from 609 nm in plain buffer to 613 nm at 52.6 mM of Naproxen can also be observed.

The next step of the research consisted on the immobilization of the fluorescent chemosensor **2** to polymeric matrixes, namely into polyacrylamide nanoparticles, and to evaluate the selectivity of the newly synthesized nanoparticles towards Naproxen and the interfering anionic molecules. A full description on the preparation and characteristics of the nanoparticles is given in the following sections.

3.3. Fluorescent nanoparticles as tools for analyte sensing

3.3.1. Introduction to nanosensors

The use of nanostructures for sensing in biosamples is a relatively recent approach for studying biological processes and ultimately for in-vivo medical research and diagnostics.

Sensor nanoparticles^{23, 24, 25}, in their broad range of polymer materials and preparation conditions appear as complex but also attractive small-sized analytical tools with variable designs, recognition chemistries and transduction principles. Nanosensors have the potential to be mass-produced at a relatively low cost and good reproducibility in terms of size homogeneity. They are applied in various fields including screening as well as quantitative analysis^{26, 27}.

Typically, the property used to measure the recognition process by optical nanosensors relies on luminescence, detecting both fluorescence^{28, 29} and phosphorescence.^{30, 31} The research efforts during the last few years have led to the development of new strategies for the fabrication of nanoparticles using different routes of synthesis e.g. miniemulsion polymerization³² where small, homogeneous and stable droplets of suitable precursors are directly reacted to the final polymer dispersion; emulsion polymerization³³ being limited to the radical polymerization of weakly water-soluble monomers such as methacrylates or styrene; nanogel synthesis³⁴ and the spontaneous formation of nanoparticles from fluorescently labelled dextrans³⁵.

Various materials^{36, 37} and approaches can be used for the nanoparticles preparation, resulting in different architectures of nanoparticles e.g. with a polymeric^{38, 39} or metal core⁴⁰, core-shell^{41, 42} or even multishell.⁴³ These approaches generally deal with coating the core with a shell to form a core-shell structure for further functionalisation⁴⁴ but also with the ability to add to the nanoparticles additional properties embedded in the core e.g. magnetic^{45, 46, 47} or fluorescent.⁴⁸

In the case of fluorescent polymeric nanosensors, the polymer matrix provides a defined microenvironment, wherein the fluorescent monomer is dissolved.⁴⁹ The particle has the function to retain the fluorescent monomer in place providing physical and chemical stabilization and thus reducing bleaching. This shielding is also very important against enzymes and biomacromolecules which can interfere with the fluorescence signal from the monomer and therefore affect sensing towards the target molecule. The immobilization can be

achieved by covalently immobilizing the fluorescent dye to the matrix but also by simply dissolving a hydrophilic and water soluble dye in a hydrophilic polymer.

3.3.2. Immobilization of chemosensor **2** into polyacrylamide nanoparticles (PAA-NPs)

In this research, compound **2** bearing a methacrylic group as the polymerisable moiety was used as the functional fluorescent monomer to be incorporated in the PAA polymeric nanoparticles. The **PAA-NPs** were prepared by inverse microemulsion polymerization as described by Clark et al.⁵⁰ (a full description can be found in the Experimental section).

The reaction was performed using acrylamide/bisacrylamide as the “backbone” monomer and *N,N,N',N'*-tetramethyl ethylenediamine (TEMED)/Ammonium Persulphate system as initiator.

Briefly, the fluorescent monomer was mixed with the aqueous phase components, since it is charged and thus water soluble. This aqueous mixture was then added to a hydrophobic organic solvent, in this case *n*-hexane, containing surfactant molecules (Brij 30, forming a micro-emulsion of small droplets, with the surfactant encapsulating the water soluble components. At this achieved stage, the initiator system was added. After polymerisation and subsequent removal of the solvent, the resulting particles were filtered in order to remove unreacted monomers. Finally, the particles were thoroughly washed and nanoparticles in the form of a pink powder were obtained and kept as such until the measurements were performed. Figure 10 shows a schematic representation of the procedure.

Through this method, the incorporation of both the functional monomer as well as the backbone monomer inside the microdroplets (and subsequently in the nanoparticle matrix) is favoured.

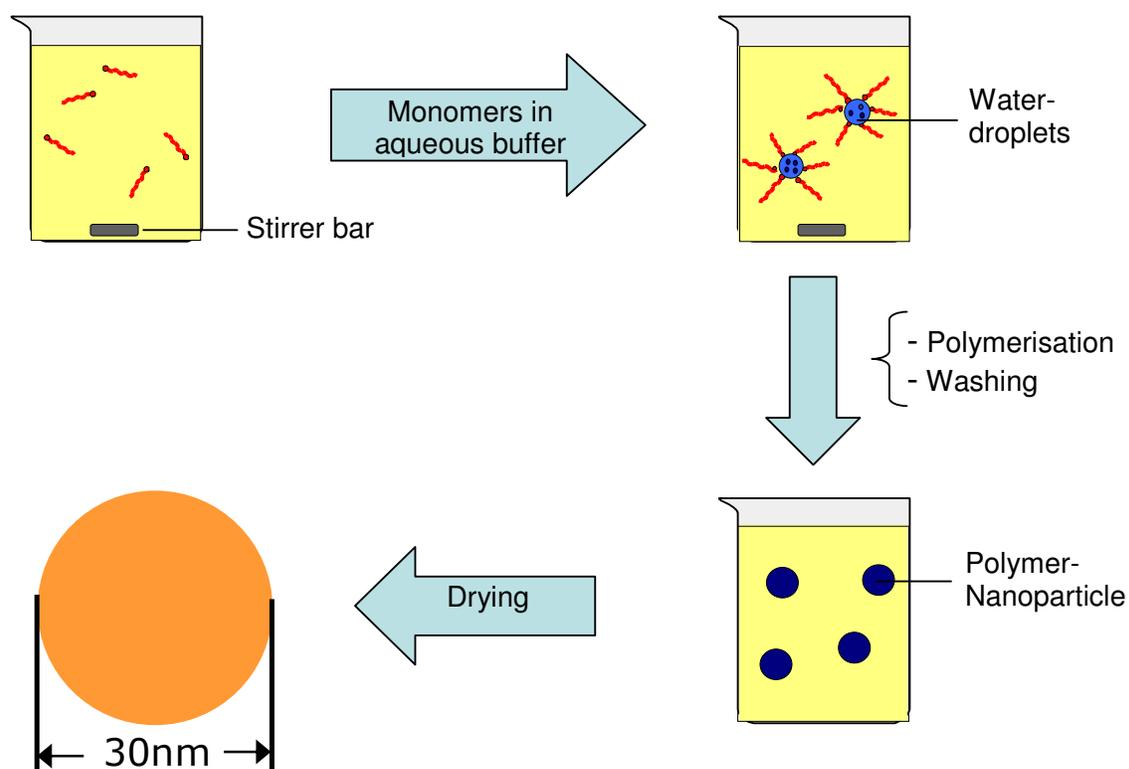


Figure 10. Synthesis of **PAA-NPs** via inverse micro-emulsion polymerization. The final size for the nanoparticles was determined to be around 30 nm (see following section).

3.3.3. Size characterization of **PAA-NPs** - Dynamic Light scattering (DLS)

A very important aspect to take into consideration when synthesizing nanoparticles is their size and homogeneity. The common method to characterise nanoparticles regarding their size is the so-called Dynamic Light Scattering (DLS).

In this technique, the size of nanoparticles is determined according to their diffusion in that the bigger the particles, the slower their diffusion will be in a certain medium. The hydrodynamic diameter, d_H , can therefore be calculated using the Stokes-Einstein equation [1]:

$$d_H = \frac{kT}{3\pi\eta D} \quad [1]$$

in which k represents the Boltzmann constant, T is the temperature, η is the viscosity of the media and D is the translational diffusion coefficient.

The analysis of the nanoparticles suspension yielded a graph describing the size distribution of the nanoparticles.

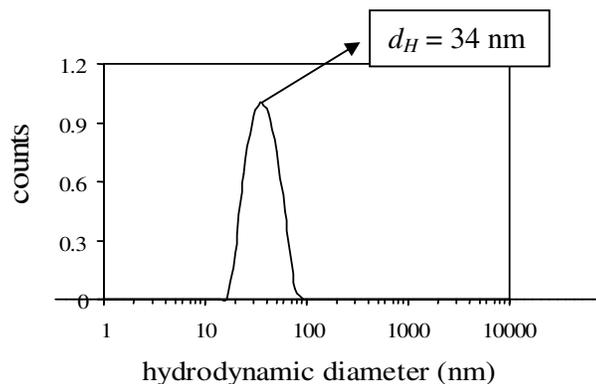


Figure 11. Graph describing the size distribution of the **PAA-NPs**. The hydrodynamic diameter was determined to be 34 nm and the polydispersity index to be 0.10.

The polydispersity index (PDI) determines the homogeneity in the size of the nanoparticles. The bigger the PDI, the less homogeneous they are. In this particular case, the obtained PDI value was 0.10 which indicates that the synthesized **PAA-NPs** are monodisperse (typical values from 0.01 to 0.20 are conventionally assumed to be monodisperse).

3.4. Naproxen sensing using fluorescent PAA-NPs

3.4.1. Sensitivity studies

As was described in 3.2.2, the interaction between the nanosensor and the analyte is based mainly on electrostatic forces, since the fluorescent monomer allocated within the nanoparticles matrix bears a positive charge. Figure 12 shows a schematic representation on the sensing mechanism of the nanoparticles towards negatively charged analytes.

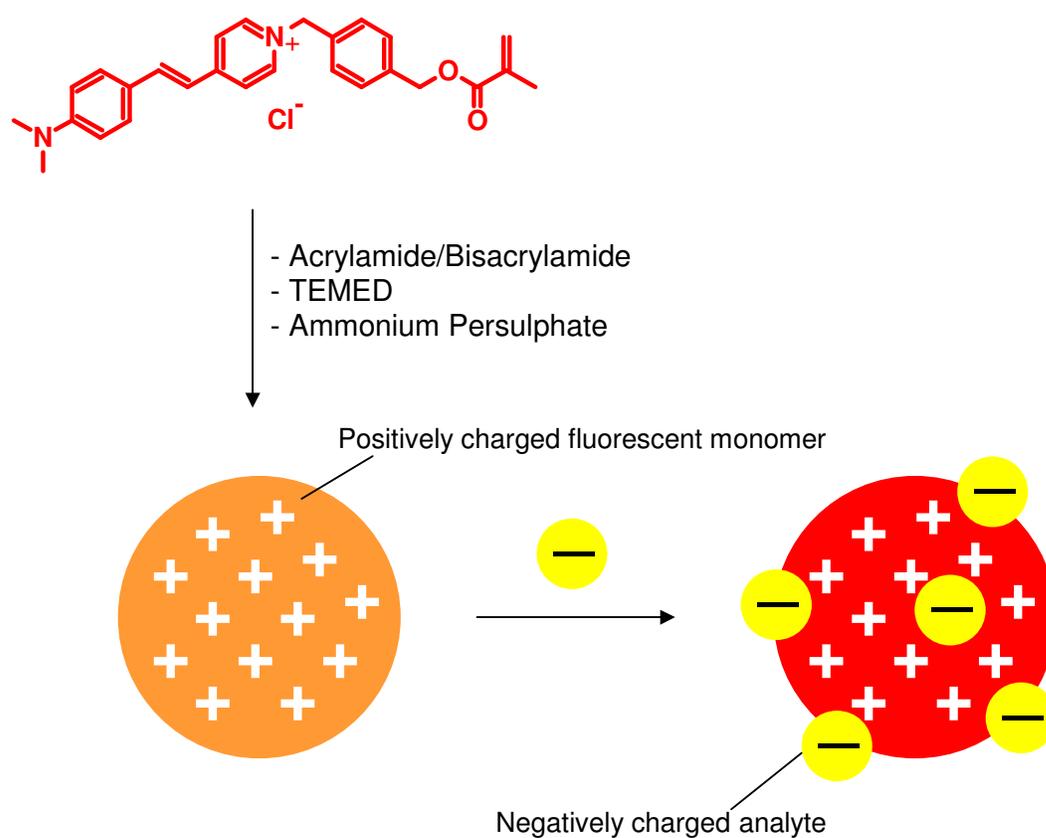


Figure 12. Molecular structure of the fluorescent monomer **2** and schematic representation of nanosensor interaction with negatively charged analytes.

In the studies involving polyacrylamide nanoparticles, three analytes were at first studied in more detail, namely Naproxen, cAMP and cGMP, since these were the ones that induced the strongest response from fluorescent chemosensor **2** in solution. In a later section (3.4.2), the selectivity for interfering species was evaluated.

The following graph describes the changes in fluorescence of the nanoparticles upon increasing concentrations of Naproxen, cAMP and cGMP.

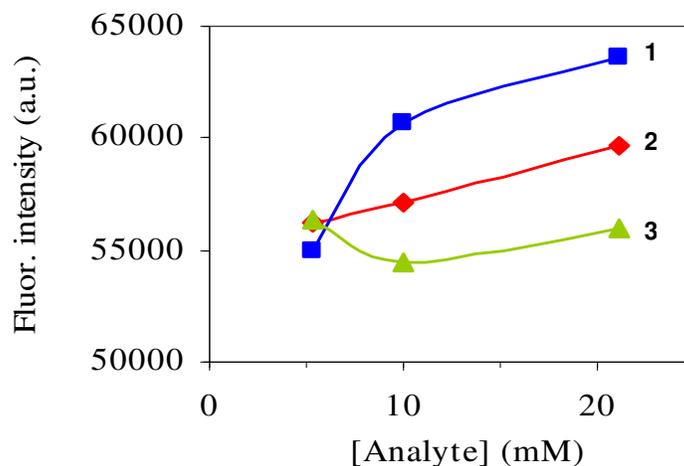


Figure 13. Fluorescence intensity changes of the signal from **2** in PAA-NPs with different concentrations of analyte: (1) Naproxen, (2) cAMP and (3) cGMP ($\lambda_{exc} = 460$ nm).

The first observation is that the fluorescence of the incorporated chemosensor **2** exhibits significantly smaller changes in intensity when compared to the free dye in solution (see Figure 9). This phenomenon is commonly observed for immobilized fluorescent dyes and is related to factors such as (1) constraint of the molecule within the matrix that affects its excited and/or ground state conformations, and (2) analyte diffusion into the matrix being prevented due to sterical hindrance or electrostatic repulsions.

A more important observation, however, is made when comparing plots 1, 2 and 3, which correspond to the three analytes. From the changes in fluorescence intensity upon different concentrations of the analytes, it is clearly visible that a significantly stronger enhancement in fluorescence is seen in the case of Naproxen than for cAMP or cGMP. One possible explanation for this observation can lie on the differences in the structures of these analytes (see Table 1). Although all three possess a negative charge, Naproxen presents a smaller molecular size than both cyclic nucleotides. This may indicate that the latter analytes are

prevented more strongly from penetrating the nanoparticle matrix to interact with the “interior” chemosensor molecules than in the case of Naproxen.

To assess more thoroughly the sensitivity of the nanoparticles towards Naproxen and to fully characterize their sensing properties, a wider range of concentrations was used. Figure 14 displays the changes in the fluorescence spectra of the sensor nanoparticles in phosphate buffer (pH 7.2) with Naproxen concentrations ranging from 0 to 52.6 mM.

Examining the obtained curves in this case, one can see an additional signal apart from the expected one for the fluorescent monomer **2**. This peak, with a maximum at around 520 nm can be explained based on the scheme presented in Figure 1 (see section 3.1). It is assumed that the main mechanism for fluorescence emission of the free monomer **2** is the TICT previously described. However, when immobilized in the **PAA-NPs**, the structure of the fluorescent monomer is more constrained, leading to a decrease in the TICT effect. In contrast, an increase is also denoted regarding the locally excited (LE) state of the monomer which does not involve any twisting of the molecule. The peak corresponding to the radiative decay from this LE is situated at higher energy, as is shown in the example from figure 1. In the presence of Naproxen an increase in the TICT form is favoured, and due to this, a decrease of the LE state is observed.

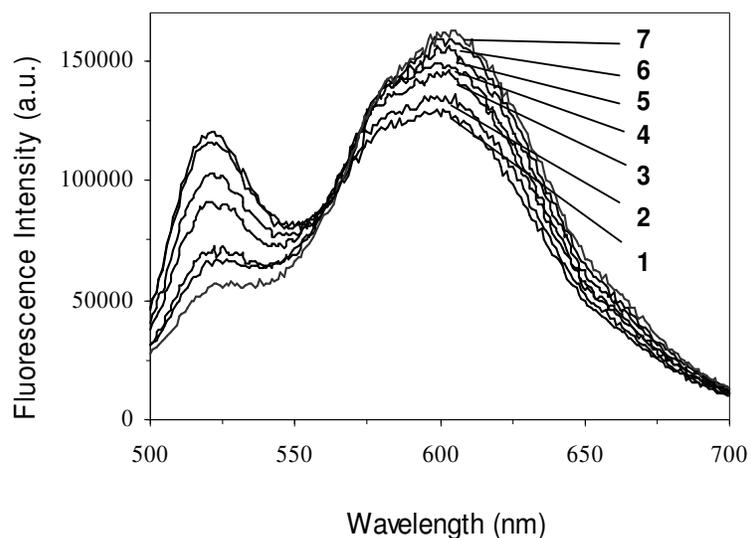


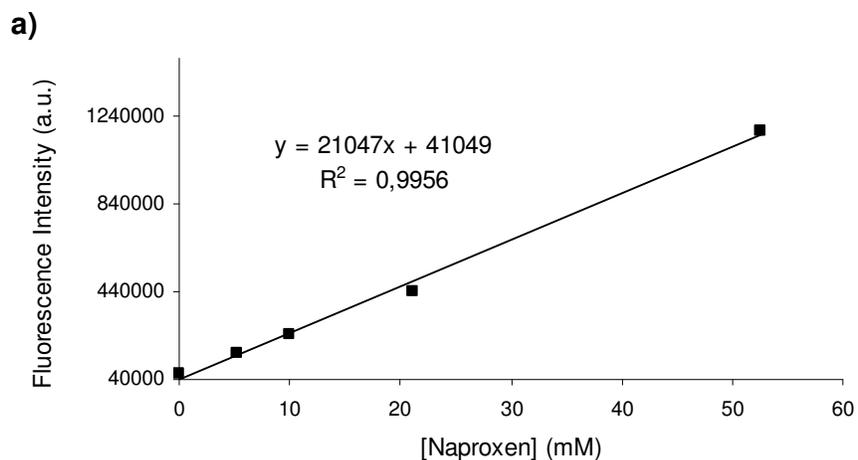
Figure 14. Fluorescence spectra of **PAA-NPs** suspended in phosphate buffer pH 7.2, and their response to increasing concentrations of Naproxen: (1) 0, (2) 1.0, (3) 5.3, (4) 10.1, (5) 21.1, (6) 35.0 and (7) 52.6 mM ($\lambda_{\text{exc}} = 460$ nm).

The response of the **PAA-NPs** against the concentration of Naproxen was evaluated and a linear plot was obtained using the logarithm of Naproxen concentration as the “x” axis and the intensity at the emission maximum as the “y” axis. For comparison purposes, the fluorescence response of the free monomer in solution towards Naproxen was also plotted. Both graphs are shown in figure 15.

The statistic parameters calculated from the linear ordinary least-square (OLS) regression and the performance characteristics are presented in Table 2. The limit of detection (LOD) was estimated according to the IUPAC guidelines⁵¹, using equation [II]:

$$\text{LOD} = \frac{3\sigma}{a} \quad \text{[II]}$$

where a represents the slope of the curve and σ is the standard deviation obtained from 6 replicates of the fluorescence intensity of only the dissolved dye or the **PAA-NPs** in buffer solution (i.e. no other analytes were added). In the case of the **PAA-NPs**, the obtained value x for the LOD was directly converted from the logarithmic scale ($\text{LOD} = 10^x$).



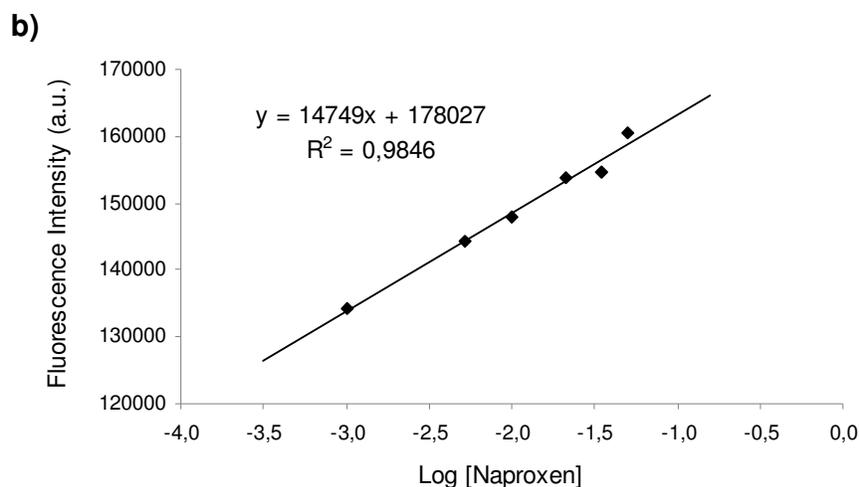


Figure 15. Changes in the fluorescence intensity maxima of (a) the free monomer **1** in solution and (b) the **PAA-NPs**, with different concentrations of Naproxen (λ_{exc} (a) = 475 nm, λ_{exc} (b) = 460 nm).

Table 2. Statistical parameters from the linear regression for each calibration curve concerning Naproxen detection with **2** in solution and in **PAA-NPs**.

	Nanoparticles	Solution
Intercept	178027	41048.8
Standard deviation of intercept	1872.6	20851.8
Slope	14749.4	21046.7
Standard deviation of slope	920.87	806.96
Determination coefficient (R^2)	98.47%	99.56%
Linearity on-line	93.76%	96.17%
L.O.D. (mM) ^a	0.50	0.054
Dynamic Range (mM)	0.50-52	0.054-52

^a: calculated as mentioned previously, according to the previously presented formula (page 27).

Although these results are satisfactory in terms of selectivity, the LOD in **PAA-NPs** is 0.50 mM, which is ten times higher than compared to the value in solution (0.054 mM). This decrease in the LOD using nanoparticles comparing with the LOD obtained in solution can be explained by the immobilization of chemosensor **2** in the polymeric matrix. It is assumed that

in the polymer nanoparticles the access to the dye is hindered, which leads to a decrease in the probability of encounters between the fluorescent monomer and Naproxen.

Furthermore, the polymer matrix may also confer some sterical constrictions to chemosensor **2** which can affect its recognition abilities towards Naproxen. Eventually, certain conformational changes which may be relevant for the interaction of chemosensor **2** with Naproxen are restricted or no longer possible.

Despite the fact that the LOD is significantly higher than in solution (around 10-fold), the **PAA-NPs** may still find applications in rapid screening procedures of plasma samples for individuals that present symptoms of Naproxen overdose. Moreover, they may also be used in analysis of waste waters and industrial routine tests for monitoring Naproxen.

3.4.2. Selectivity studies

In order to assess the selectivity of the sensor nanoparticles in water analysis, a systematic study was conducted in aqueous buffer on the effects produced by the presence of interfering species, including drugs and biomolecules, on the determination of 1.0 mM of Naproxen. The concomitant species were tested at different concentration levels, and if interference occurred, the concentration of these species was reduced until the result was included in the interval defined by $[\pm t_{(n-2; \alpha:0.05)} \cdot S_R]$ (at 1.0 mM of Naproxen), being S_R the standard deviation for four different replicates of **PAA-NPs** equilibrated in 1.0 mM of Naproxen and equal to 0.0041, and the t-student of 2.132 (freedom degrees: $n-2$, $\alpha=0.05$). The predicted response⁵² coming from the calibration function was found to be 0.0134, so that, the tolerance interval was of 0.0223 ± 0.0046 . This interval was used as the reference and the maximum concentration of interfering species producing a value higher or lower to this interval was taken as the tolerance level. Table 3 shows the obtained tolerance levels for the fluorescence response of the **PAA-NPs** relative to all the studied analytes in the presence of Naproxen (1 mM).

Table 3. Effect of potentially interfering molecules on the determination of 1 mM of Naproxen using the synthesized **PAA-NPs**.

Analyte molecules	Tolerance level (mM)
<i>Anions</i>	
Perchlorate	23
Pyrophosphate	32
Citric Acid	13
<i>Negatively Charged Aminoacids</i>	
L-Glutamic Acid	>21
L-Aspartic Acid	>21
<i>Non-steroidal anti-inflammatory drugs (NSAID)</i>	
Acetylsalicylic Acid	>50
Sodium Salicylate	14
Ibuprofen	13
Metamizole	>50
<i>Non-NSAID</i>	
Acetaminophen	>21
<i>Nucleotides</i>	
Adenosine 3':5'-cyclic monophosphate (cAMP)	1.6
Guanosine 3':5'-cyclic monophosphate (cGMP)	5.6

For almost all of the studied anionic species, the interferences were minimal, especially when considering the drug molecules (NSAIDs and non-NSAIDs). However, cAMP interference is high (1.55 mM) as expected, taking into account the similar response in solution for both cAMP and Naproxen (see experimental points in figure 8). This synergistic effect can be explained on the basis that, although chemosensor **2** binds to Naproxen more favourably than cAMP, a high concentration of the latter leads to a decrease in Naproxen interaction. Despite the increase in cAMP interference when it was mixed with Naproxen, the obtained tolerance level is sufficient for analysis of plasma samples, since concentrations of cAMP found in human plasma samples are in the nanomolar range.⁵³ Tolerance levels for other compounds were also found to be sufficient for application in environmental analysis.^{54,55} As such, the synthesized **PAA-NPs** can be suitable for analysis of waste waters from pharmaceutical industries, or simply for fast screening of Naproxen in aqueous samples.

3.5. Conclusions

A new polymerisable chemosensor **2**, based on a styrylpyridinium structure was successfully synthesized. The chemosensor bears a positive charge and changes its optical properties (fluorescence emission) in the presence of anionic species. The sensing mechanism is essentially based on electrostatic interactions which affect the TICT efficiency of **2**, leading to a significant increase in fluorescence intensity.

The chemosensor was studied against a wide variety of anions, providing the strongest interactions towards Naproxen, a drug belonging to the group of Non-Steroid Anti-Inflammatory Drugs which are commonly produced and marketed by the pharmaceutical industry. The limit of detection (LOD) of **2** in aqueous phosphate buffer at pH 7.2 against Naproxen was found to be 0.054 mM, with a linear response in the studied concentrations (up to 50 mM).

Apart from its desirable optical properties i.e. absorption and emission maxima in the visible range – 478 nm and 610 nm respectively –, the methacrylic group within the chemosensor structure allowed for its use in the production of fluorescent polyacrylamide nanoparticles (**PAA-NPs**). The covalent attachment of **2** minimized leaching of the chemosensor from the nanoparticle matrix into the sample solution. The synthesized **PAA-NPs** exhibited a homogeneous size distribution, with a measured diameter of 34 nanometers and fluorescence emission maximum at 590 nm.

The **PAA-NPs** were fully characterized regarding their fluorescent response to Naproxen. The LOD for the fluorescent **PAA-NPs** was about ten times higher (0.50 mM) when compared to **2** in solution. It is assumed that this loss of sensitivity was due not only to the physical constraint of **2** inside the **PAA-NPs** which affected its sensing properties, but also due to sterical hindrance that impeded Naproxen from entering the highly cross-linked polymeric matrix of the nanoparticles. Although the nanoparticles present a higher LOD than the free monomer in solution, it is still low enough for fast analysis of human plasma, to diagnose possible Naproxen overdose. The selectivity studies against other analytes showed that cAMP acts as a strong interfering species. Nevertheless, the concentrations of cAMP in human plasma samples are too low to interfere with Naproxen analysis using the synthesized **PAA-NPs**. Apart from biological samples, the nanoparticles may also be used for environmental tests of pharmaceutical waste waters or rapid monitoring of Naproxen in aqueous samples.

4. An ATP Fluorescent Chemosensor Based on a Zn(II)-Complexed Dipicolylamine Receptor Coupled with a Naphthalimide Chromophore

4.1. State of the art – Photoinduced Electron Transfer (PET) based fluorescent probes

Several photochemical mechanisms are available that can be used as a recognition process for specific interactions between indicator and analyte molecules. Along with ICT, PET is one of the most common mechanisms in fluorescent sensor molecules.

PET is a fluorescence quenching process which generally involves two components: an electron donor and an electron acceptor. Its principle is based on the fact that, in the excited state, the oxidative and reductive properties of molecules are enhanced and therefore, electron transfer processes may take place. A scheme for oxidative and reductive electron transfers is presented in Figure 16.

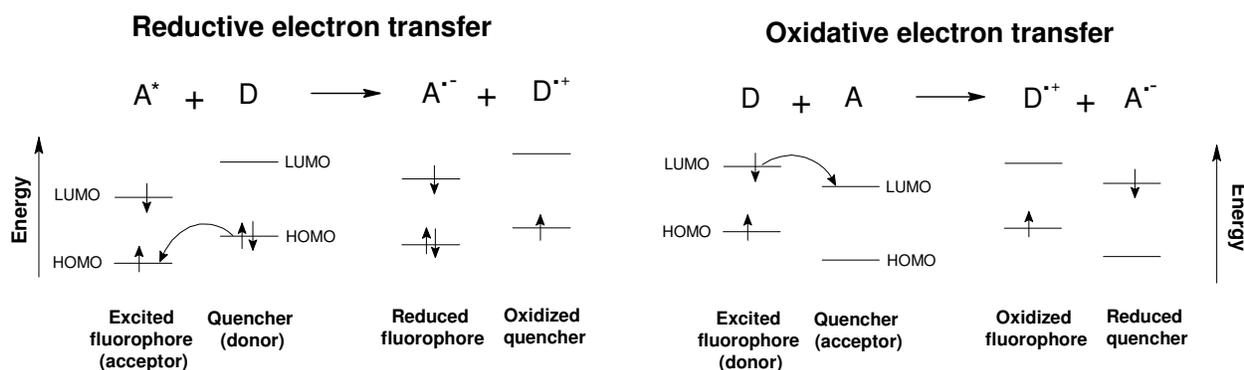


Figure 16. Scheme for oxidative and reductive PET between an excited fluorophore and a quencher.

PET can be an extremely useful tool when designing fluorescent sensors, particularly in the case of cation detection. The typical architecture for such a fluorescent sensor involves a receptor unit as the electron donor and a fluorophore as the acceptor, often with a carbon chain acting as a spacer. Upon reacting with the target cation, the electron donor strength of the receptor is affected and PET quenching is decreased or completely prevented (Figure 17).

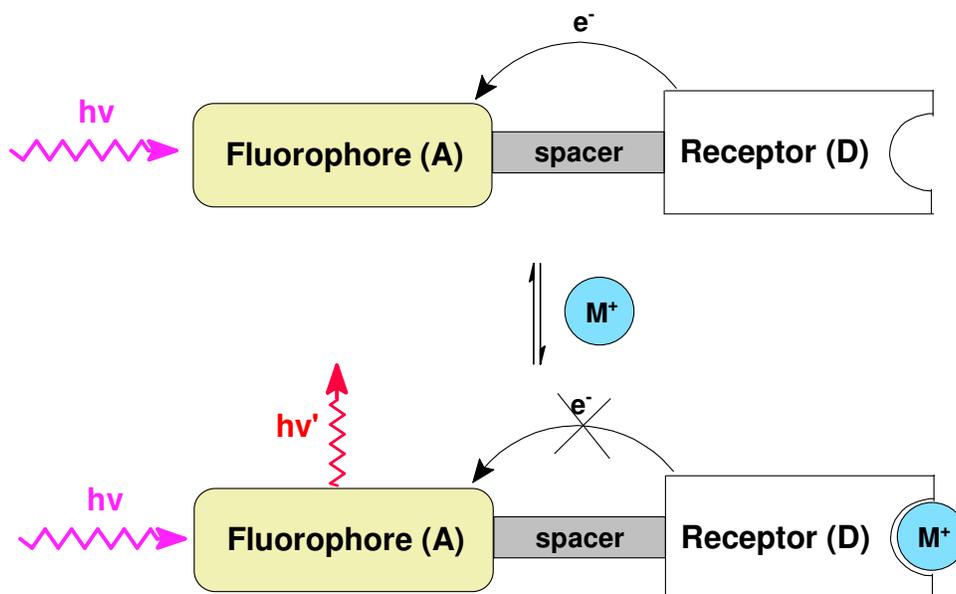


Figure 17. A typical scheme for PET-based cation sensing.

The PET sensing mechanism can be found in a wide range of fluorophore molecules. The first and perhaps most commonly found in the literature are systems based on naphthalene, anthracene and pyrene groups. De Silva et al.⁵⁶ reported a PET-based pH indicator consisting of an anthracene fluorophore connected to an amine via a methylene spacer. By changing the amine donor group, it was possible to tune the pKa value of the indicator dye in the range from around 2 to 8.

Fluorescein is one the most studied cases regarding fluorescent indicator molecules. Its high quantum yield presents perhaps its most attractive characteristic, and its pKa in the physiologically relevant range (around 7) allows for its use as a highly sensitive pH probe. Although not usually considered a PET fluorescence sensor, some derivatives of fluorescein were reported as cation sensors using a PET-based sensor mechanism. These findings were made by Walkup et al.⁵⁷, who designed a derivative of fluorescein linked to two dipicolylamine moieties with a methylene spacer (Figure 18).

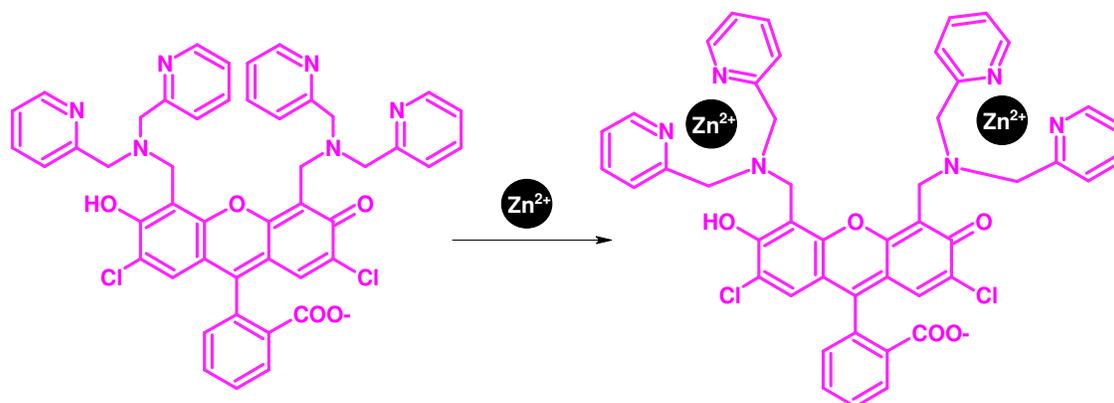
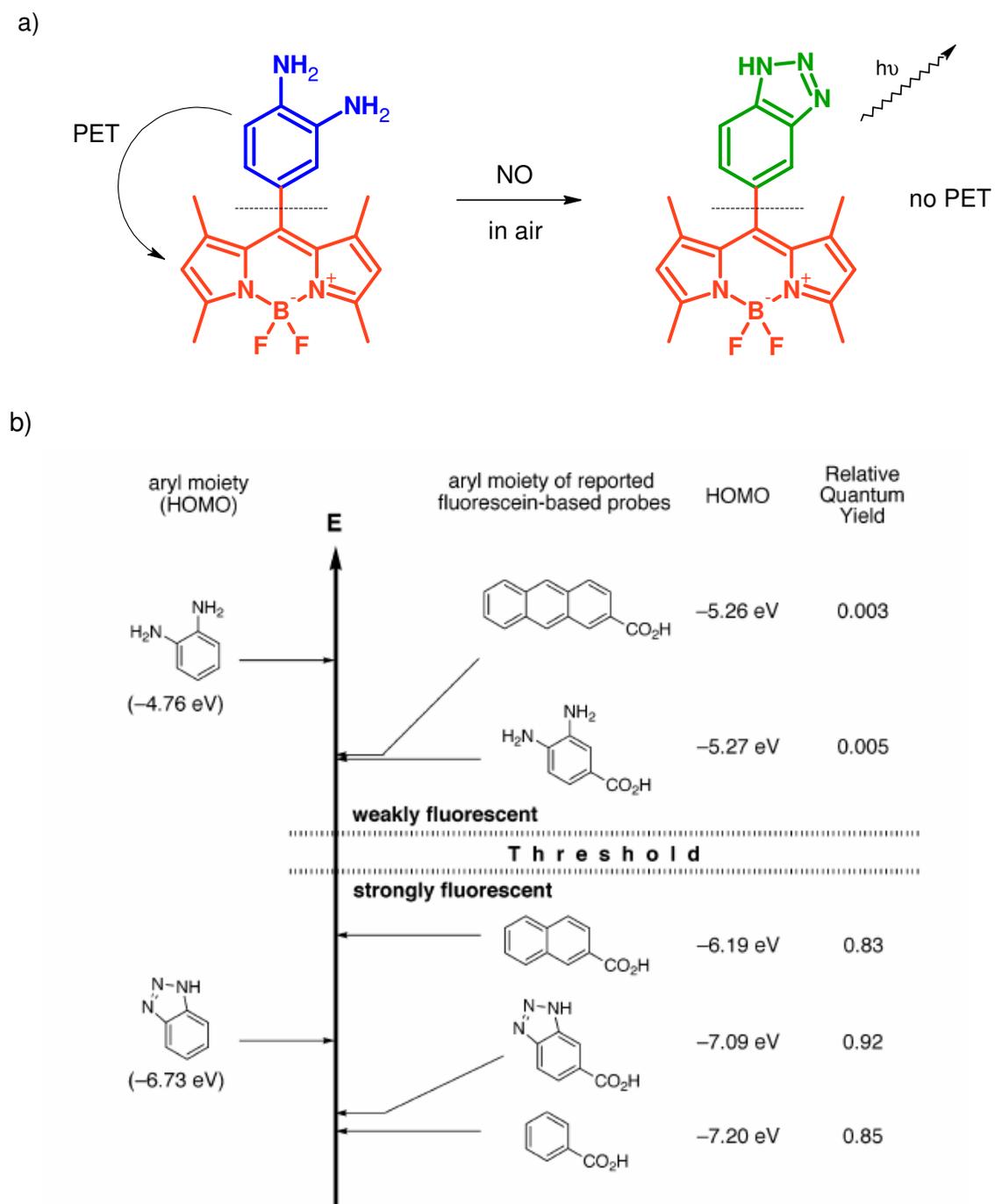


Figure 18. Complexation of Zinpyr-1 with Zn^{2+} ions. The dye is highly sensitive and exhibits a significant fluorescence enhancement upon Zn^{2+} concentrations down to the nanomolar range in aqueous buffer at pH 7.0.⁵⁷

Upon binding of Zn^{2+} ions to the chelating groups, a strong increase in fluorescence was observed, with virtually no signal changes in the presence of Ca^{2+} or Mg^{2+} . Furthermore, the sensor was successfully tested in living cells and the response allowed for detection limits down to nanomolar concentrations. Later, Lippard et al.⁵⁸ modified the structure of the receptor moieties with the advantage that the pK_a of the donor groups was lower and therefore, the response to Zn^{2+} was increased when compared to its predecessor.

An interesting fluorophore which has been attracting much attention in recent years is the class of the BOron-DIPYrromethene (BODIPY) dyes. The main advantages of this system lie on its high photostability and quantum yields. Several examples of PET sensors using this fluorescent group can be found in the literature.⁵⁹

Nagano et al.⁶⁰ were amongst the first to thoroughly study the PET effects on BODIPY fluorescence and to use these findings for the design of sensors. Figure 19 describes a BODIPY fluorescent probe for nitric oxide. When the donor phenyl ring (blue) is present in unreacted form, the oxidative potential of its LUMO orbital is higher than the HOMO from the BODIPY core and therefore, reductive PET is observed. However, upon reaction of the aromatic amines of the donor with nitric oxide, the formed benzotriazole species (green) presents an oxidation potential which is lower than the potential of the HOMO from the BODIPY. As a consequence, PET is no longer observed and the quantum yield of the probe is strongly increased.



Another example of this rational method for sensor design was later reported by Urano et al.⁶¹, who designed a series of pH-sensitive BODIPY compounds for selective cancer cell imaging (Figure 20).

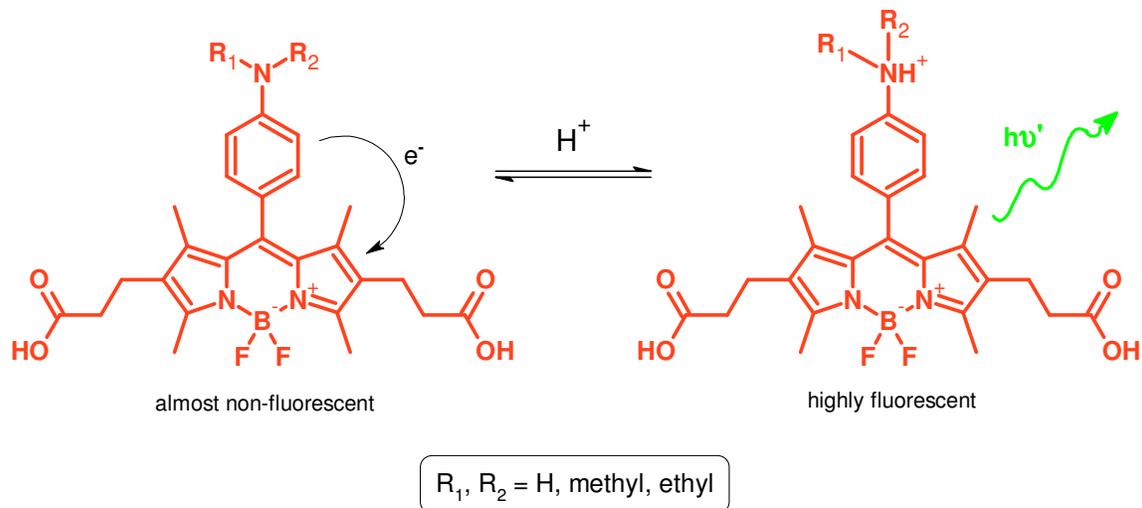


Figure 20. BODIPY pH probes. The different substituents dictate the final pKa of the aniline moiety, which modulates the emission of the BODIPY fluorophore.⁶¹

The methodology is based on the fact that, in some types of cancer cells, lysosomal pH reaches more acidic values than healthy cells. The sensors were tested *ex-vivo* and *in-vivo* in lung cancer cells, with the fluorescence being turned on at acidic pH. The principle was the same as in the previous case (for the nitric oxide sensor), with the chemosensors presenting pKa values ranging from 4 to 6, depending on the different substituents of the donor aniline group. The only difference in comparison with the previous case is that, in this case, it is the HOMO of the donor that upon protonation raises its energy to a higher level than the LUMO of the acceptor, thus preventing PET quenching. Other cases of BODIPY-based sensors using PET were also reported for metal ions, including some NIR BODIPY derivatives.⁶²

Despite all these characteristics, the vast majority of the BODIPY dyes possess a very small Stokes' shift, which complicates the separation of the excitation from the emission light.

4.2. Design of a naphthalimide-based chemosensor

4.2.1. THE FLUOROPHORE – Is naphthalimide the perfect system for sensor applications?

In many aspects, the answer to the previous question is “yes”. The naphthalimide group is constituted by a naphthalene ring fused with a succinimidyl moiety. Its 4-aminonaphthalimide derivative, which is the most commonly presented form (and therefore it’s simply known as “naphthalimide”), possesses numerous desirable characteristics such as high quantum yields, good photostability and both absorption and emission in the visible spectral range (figure 21).

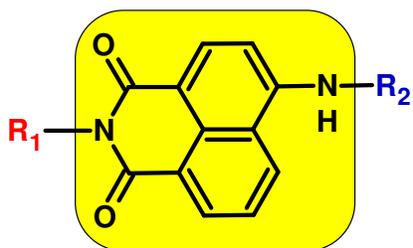


Figure 21. General structure of a 4-aminonaphthalimide. The fluorophore is represented inside the yellow rectangle, with R₁ and R₂ representing possible functionalizations on the fluorophore molecule.

Perhaps the most noticeable advantages of this core, in comparison for example with the BODIPY, are: (1) its high chemical versatility which permits a relatively easy and independent functionalization of two parts of the molecule (if the synthesis starts from 4-bromo-8-naphthalic anhydride, for example) through selective nucleophilic attack; and (2) the large Stokes’ shift that allows for the excitation to be made at the maximum of absorption and therefore, maximum emission signal intensity is achieved.

Due to all of these advantages, the naphthalimide unit is one of the most used, and also one of the most promising fluorescent groups in optical sensing. However, one major limitation is that it absorbs at too short wavelength to be excited with the common 488 nm laser.

Most of the naphthalimide-based sensing approaches rely on intramolecular PET mechanism. The sensor molecule usually possesses an electron donor group within its structure that acts as quencher. Upon reaction of the target analyte with this donor group, the energy of its HOMO is lowered down to a level where it does no longer interfere with the radiative decay of the excited electron of the fluorophore to the ground state, resulting in an increase in its fluorescence emission (figure 22).⁶³

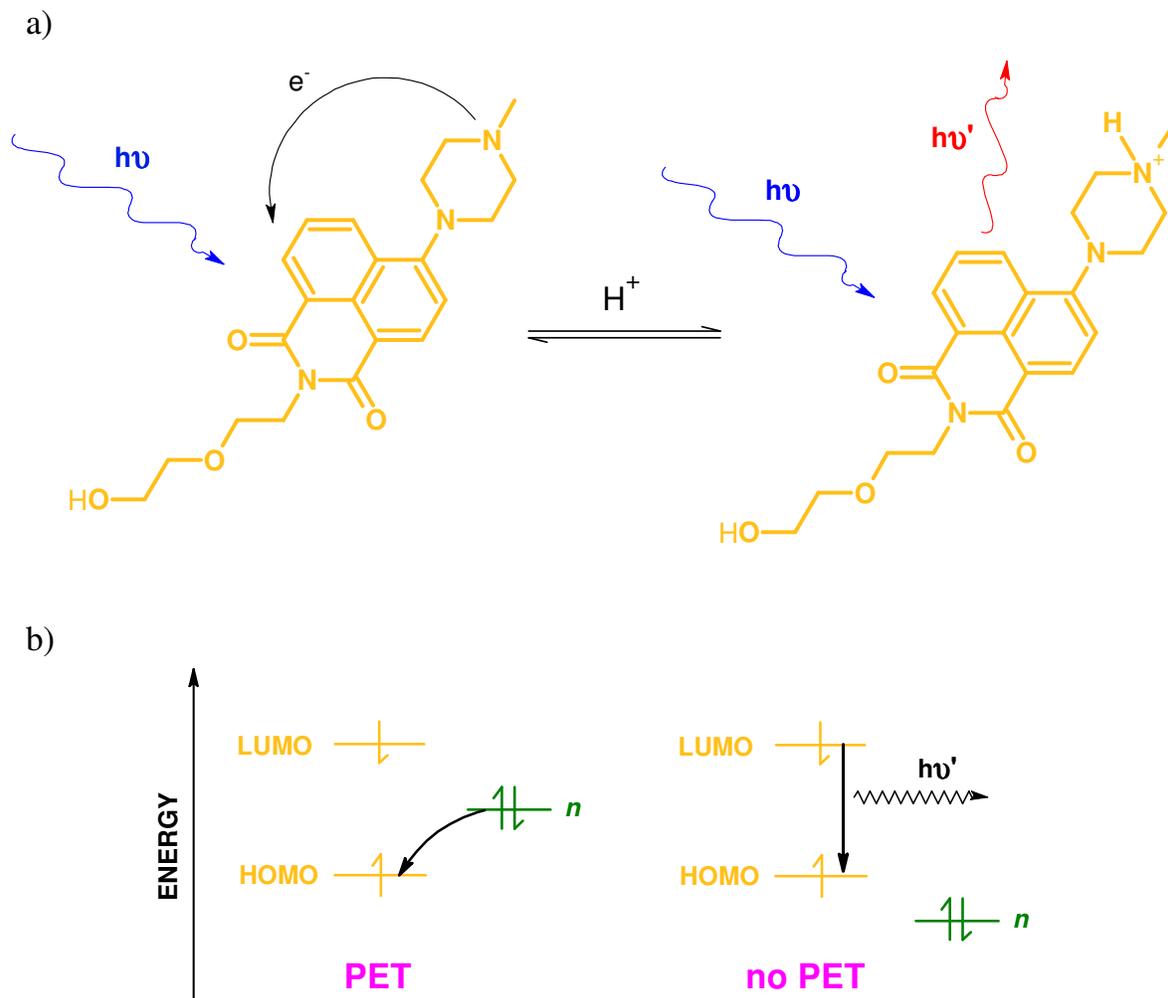


Figure 22. Schematic representation of the PET mechanism in 4-aminonaphthalimides. a) A fluorescent naphthalimide sensor for pH.⁶³ Upon protonation of the methyl piperazine group, fluorescence is enhanced. b) Molecular orbitals scheme referring to a). When the n -orbital (green) is not-protonated, its energy resides between the energies of the HOMO and LUMO from the fluorophore and PET is observed. If the n -orbital is used to bind a proton, its energy is drastically lowered and PET no longer occurs.

A vast amount of examples for these sensors can be found in the literature.⁶⁴ In the next paragraphs, some of the latest and significant contributions will be addressed.

The most significant impact using naphthalimides was made on the development of sensors for metal cations. The strategy for the design of such sensors is also based on the PET mechanism. It usually involves the attachment of an electron donor chelating unit to the naphthalimide which, upon binding of the metal ion undergoes an increase in fluorescence emission (due to the decrease of the PET effect).

He et al.⁶⁵ successfully developed a selective fluorescent sensor for potassium ions, which presented almost no response to sodium and calcium. In this case, the receptor unit was composed of a complex macrocycle, possessing an aniline moiety as the electron donor to the naphthalimide (figure 23).

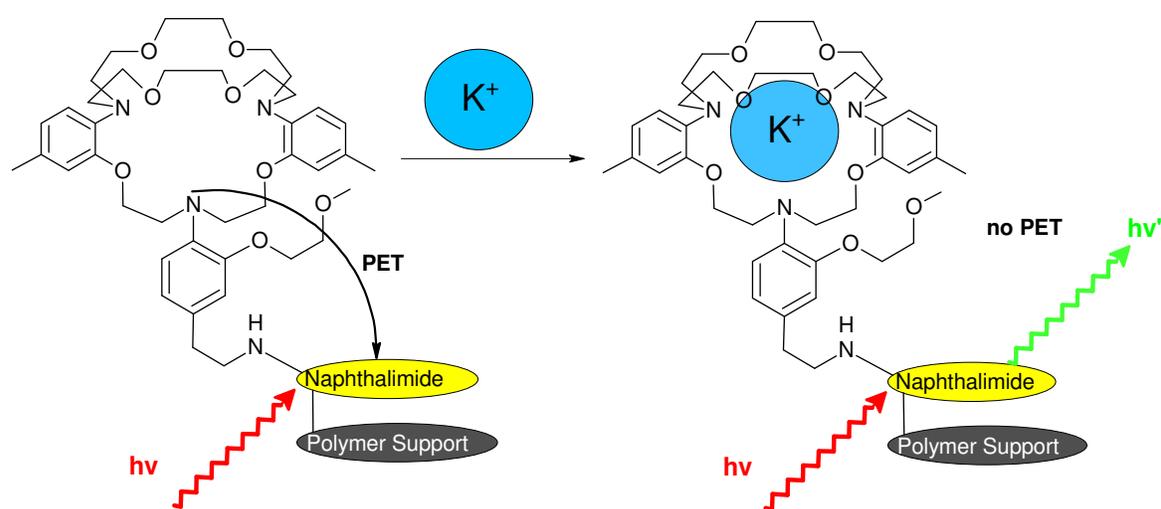


Figure 23. Scheme for the sensing mechanism of the fluorescent potassium sensor developed by He et al..⁶⁵

Upon chelation of potassium, the free electron pair from the aniline participated in the complexation of the cation and therefore, PET effect decreased significantly. The authors also attached the fluorescent sensor to a polymer support using the succinimidyl-ester approach. The same group also presented a similar sensor molecule for sodium.⁶⁶

Another interesting report was made by Guo et al.⁶⁷, who used a two-naphthamidine system towards the sensing of mercury ions (Figure 24). The binding of mercury was found to be much higher than for a wide range of other metal ions, with fluorescence increasing about 17 fold when compared to its unbound form.

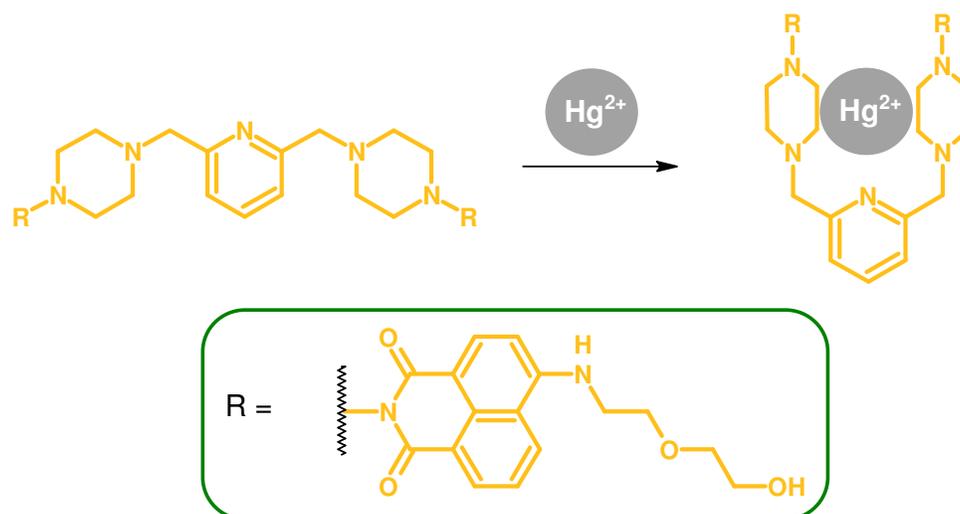


Figure 24. “Capturing” Hg^{2+} ions with the sensor from ref. 67. Upon binding of the metal, strong fluorescence enhancement is observed.

All of the previous examples showed sensors in which the target analyte was a metal cation, which can be captured with relative ease using different chelating rings. However, a significantly tougher challenge is presented when the target analyte is an anion or non-charged compound, since many of the reported sensors establish highly unspecific interactions with these analytes. Even in the case of some sensors which are denoted selective, a clear explanation for the selectivity is often not present.

In the particular case of phosphate anions, which we are primarily focusing on with our research, several approaches can be undertaken for binding of the target analyte. The following section describes different receptor functions which are currently being applied for the detection of phosphate and its known derivatives.

4.2.2. THE RECEPTOR – Different strategies for sensing of ATP and other phosphate derivatives

The design of fluorescent anion sensors has been, and still remains a challenging task even today. Nevertheless, an enormous effort is made in the direction of finding new and interesting molecules to detect anionic species, due to their relevance in biological processes at cellular level.⁶⁸

Phosphates are among the most important anions in biological systems, as they perform essential functions in living organisms. Within this class, phosphate nucleobases are highlighted due to their roles in various intracellular metabolic pathways. Adenosine-5'-triphosphate (ATP) is one of the most studied since it is responsible for the energy production and storage in living cells. The production of energy is achieved through the cleavage of one or two phosphate groups from ATP, yielding adenosine-5' diphosphate (ADP) and adenosine-5'-monophosphate (AMP), respectively. ATP may also be used in the production of other metabolic regulators such as 3'-5'-cyclic adenosine monophosphate (cAMP) (figure 25). Other derivatives such as guanosine-5'-triphosphate (GTP) and 3'-5'-cyclic guanosine monophosphate (cGMP) also perform similar functions in biological processes.

The ratio between ATP and its metabolic products dictates a great part of the cellular processes. Therefore, the continuous monitoring of ATP levels can be extremely useful for the study of multiple cellular mechanisms, including numerous enzymatic processes as well as cell apoptosis.^{69, 70, 71, 72}

Lanthanoid complexes

A common approach for the sensing of ATP and its derivatives is through the use of lanthanoid complexes. Wolfbeis and Schäferling⁷³ reported the use of a Eu(III)-tetracycline complex for sensing of nucleobase phosphates. In the presence of ATP, a strong quenching effect on the luminescence of the complex was observed. Other examples of lanthanoid metals with the same purpose are Tb (III)⁷⁴ and Yb (III).⁷⁵

Despite their advantages, namely long lifetime and large Stokes' shifts, most of the lanthanoid complexes are unspecific and therefore difficult to evaluate. Furthermore, it frequently involves fluorescence quenching, whereas an enhancement is more desirable for sensing applications.

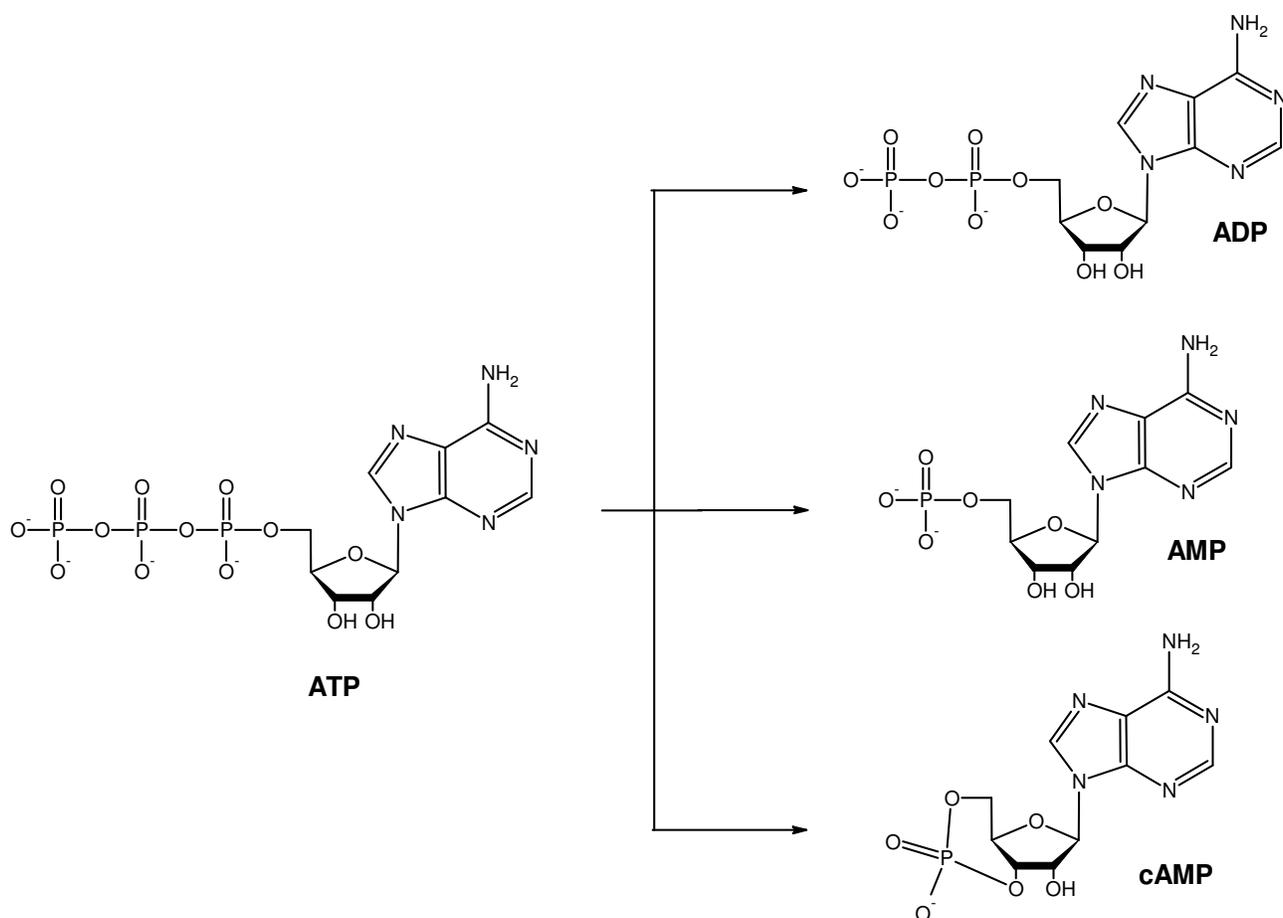


Figure 25. ATP and its metabolites.

Multi-point nitrogen-based receptors

In the previous section 4.2.1, the versatility of the naphthalimide fluorophore was highlighted. Referring to figure 21, the vast majority of naphthalimide-based sensors possess their binding (or receptor) unit in the R₂ end of the structure, since it is upon binding of an amine compound to position 4 of the naphthalimide core that optical properties are “potentiated” (namely, absorption and emission are shifted to the visible range, with a strong increase in its fluorescence quantum yield).⁷⁶

The group from Gunnlaugsson made some interesting contributions using naphthalimide-based sensors for the detection of anionic species. Most of their recent work involved the use of a di-aromatic thiourea moiety as the receptor group (figure 26).^{77, 78}

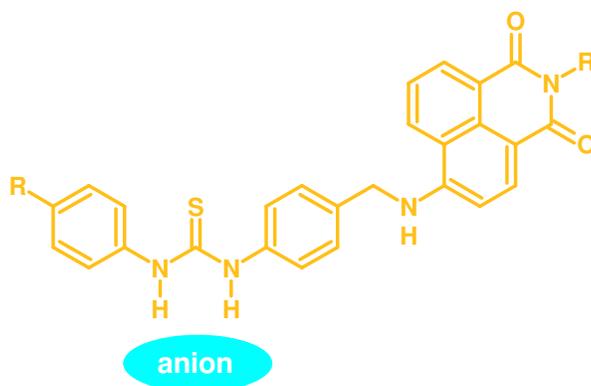


Figure 26. Anion sensing with di-aromatic thiourea receptors.^{77, 78}

The different substituents and their respective position dictated the binding strength towards different anions, namely fluoride, acetate and dihydrogen phosphate.

Fu et al.⁷⁹ used a similar approach to develop a sensor for pyrophosphate. By adding a hydrazino-guanidiniocarbonyl pyrrole instead of the usual thiourea unit, the authors were able to obtain a high selectivity towards the pyrophosphate when compared to other related anions. The sensing mechanism was based on the combination of electrostatic forces and hydrogen bonding between the receptor and the pyrophosphate, reflected in a significant increase in fluorescence emission of the naphthalimide fluorophore in aqueous buffer at pH 7.0 (figure 27).

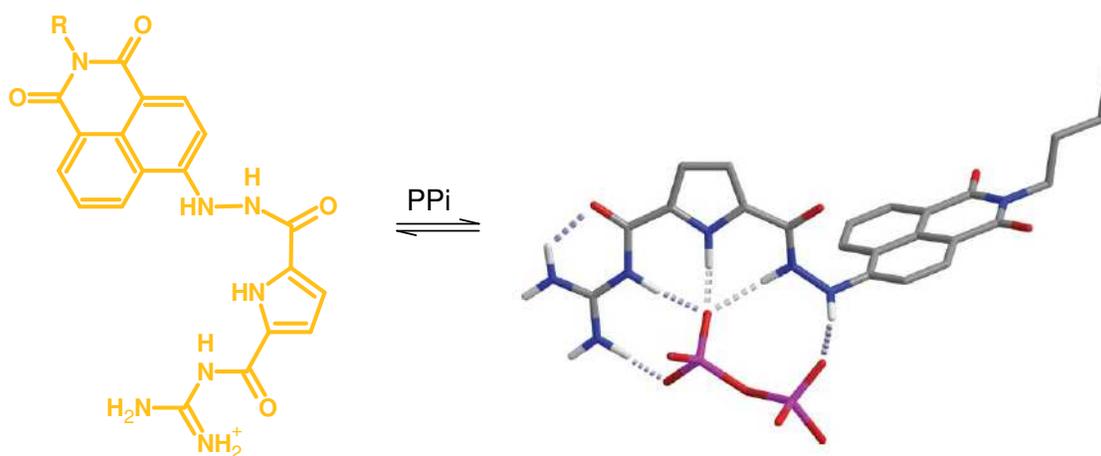


Figure 27. Interaction between pyrophosphate anion (PPi) and the naphthalimide sensor in reference 79. The picture on the right was taken directly from the same reference.

However, to the best of our knowledge, such an approach has yet to be tested towards the sensing of phosphate nucleobases.

Chelated transition-metal complexes

The use of a transition metal chelator coupled with a fluorophore is another promising approach for fluorescence-based sensing of phosphate and its derivatives. Furthermore, it frequently induces fluorescence enhancement which is more desirable in sensing than fluorescence quenching.

Kikuchi et al.⁸⁰ utilized this strategy for designing a coumarin-based chemosensor for ATP with a Cd(II)-cyclen unit as receptor (figure 28).

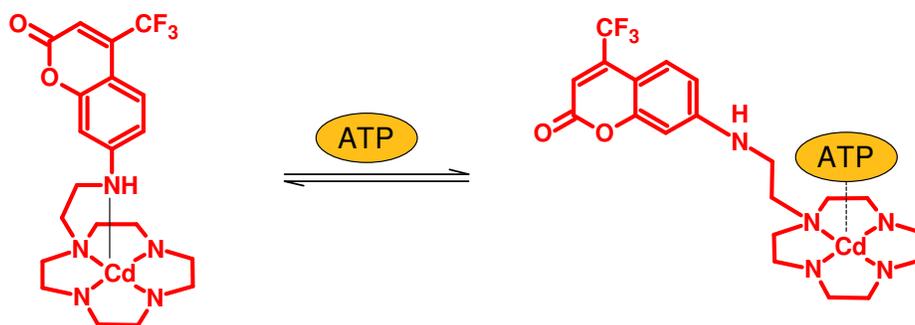


Figure 28. ATP Sensing with the coumarin-Cd(II)-cyclen system.⁸⁰

The sensor molecule exhibited a shift in its excitation maximum in the presence of ATP and other phosphate species, and was used in a fluorescence assay for monitoring phosphodiesterase 3',5'-cyclic nucleotide activity, successfully detecting the transformation of cAMP to AMP. Recently, the same authors used a similar fluorescent system for ratiometric measurement of protein kinase activity, by attaching the sensor directly onto a target peptide.⁸¹

One of the most common chelating groups for this purpose is the dipicolylamine (DPA) unit. Its structure possesses three nitrogen atoms that are used for complexation of metals, in the majority of the cases Zn (II) or Cd (II). Since only three positions of the chelating sphere are used for metal complexation, the fourth position is ideal for binding of phosphate.

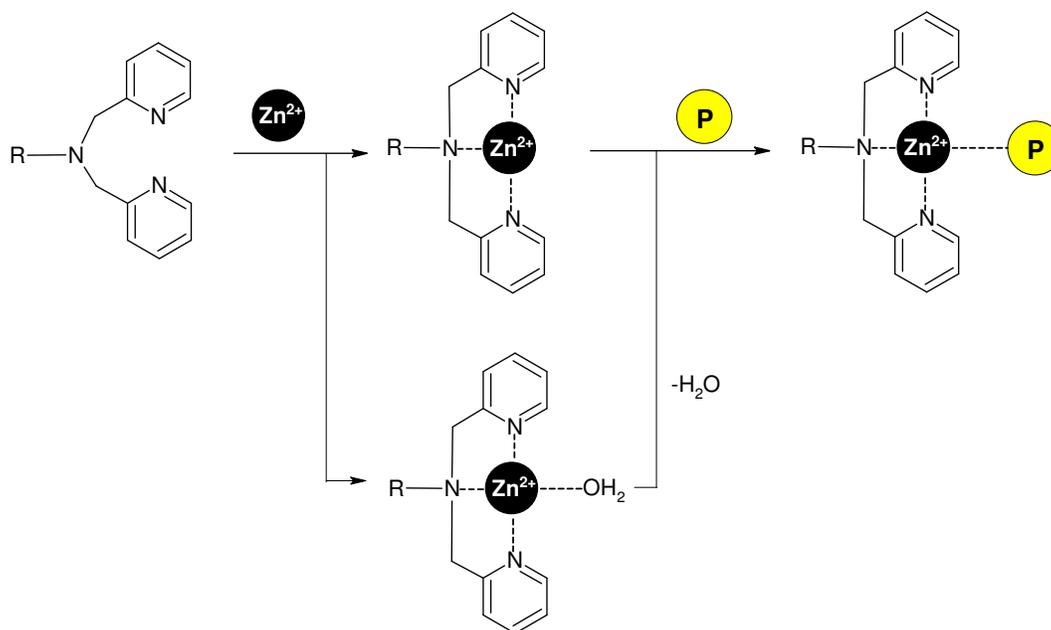


Figure 29. Stepwise binding of, first Zn^{2+} and second phosphates (P), to the DPA unit. “R” represents a fluorophore which is either directly attached, or attached via a spacer (e.g. methylene (ethylene) chains).

In some cases, this extra position can be occupied by a water molecule which is later substituted by the phosphate derivative (figure 29).

The first report of phosphate sensing based on a DPA-metal complex was made by Hamachi et al.⁸². Taking the premise that many phosphatase enzymes possess a metal centre for the binding and cleavage of phosphate groups from their substrates, the authors used a Zn (II)-DPA complex as a receptor for phosphorylated peptides, which was coupled to an anthracene fluorophore. Since then, Hamachi and co-workers have developed other structures with the same DPA-metal motif but with different fluorophores (figure 30).⁸³ In all of the chemosensor molecules presented in this figure, a methylene spacer is used between the fluorophore and the DPA receptors.

Lee et al.⁸⁴ presented a sensor for pyrophosphate (PPi) which was also based on a binuclear Zn (II)-DPA complex (figure 31). The metal also formed a coordinating bond with a phenol group of the fluorophore. In this manner, apart from the changes in the emission of the fluorophore, binding of PPi also caused changes in the absorption spectra of the chemosensor. The chemosensor was found to be quite selective, although some interaction with ATP was also observed.

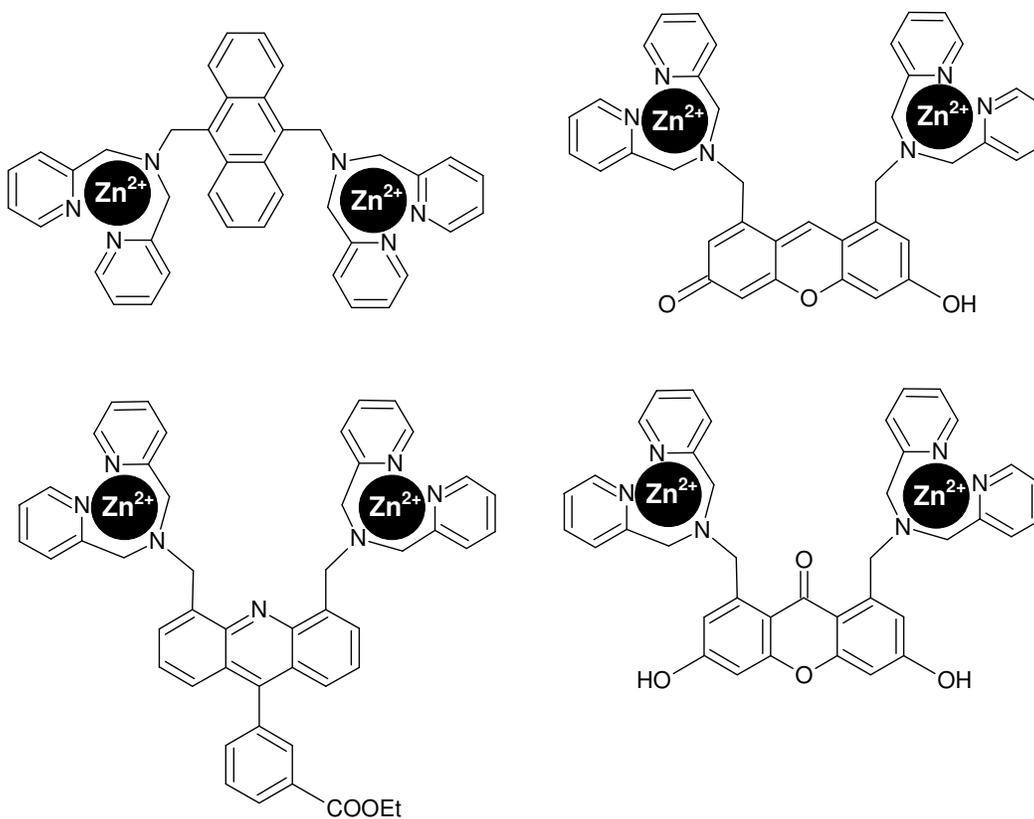


Figure 30. Chemosensors for phosphorylated peptides developed by Hamachi and co-workers.⁸³

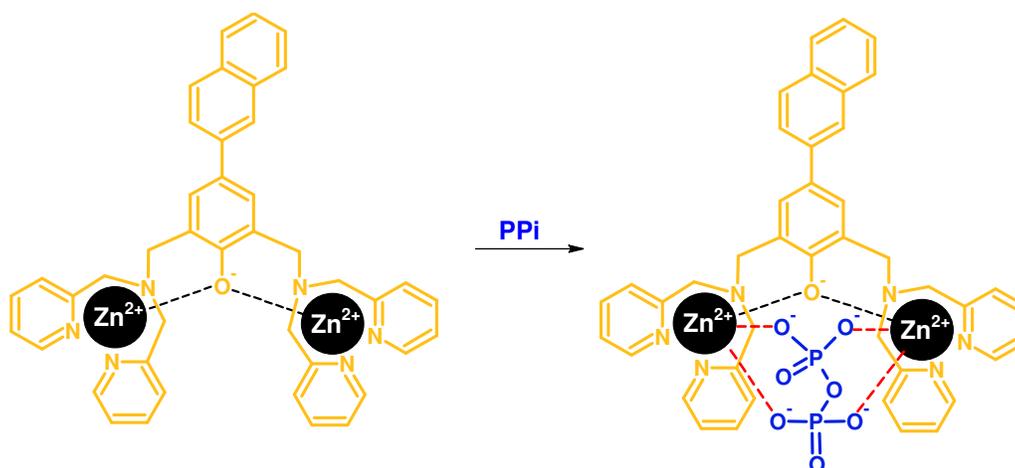


Figure 31. Proposed mechanism for the interaction of pyrophosphate (PPi) with the chemosensor reported by Lee et al.⁸⁴

Recently, Huang et al.⁸⁵ designed a dicyanomethylene-4*H*-chromene sensor dye bearing a DPA unit which is directly connected to the conjugated system of the chromophore. The single DPA group complexed with Cu (II), which translated into a strong quenching effect from the metal (figure 32). Other metals did not induce any change in the fluorescence emission of the molecule. The complexed chemosensor was then used for the detection of pyrophosphate through ICT effects yielding an increase in fluorescence, while it presented no significant interactions with other anions. However, one must stress out that, in this case, the chemosensor was not tested for closely related derivatives, namely (tri)phosphorylated nucleotides (e.g. ATP, GTP).

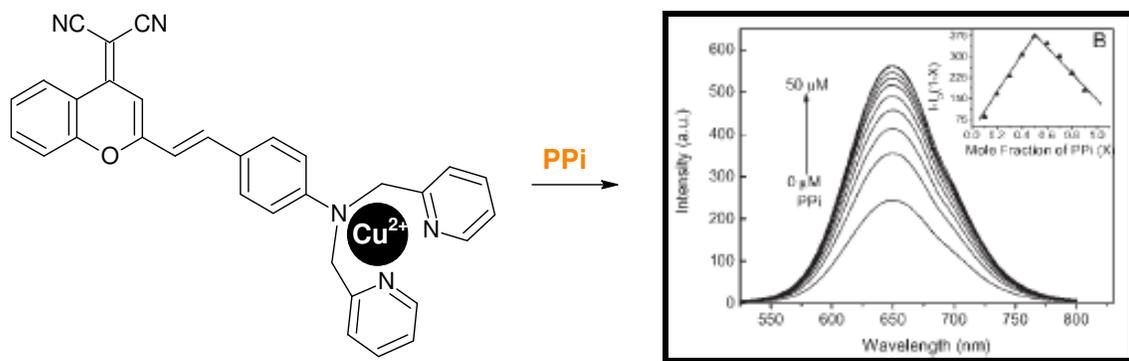


Figure 32. A dicyanomethylene-4*H*-chromene-DPA-Cu (II) complex for pyrophosphate detection. The figure of the spectra was taken directly from reference 85.

Although non-fluorescent, an interesting and very simple chemosensor was reported by Jose et al.⁸⁶. The molecule is based on a donor-acceptor azo-dye chromophore and possesses a Zn (II)-DPA group at the terminus of the conjugated system. The receptor bound selectively to ATP and CTP with a change in color visible to the naked eye. The same dye was successfully used as a staining agent of bacteria and yeast cells, and the cellular growth was measured with time through the difference in absorbance which indicated the quantity of ATP present in the biological sample.⁸⁷

Despite all the progress demonstrated by the above cited examples, there remains still a significant challenge regarding the selective sensing of phosphate anions and derivatives. Nevertheless, the most promising developments have been reported only recently and therefore, these new paths must still be explored in more detail.

4.3. Strategy and synthetic pathway of a fluorescent chemosensor for ATP

Given the reported examples of receptor functions in phosphate sensing, we decided to focus our efforts towards developing a sensor molecule based on the naphthalimide fluorophore. The final chemosensor should be capable of, on one side (**R**₁ in figure 21), covalent attachment to functionalized surfaces using NHS-ester activation of a carboxylic acid function, and on the other side (**R**₂ in figure 21), to append a chelating unit to enable phosphate sensing through changes in the fluorescence emission of the fluorophore.

The synthetic strategy involved a converging synthesis, meaning that the naphthalimide core would be bound stepwise to **R**₁ and **R**₂, performing the complexation with a transition-metal in the last step.

The synthetic pathway led us to start from commercially available 4-bromonaphthalic anhydride. The first reaction step consisted of the introduction of 6-aminohexanoic acid as the **R**₁ group. The mechanism of the reaction is fully described in figure 33.

The nucleophilic attack of the primary amine from 6-aminohexanoic acid is favoured due to the electrophilic nature of the anhydride. Sequential rearrangement of the intermediate species leads to the expulsion of one water molecule, yielding structure **3**. The characterization of product was performed through mass spectrometry and NMR spectroscopy, revealing the desired structure.

At this point, we had to choose which receptor group would be suitable for our purposes, i.e. detection of phosphates. Our initial approach was to use the cyclen group, in analogy to the work reported by Kikuchi *et al.*⁶³. As was done in this reference, a cyclen unit with a spacer had to be synthesized and coupled with the naphthalimide derivative **3**. The cyclen ring would then be complexed with a transition metal to bind phosphate derivatives.

The synthesis of the cyclen receptor group was planned in four steps. The strategy is presented in figure 34.

The first step consisted on the protection of three of the amine functions with di-*tert*-butyl dicarbonate (di-Boc), which was achieved in relatively good yield. The second step was the addition of the spacer, through nucleophilic attack of the free amine group in **4** to the electrophilic centre in 2-bromoacetonitrile. The last step would be the reduction of the nitrile group using nickel (II) boride (supplied by Dr. Martin Schulz, Institut für Anorganische

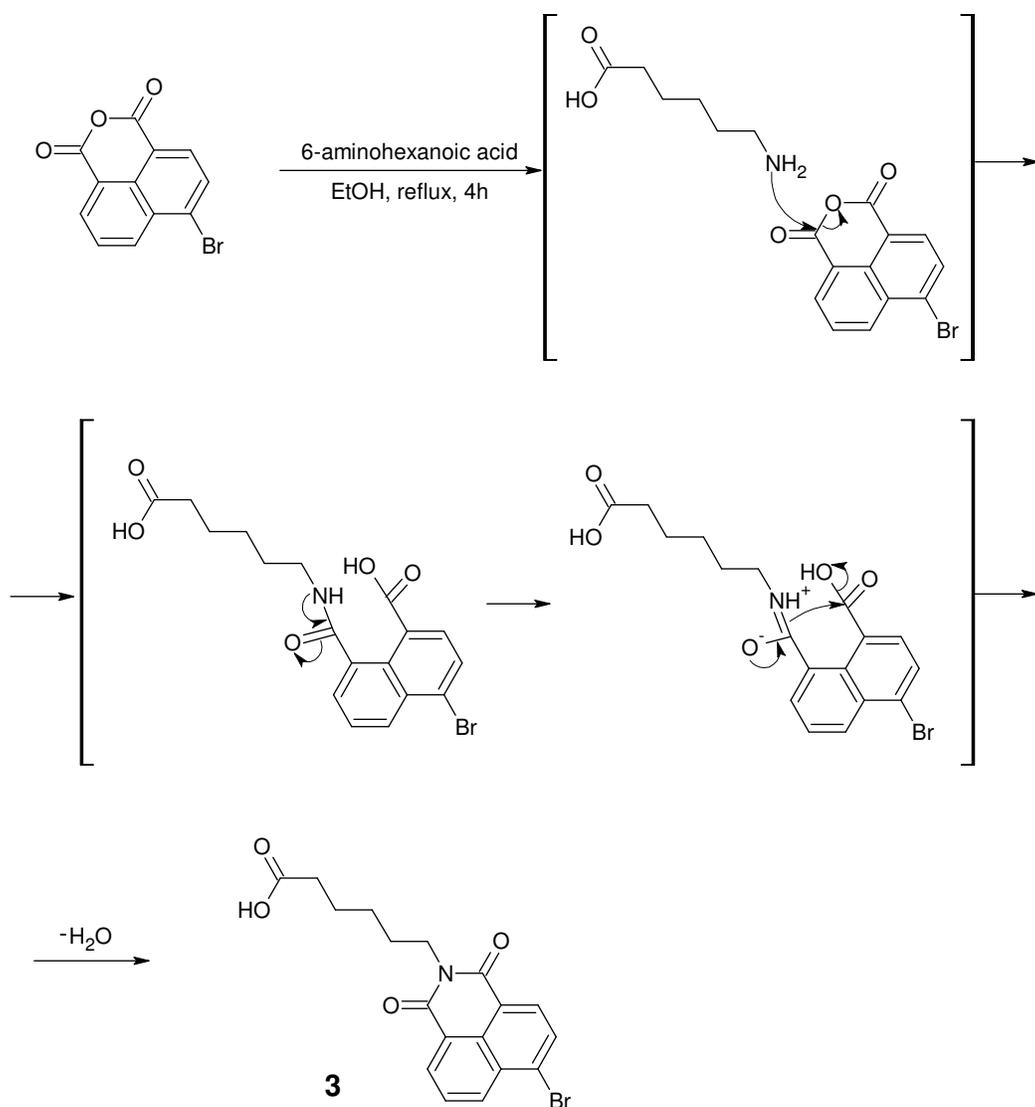


Figure 33. Mechanism for the reaction between naphthalic anhydride and 6-aminohexanoic acid to yield **3** as the final product. Between brackets are shown the intermediate species of the reaction.

Chemie, FSU Jena) and sodium borohydride (to help regenerate the Ni (II) boride) to afford the final desired primary amine.^{88, 89} However, instead the desired product, a side-product consisting on the loss of the cyanide group from the initial compound **5** was observed through MS and NMR characterization (absence of the peak from cyanide carbon at 114.4, which was present in the ¹³C NMR of **5**). An explanation to this fact can be that the hydride anions present in the reaction simply acted as nucleophiles, with consequent exit of the cyanide group.

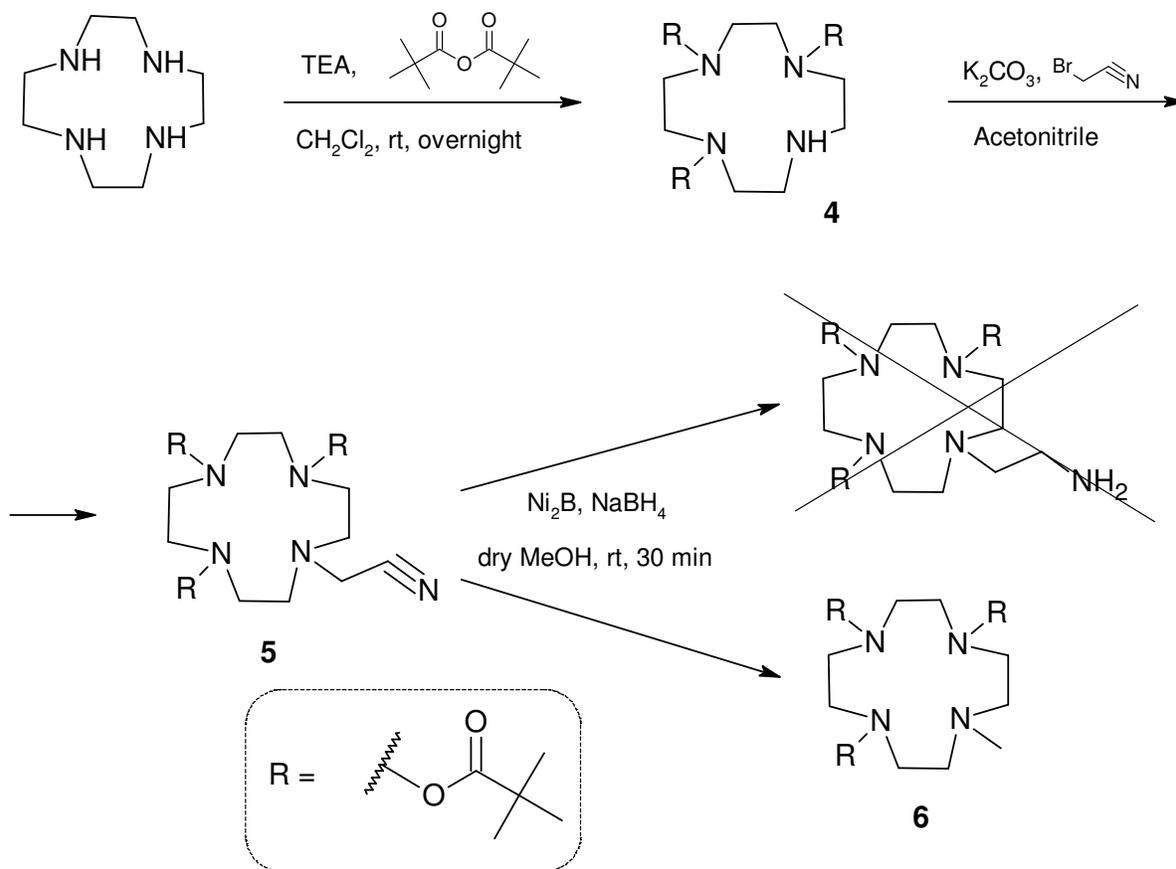


Figure 34. Synthetic pathway for the cyclen receptor unit. The final reaction yielded an undesired side-product with structure **6**.

At this point and due to the difficulties in the last step, the idea of using the DPA unit as a receptor was adopted.

The initial strategy was to couple the actual DPA directly in position 4 of the aromatic ring from the previously synthesized naphthalimide derivative **3**, since DPA as a pure compound is commercially available. However, the reaction, which involved nucleophilic aromatic substitution of the bromine with the DPA, did not occur. This fact can be explained by two effects: first, the DPA possesses a secondary amine connected to two aromatic rings, conferring it a less nucleophilic character; secondly, the two pyridine rings can cause sterical hindrance due to the proximity with the volumous naphthalimide group. Therefore, a different approach had to be evaluated.

The new path was to use an ethylene chain as a spacer between the DPA receptor and the naphthalimide fluorophore. Thus, the receptor and the spacer were synthesized separately.

Based on the work reported by Nagano⁹⁰ (except for the second step, which was adapted from other work⁹¹), who used a DPA with an ethylene spacer coupled with a Near-Infrared (NIR) cyanine dye for Zn²⁺ ion detection, the same unit was synthesized to be coupled with our naphthalimide structure **3**. The synthetic route of this receptor is shown in figure 35.

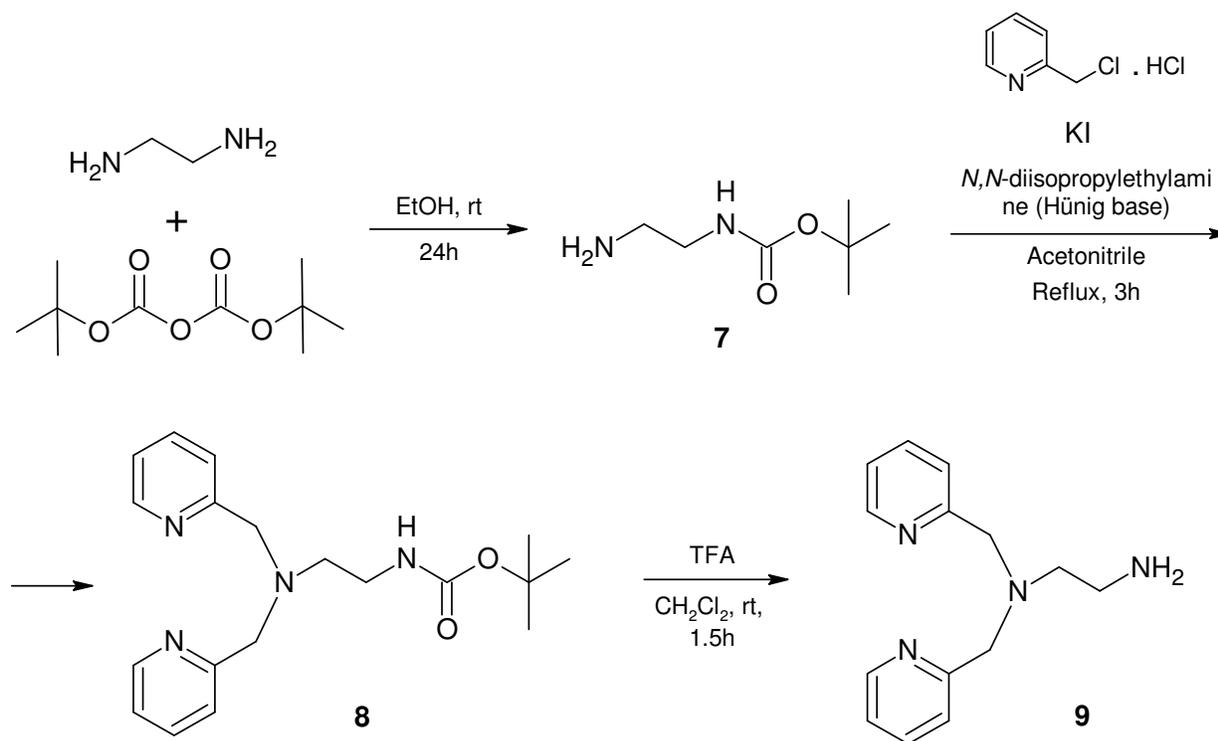


Figure 35. Synthesis of the receptor, a DPA unit with an ethylene spacer (structure **9**).

The synthesis of the receptor unit started from ethylenediamine. The first step consisted on the protection of one of the amines in the molecule through reaction with di-Boc, originating intermediate **7**. The second step was the “attachment” of two methylpyridine groups to the unprotected amine, via a S_N2 mechanism (compound **8**). The final step was the removal of the Boc protective group to yield compound **9**.

At this point, the synthesis of the chemosensor converged. The receptor **9** was connected to compound **3**, through aromatic nucleophilic substitution of the bromine (Figure 36). This mechanism is facilitated by the electron withdrawing nature of the naphthalimide ring which is able to stabilize negative charges through multiple resonance structures. The product **10** was characterized through MS and NMR.

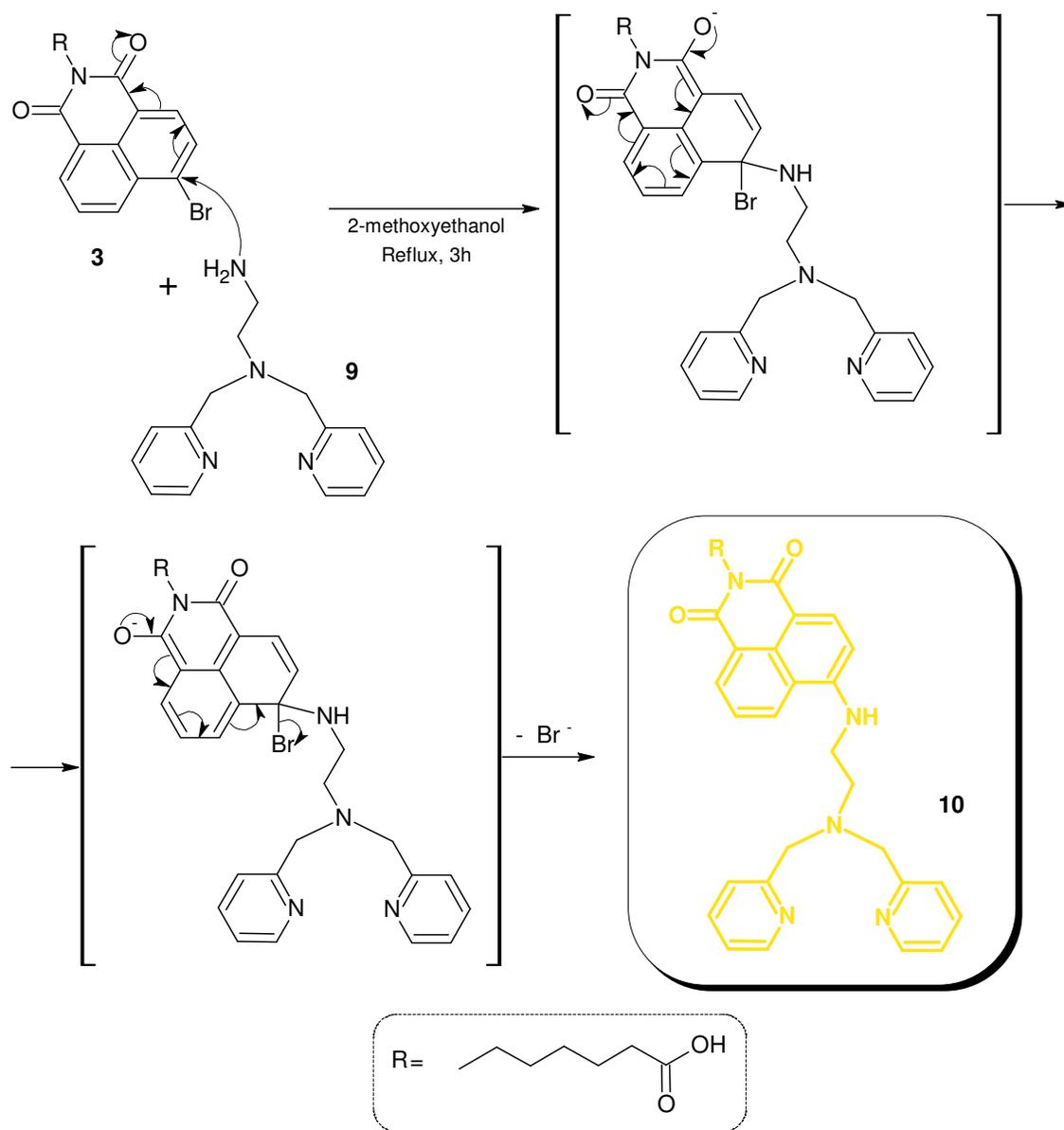


Figure 36. Converging step of the synthesis of chemosensor **10**: “joining” the fluorophore (compound **3**) and the receptor group (compound **9**).

Once structure **10** was obtained, our intention was to assess which transition metal would be the most suitable for complex formation with the DPA moiety and which one would be the best to bind phosphate species. Therefore, a thorough study was performed with **10** and a wide range of metal ions, using both absorption and fluorescence spectroscopy.

4.4. Spectroscopic characterization of **10**

4.4.1. General studies on the fluorescence of **10** – Influence of concentration and pH

Although chemosensor **10** showed some solubility in water, a far better solubility was obtained in methanol. Thus, in all absorption and fluorescence measurements (except when denoted otherwise), solutions of **10** in methanol were used and mixed with aqueous solutions of HEPES buffer 0.1M (HEPES - 2-(4-(2-Hydroxyethyl)-1-piperazine)ethanesulfonic acid sodium salt) with the pH adjusted to 7.4. Using a pH-meter, it was possible to assess that the used amount of methanolic solutions (less than 2% of the total volume inside the quartz cuvette) did not affect the final pH of the measured solution mixture.

In order to determine which would be the best concentration of chemosensor **10** to use in the measurements, the concentration-dependent fluorescence was evaluated. Two solutions of **10** with different concentrations ($[\mathbf{10-A}] = 3 \times 10^{-4}$ M and $[\mathbf{10-B}] = 3 \times 10^{-3}$ M) in methanol were prepared. These solutions were successively added to a cuvette containing solely HEPES buffer (0.1 M, pH 7.4) and after each addition, the fluorescence spectrum was acquired. The total volume of added methanolic solutions in this particular experiment reached 3.1% (pH was controlled and did not change during the measurements). The concentration of **10** in the cuvette ranged from 0.5 to 50 μ M. The results for this experiment are shown in figure 37.

As can be seen, a linear response can only be obtained at highly diluted concentrations (see Inset on figure 37b). At concentrations higher than 10 μ M, the response is affected since the chemosensor molecules start to interact and quench each other due to aggregation within the bulk of the solution. With these results in mind, we set a concentration of 5 μ M as the standard for all the following measurements.

Another important aspect for the characterization of chemosensor **10** is to determine whether or not its fluorescence properties are pH dependant since ultimately, the goal is to be able to use **10** under physiological conditions. As such, the fluorescence emission of **10** was measured at different pH values in 0.067M phosphate buffer (the preparation of buffers is described in the experimental section). These results are presented in figure 38. The experimental values were fitted to a sigmoidal function using the program *Origin 8.0*[®], yielding a pKa of 5.8 for chemosensor **10**.

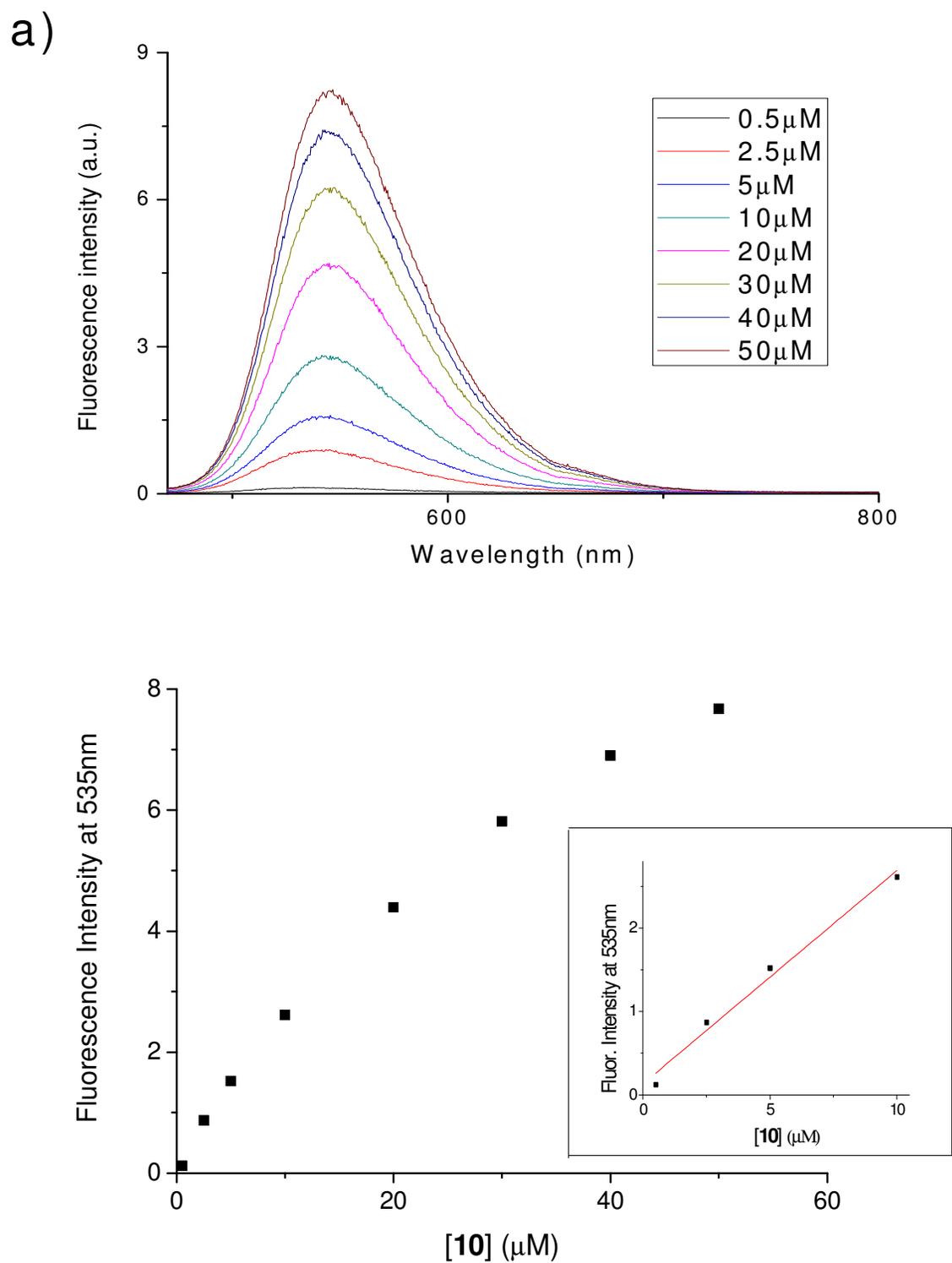


Figure 37. Influence of the concentration in the fluorescence intensity of **10**. a) collected fluorescence emission spectra at different **10** concentrations ($\lambda_{\text{exc}} = 450 \text{ nm}$); b) tendency plot of the fluorescence intensity maxima (535nm) of **10** at different concentrations. Inset: zoom on the range from 0.5 to 10 μM , with respective linear regression ($R^2 = 0.9789$).

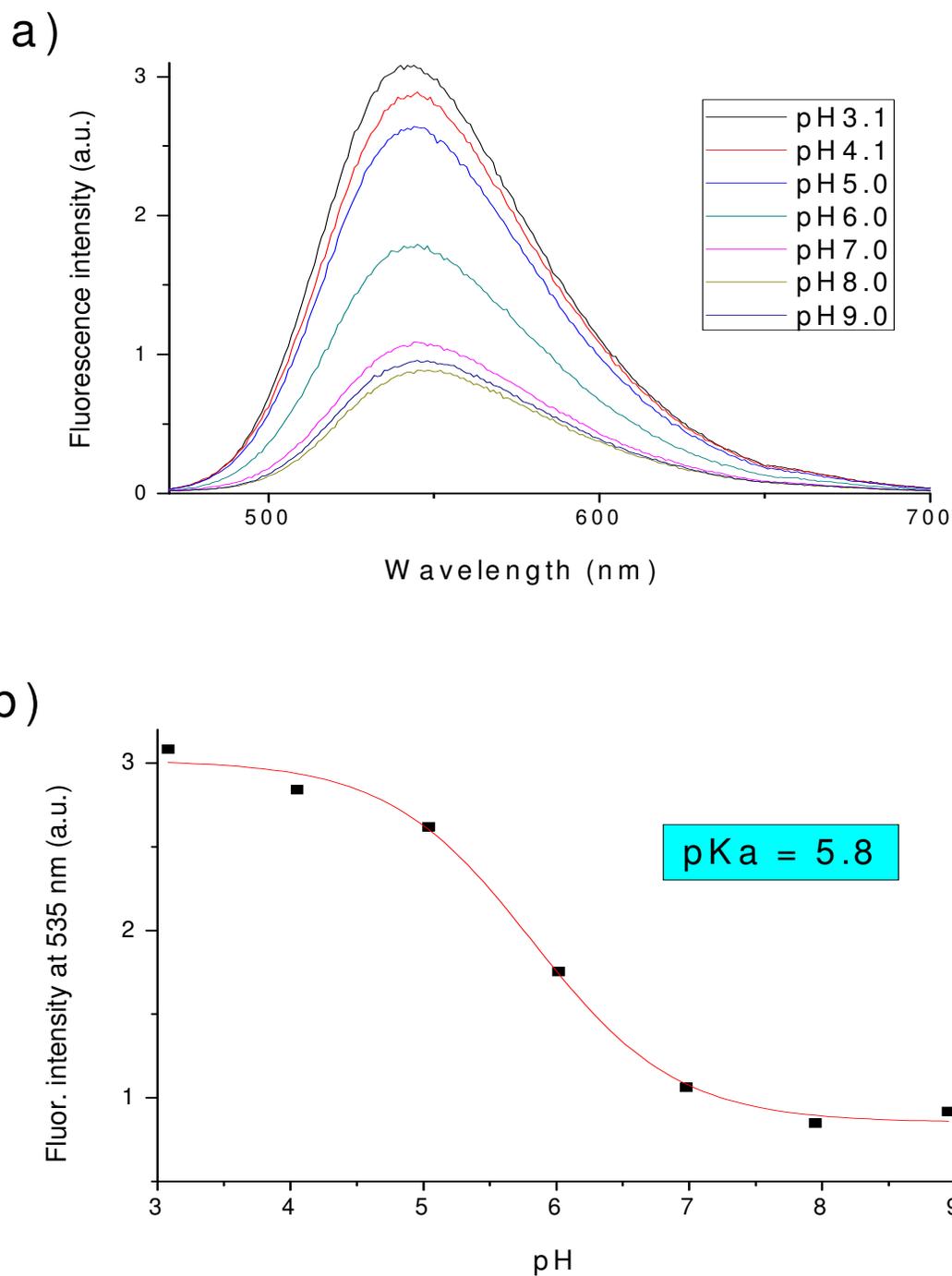


Figure 38. Influence of pH in the fluorescence emission of chemosensor **10**. a) collected fluorescence emission spectra at different pH ($\lambda_{\text{exc}} = 450 \text{ nm}$); b) plot of the fluorescence intensity maxima (535nm) of **10** at different pH. From the sigmoidal fit (red line) to the experimental points, a pKa value of 5.8 was obtained.

It was observed that, at pH values above 5, the fluorescence emission of **10** is strongly decreased. This is a consequence of the deprotonation of the tertiary amine from the DPA group. Upon deprotonation, the lone pair of electrons from the tertiary amine is “free” to perform PET to the fluorophore, quenching its emission. At higher pH values, the lone pair of electrons from the tertiary amine is used for binding a proton and the *n*-orbital is stabilized. Therefore, no PET is observed (these effects are analogous to the ones highlighted in figure 22, section 4.2.1).

The results indicate that, for binding of metal ions, the pH of the medium has to be above 6 for the tertiary amine to act as a coordinating ligand to the metal ion. Therefore, we can assume that the chemosensor is suitable to work under physiological conditions (pH between 6.8 - 7.4). For that reason, all following measurements were performed at a pH of 7.4.

4.4.2. Complexation of **10** with metal cations

As was previously pointed out, DPA forms complexes with various metal cations, forming three coordination bonds with the aromatic nitrogen atoms from the two pyridine rings as well as with the remaining aliphatic nitrogen.

The most commonly referred metals to complex with DPA are Zn (II), Cd (II) and Cu (II). Nevertheless, other metals were also studied since the objective was to observe how the different metals affect the optical properties of the naphthalimide fluorophore. With this in mind we decided to study also Ni (II) and Co (II), apart from the three previously mentioned metal ions.

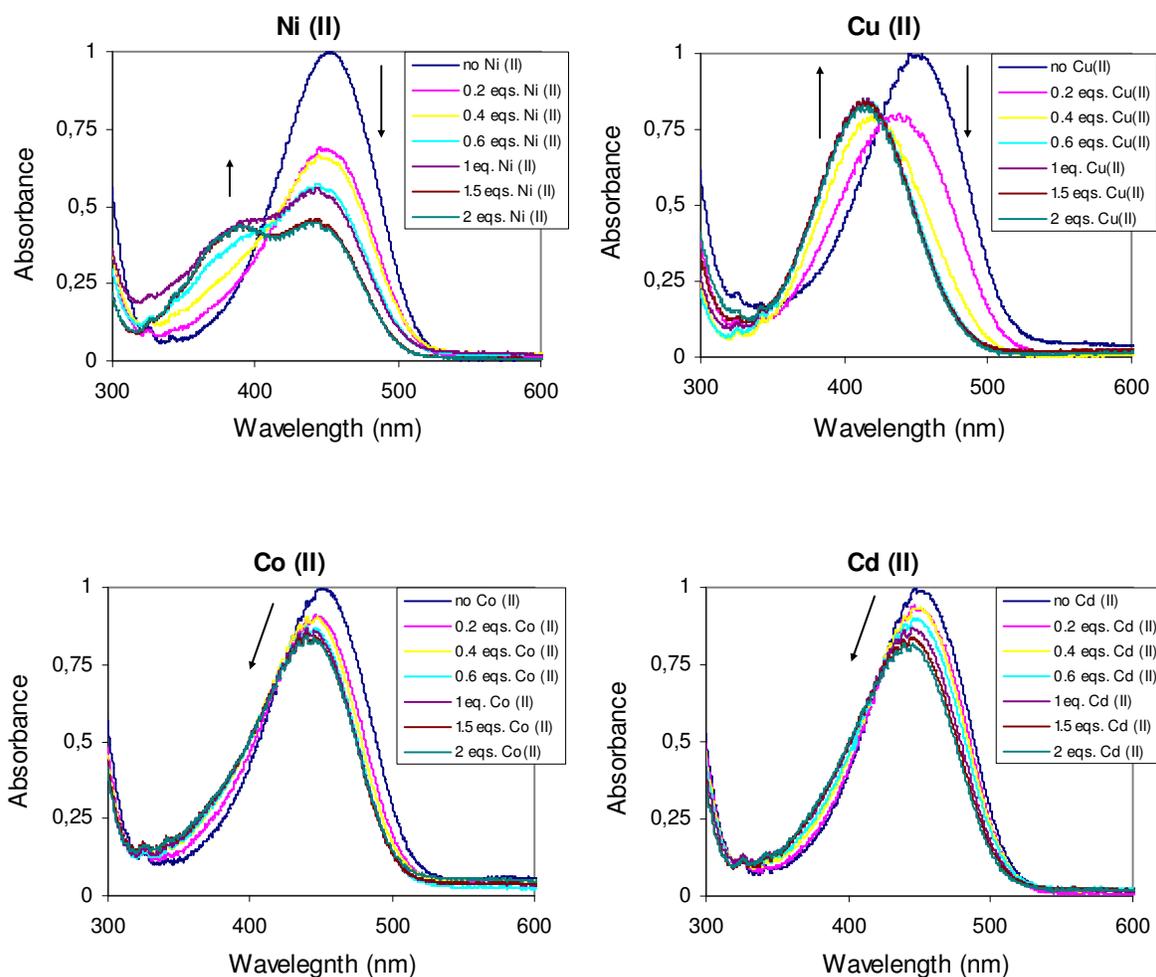
The spectroscopic studies were performed in the following manner: an small aliquot (50 μ L) from a solution of **10** in methanol was added to a cuvette containing HEPES buffer (2950 μ L) at a 0.1M concentration with pH adjusted to 7.4. Then, small amounts of an aqueous solution of the metal were progressively added until the metal was twice the quantity of **10**, to ensure the full complexation of the DPA. The added amounts of volume were small enough to have no relevant effect on the final concentration of both the chemosensor and the metal, with no changes being observed on the pH of the solution.

The results for these studies are described in the next sections.

Absorption studies

The following graphs (figure 39) represent the changes in the absorption spectra resulting from the complexation of **10** with the five different metals.

Since the aliphatic amine from the DPA group is not directly connected to the fluorophore, one could assume that no changes in the absorption spectra upon complexation with a metal are to be expected. However, and according to the findings of Nagano⁹⁰, the presence of another nitrogen directly adjacent to the aromatic naphthalimide may induce an additional coordination bond to the metal. This effect would result in a blue shift of the absorbance maximum from the fluorophore, since the donating strength from the free electron pair of the aforementioned nitrogen to the aromatic π -system is decreased.



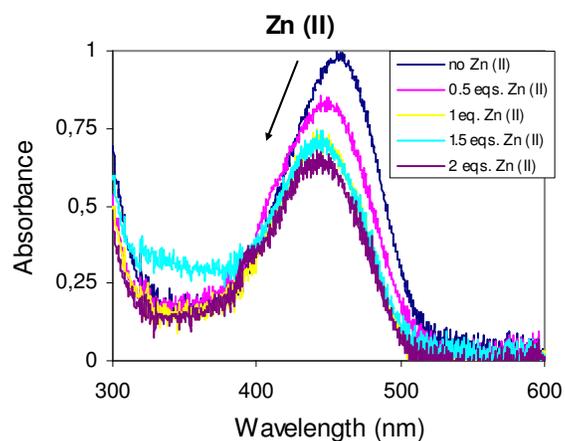


Figure 39. Absorption spectra from the complexation of **10** with different metal ions in HEPES buffer 0.1M at pH 7.4. The arrows indicate the shift of the spectra upon addition of metal to the sample solution. All graphs are normalized for better comparison.

The recorded absorption spectra present two different patterns. In the cases of Co (II), Cd (II) and Zn (II), the absorption band corresponding to pure **10** shows a slight blue shift, with a decrease in the intensity of the signal. In the cases of Ni (II) and Cu (II), the expected blue shift is stronger, leading even to a clear isosbestic point in the latter metal complex. These results demonstrate that the complexation of **10** involves a coordinating bond from the aromatic nitrogen of the fluorophore (figure 40). This fact is in accordance with the previous explanation (see beginning of this section).

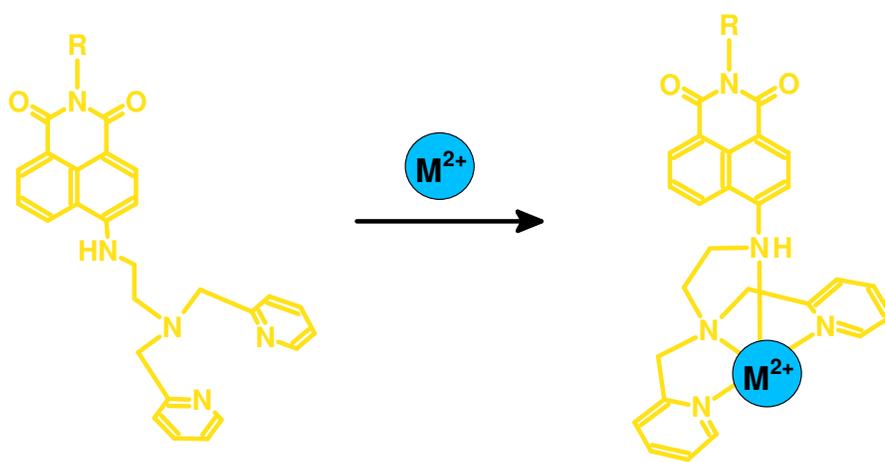


Figure 40. Mechanism for the complexation of bivalent metal ions with **10**.

Fluorescence studies

Simultaneously, a fluorescence study was also performed under similar conditions (i.e. same concentration of **10** and metal in the same buffer solution). The results are shown in figure 41.

The effects induced by the metals in the fluorescence emission of **10** can be separated into two groups: for Co (II), Cu (II) and Ni (II), a clear quenching of fluorescence is observed; for Cd (II) and Zn (II), the fluorescence intensity of **10** is significantly enhanced, accompanied by a slight red shift (around 10 nm) of the fluorescence maximum in the case of Zn (II).

The quenching in fluorescence of the fluorophore observed in the cases of Co (II), Cu (II) and Ni (II) is common due to their free *d* orbitals which can contribute extensively to non-radiative relaxation processes through electron transfer, especially in the case of Cu (II).⁸⁰

For the cases of Zn (II) and Cd (II), the formation of a coordinating bond to the metal through the lone pair of electrons from the aliphatic nitrogen atom of the DPA group strongly decreases PET, in analogy to what was said previously for protonation of the same tertiary amine (see section 4.3.1). It is quite often that fluorescence sensing of these metals is processed through strong fluorescence enhancement, particularly in reports where DPA is used as the receptor function for complexation.^{90, 91, 92} In many of these reports, Cd (II) acts as an interferent for Zn (II) sensing, though its fluorescence enhancement effect occurs to a lesser extent when compared to Zn (II). This is, in fact, what is observed in our study of **10**.

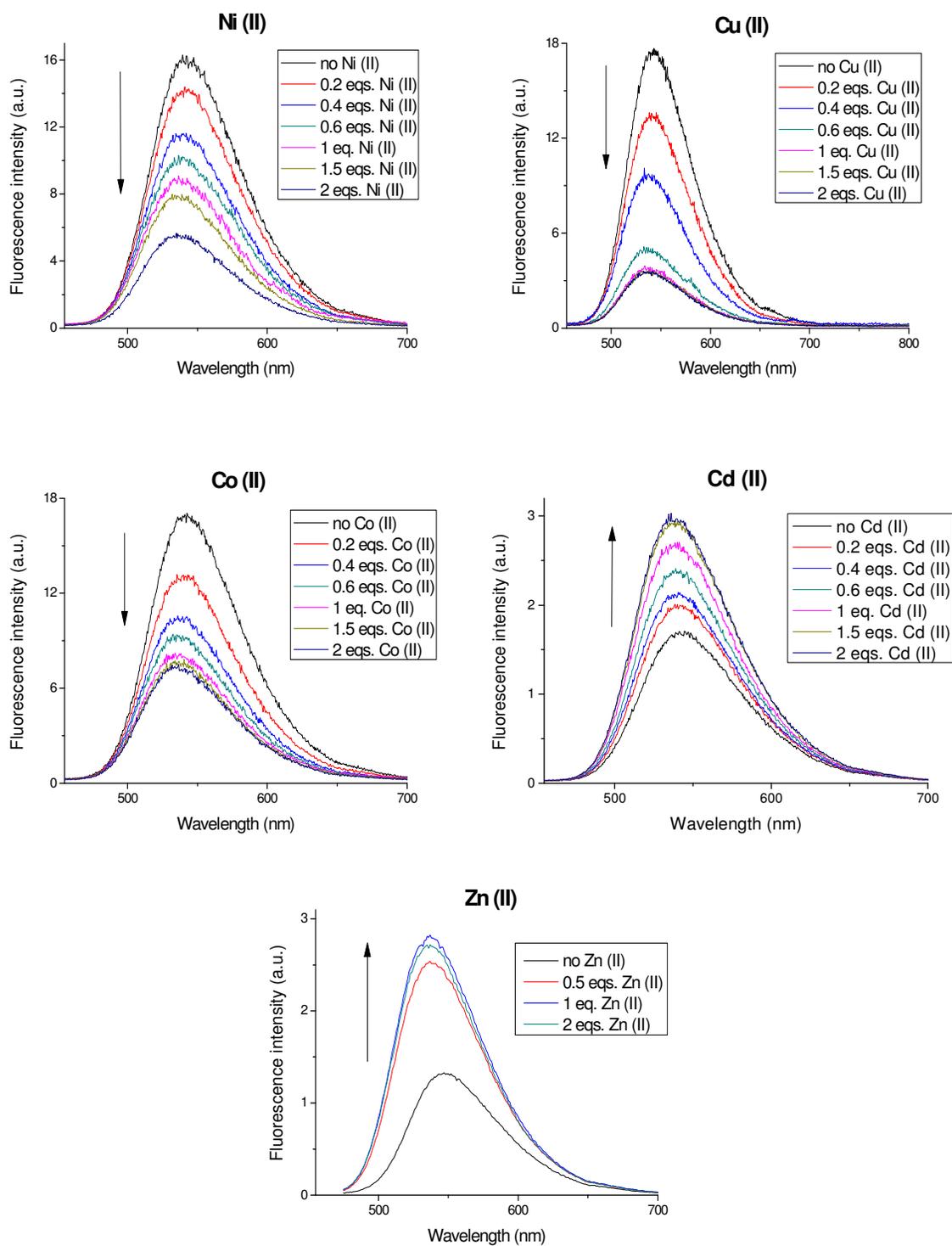


Figure 41. Fluorescence spectra corresponding to the complexation of the different metals with **10** in HEPES buffer 0.1 M at pH 7.4 ($\lambda_{exc} = 450$ nm).

4.4.3. Evaluation of [10-Metal] complexes for sensing ATP

As denoted previously (see section 4.2.2), the use of chelated metal complexes which are coupled to fluorophore systems is one of the most promising approaches for sensing of ATP and other phosphate derivatives. Given that the results presented above (section 4.4.2) show evidence for complexation of the metal ions, the behaviour of these complexes was studied in the presence of ATP through absorption and fluorescence spectroscopy, in order to assess their possible use as optical sensors for ATP detection. The complexes were generated in solution to which was added an aliquot of a freshly prepared ATP solution (as a continuation of the experiments in section 4.4.2), being the final ATP concentration inside the cuvette equal to 10 μM (i.e. two equivalents) in all cases.

Absorption studies

The absorption spectra resulting from ATP addition to a buffered solution of **10** complexed with each of the five studied metal ions are shown below in figure 43. For all cases, although not all to the same extent, a red shift of the absorbance maximum is observed. This indicates the ATP binding to the metal centre induces a weakening or a complete break of the coordinating bond to the aromatic nitrogen atom in position 4, as opposed to the previously observed blue shift upon metal complexation to the DPA unit (figure 42). As a matter of fact, the spectra reflect a total or partial return to structure **10** when unbound to the aromatic nitrogen of the naphthalimide.

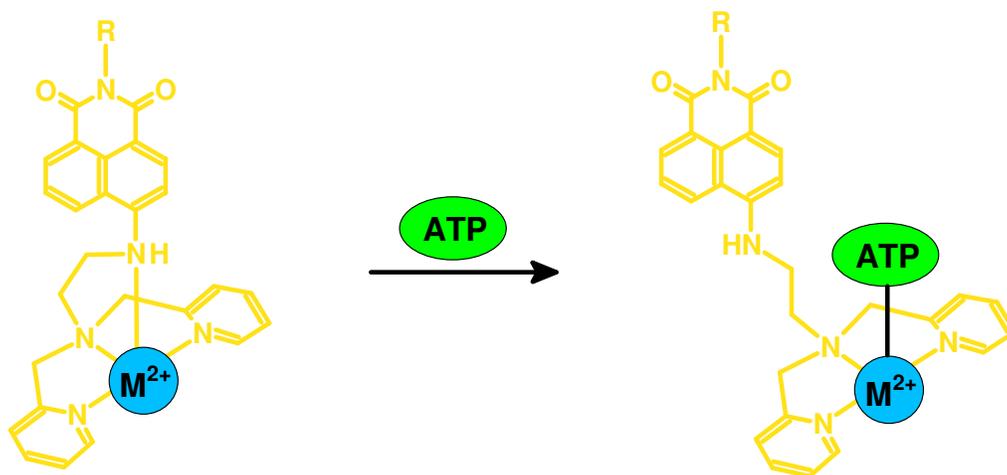


Figure 42. Schematic representation of ATP binding to [10-Metal] complexes.

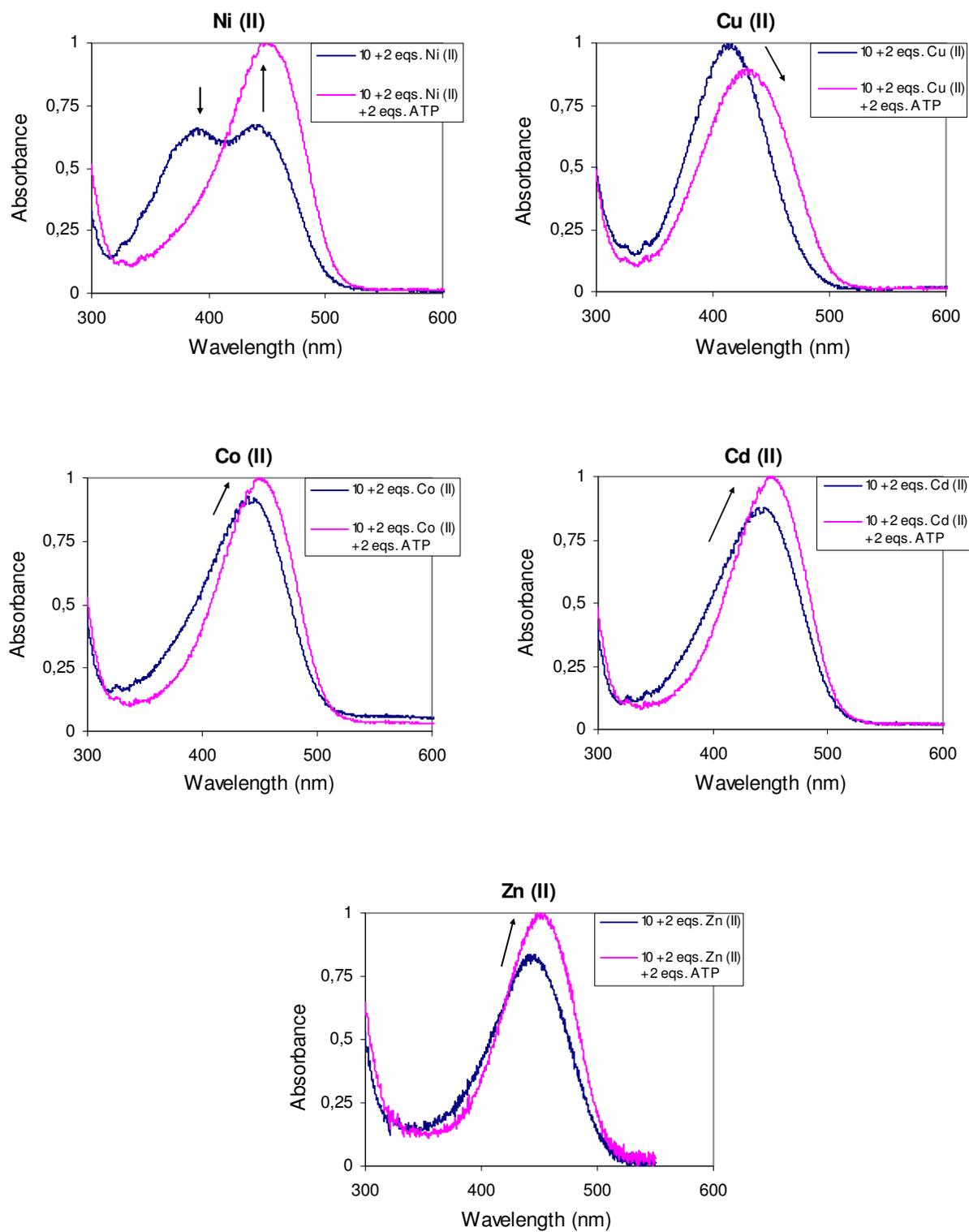


Figure 43. Spectral changes after the addition of ATP to solutions of **10** complexed with different metal ions.

Fluorescence studies

Simultaneously, fluorescence emission studies were also performed under the same conditions as the absorbance measurements. These spectra are presented in figure 44.

Analysing the spectra, it is clear to see that only the Cd (II) and Zn (II) complexes of **10** present significant changes in fluorescence upon addition of ATP. In the other cases, no changes in fluorescence were observed, probably due to the aforementioned quenching effect of the metal towards the naphthalimide fluorophore. Apart from that, one must point out that the fluorescence emission enhancement is significantly stronger (around 2-fold) in the case of Zn (II) than with Cd (II).

Therefore, and in conclusion to this preliminary study with different metal ions, we can say that the best metal complex to use for ATP sensing was found to be **10.Zn**. Further investigations using this complex were carried out to fully characterize this newly discovered fluorescent sensor.

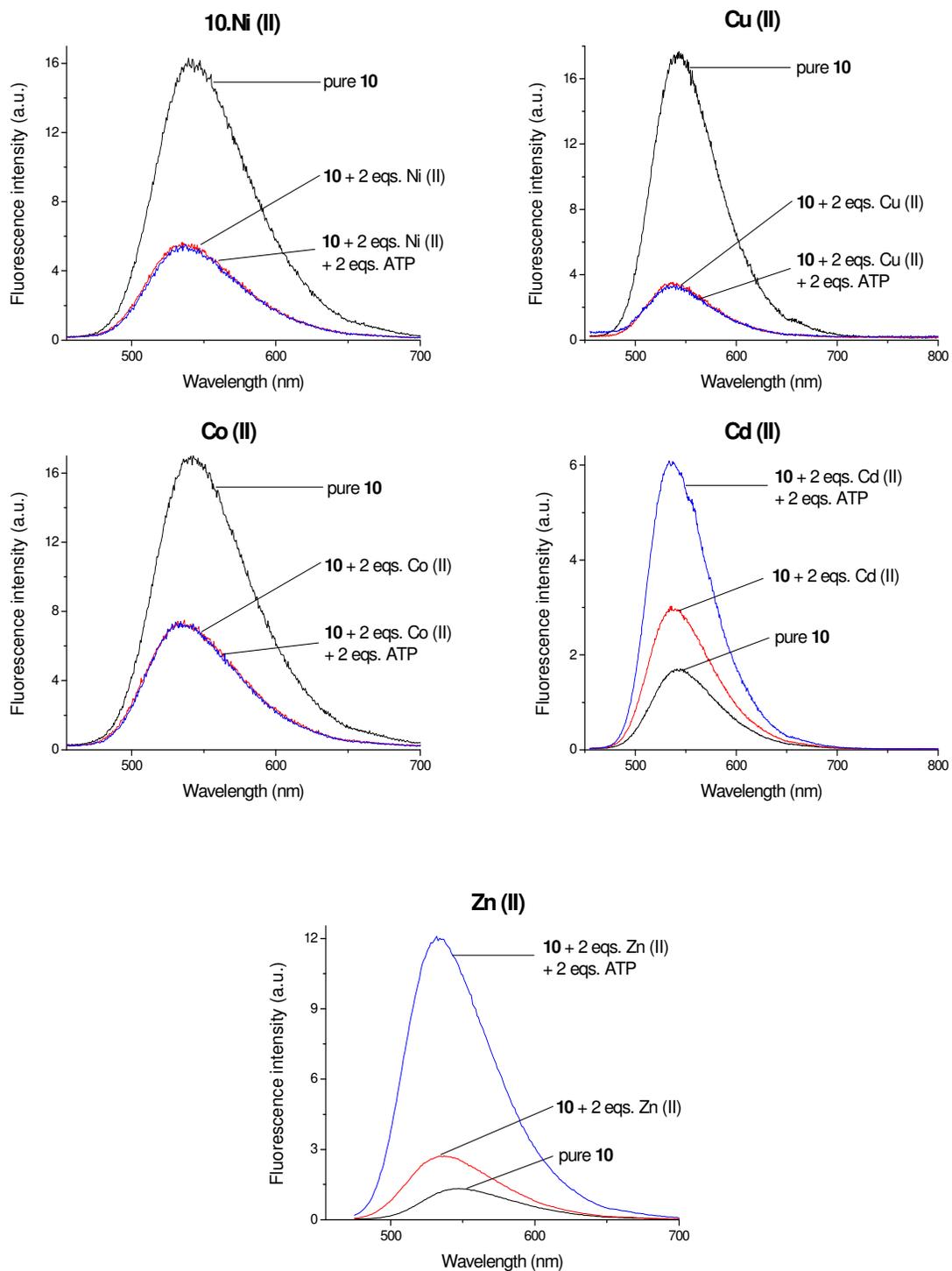


Figure 44. Spectral changes after the addition of ATP to solutions of **10** complexed with different metal ions ($\lambda_{\text{exc}} = 450 \text{ nm}$). For comparison purposes, the spectra corresponding to pure **10** for each case are also shown.

4.5. Complex **10.Zn** – a fluorescent sensor for ATP

4.5.1. Evaluation of **10.Zn** as an ATP chemosensor

Taking into consideration the preliminary results shown for fluorescence sensing of ATP using **10.Zn**, it was essential to confirm the existence of **10.Zn** as an individual structure. To obtain the isolated complex, **10** (1.65 mg) was dissolved in methanol (10 mL) with two equivalents of $\text{Zn}(\text{ClO}_4)_2 \cdot 6\text{H}_2\text{O}$ (2.2 mg) and the mixture was stirred at room temperature overnight. A small aliquot (1 mL) from this solution was evaporated and analysed through mass spectrometry as seen below (figure 46).

Analysing the obtained mass spectrum, it is noteworthy that the molecular ion corresponds to the only significant signal. The isotope pattern confirms the presence of the several zinc isotopes, confirming the structure of complex **10.Zn**.

The remaining solution (“mother” solution) was used for all the subsequent measurements. The spectra resulting from the successive addition of ATP (up to a final concentration of 100 μM) to a solution of **10.Zn** (50 μL of the “mother” solution – $[\mathbf{10.Zn}]_{\text{final}} = 5 \mu\text{M}$) in HEPES buffer are presented in figure 45.

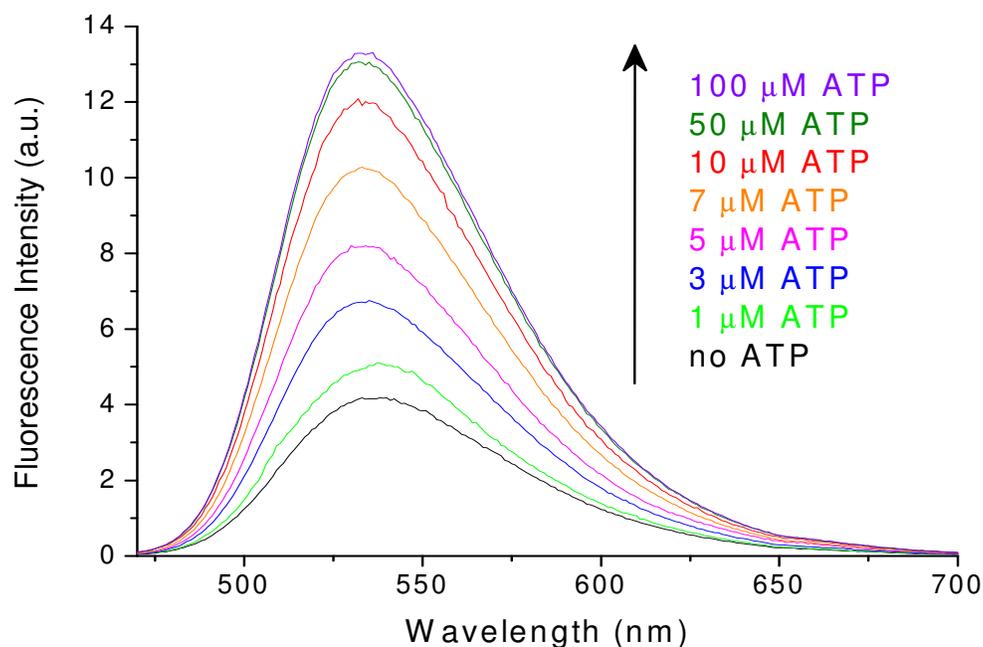


Figure 45. Changes in the fluorescence emission spectra of **10.Zn** (5 μM) upon addition of different amounts of ATP ($\lambda_{\text{exc}} = 450 \text{ nm}$) in HEPES buffer 0.1M at pH 7.4.

fluorescence (around 1-fold). Binding of ATP to the Zn (II)-DPA unit decreases the strength of the Zn²⁺-NH interaction, resulting in a significant increase in fluorescence, as already mentioned. Although to a lesser extent, a similar behaviour was observed in the case of **10** complexed with Cd (II).

An interesting observation is made in the recorded excitation spectra (figure 47).

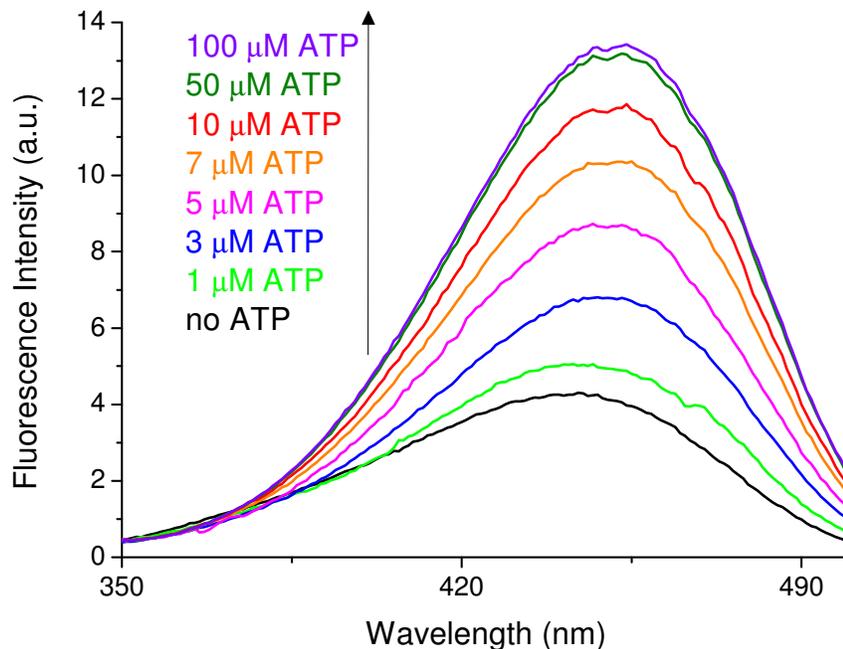


Figure 47. Changes in the fluorescence excitation spectra of **10.Zn** (5 μM) upon addition of different amounts of ATP ($\lambda_{em} = 535$ nm) in HEPES buffer 0.1M at pH 7.4.

Upon binding of the ATP to **10.Zn**, a bathochromic shift from 441 to 450 nm is registered. These results are analogous to the absorption spectra in section 4.4.3 and fully support the aforementioned hypothesis regarding the breaking of the coordinating bond from the secondary (aromatic) amine of the naphthalimide chromophore to the metal ion.

To better evaluate the sensitivity of **10.Zn** towards ATP, a calibration plot was made relating the fluorescence intensity at the maximum of 535 nm against the concentration of ATP in the sample (figure 48).

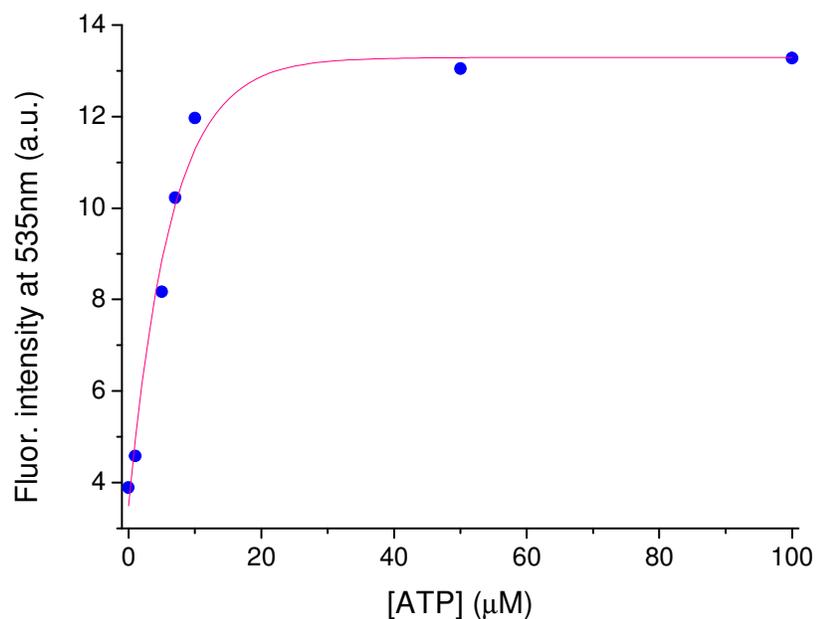


Figure 48. Calibration plot of the fluorescence emission of **10.Zn** in different ATP concentrations. Blue points: experimental data; red line: exponential fit using *Origin 8.0*[®].

In order to confirm that the complexed chemosensor **10.Zn** was indeed the molecule responsible for these fluorescence changes, a simple experiment was performed. To a solution of pure **10** was added first ATP, resulting in minor changes in the fluorescence signal. Afterwards, a solution of $\text{Zn}(\text{ClO}_4)_2$ was added, giving a strong increase in fluorescence intensity at 535nm (figure 49). These results prove that the presence of Zn^{2+} in the structure of **10.Zn** is essential for sensing ATP.

To determine if the sensing properties of **10.Zn** are influenced by the pH of the sample solution, we decided to test its sensitivity to ATP at different pH values. For this purpose, the fluorescence intensity of the chemosensor was measured in the absence and presence of ATP (50μM) in HEPES 0.1M buffered solutions, with the pH ranging from 5.6 to 8.4. The summary for this experiment is presented in the following graph (figure 50).

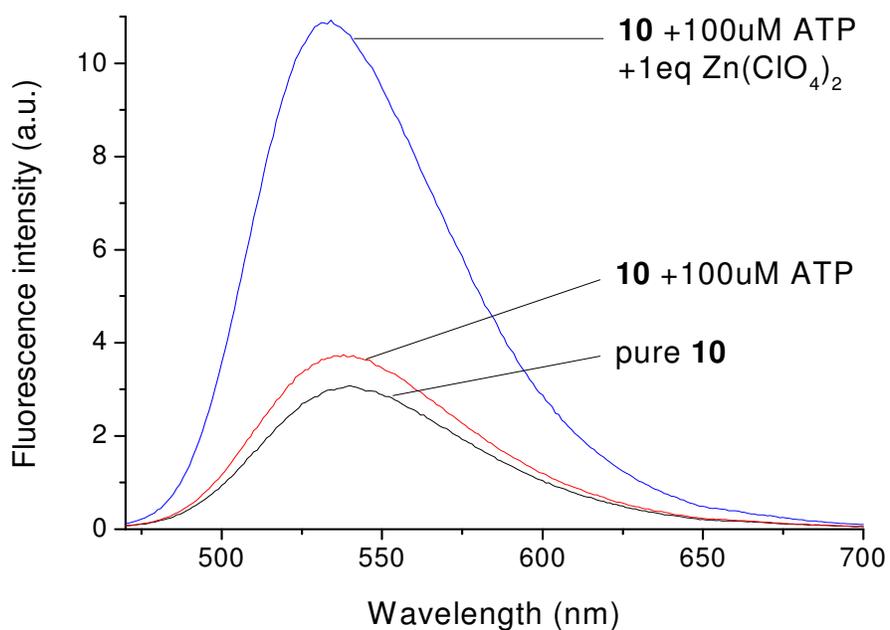


Figure 49. Determination of the importance of Zn^{2+} for the detection of ATP using **10.Zn** ($5 \mu\text{M}$, $\lambda_{\text{Exc}} = 450 \text{ nm}$).

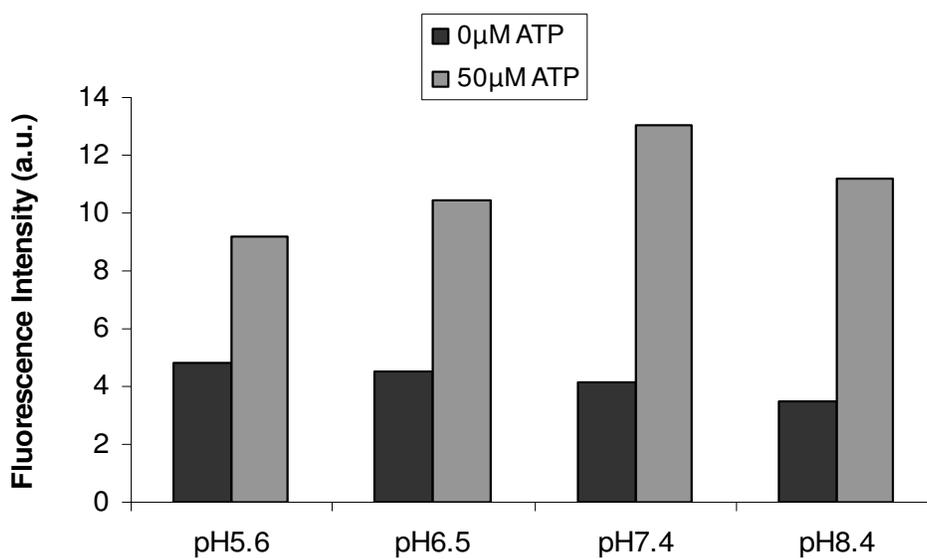


Figure 50. Influence of pH on the sensing properties of **10.Zn** ($5 \mu\text{M}$) towards ATP ($\lambda_{\text{exc}}=450\text{nm}$, $\lambda_{\text{em}} = 535 \text{ nm}$).

Although a loss of sensitivity was observed at lower pH values when compared to the neutral conditions (about 40% at pH 5.6 and 25% at pH 6.5), the changes in intensity are still significant for sensing ATP in the low micromolar range. The main reason for this loss in sensitivity is the partial protonation of the tertiary amine group of the DPA, since its uncomplexed pK_a value is around 5.8.

4.5.2. Selectivity studies on **10.Zn**

In order to determine the selectivity of chemosensor **10.Zn**, it was tested against several organic and inorganic phosphates, as well as other common anions. The results are represented in figure 51.

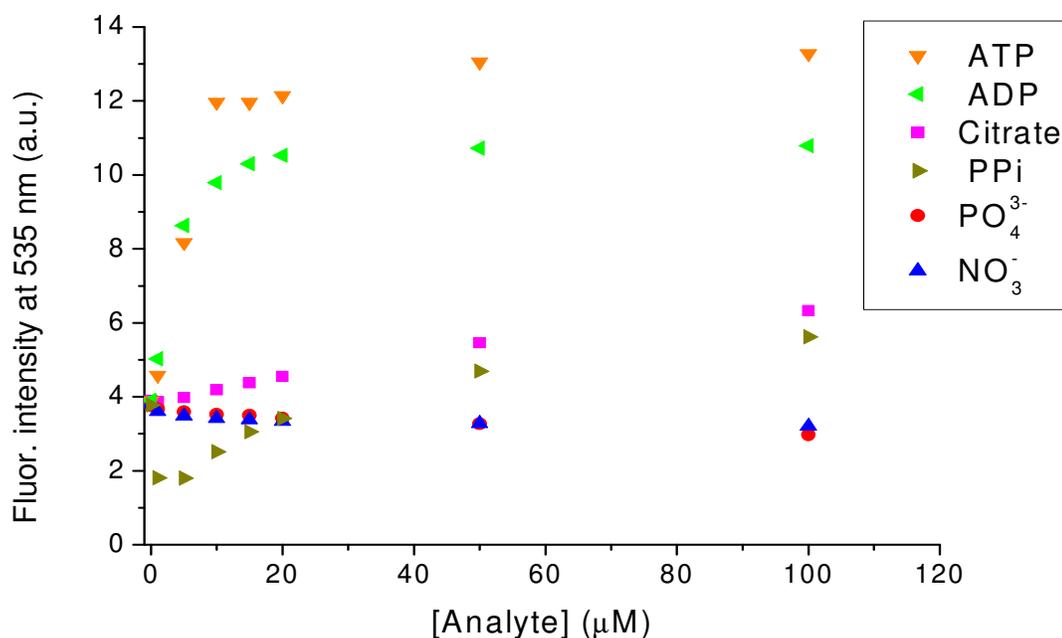


Figure 51. Changes in fluorescence intensity of **10.Zn** (5 μM) upon exposure to different concentrations of anionic analytes ($\lambda_{exc}=450\text{nm}$, $\lambda_{em} = 535 \text{ nm}$).

The plots refer to the maximum fluorescence intensity against the concentration of the different analytes in buffered aqueous solution. As can be observed, most of the studied anion species (exceptions are ADP and PPI) do not show significant changes in fluorescence in comparison to ATP, especially if we focus on the concentration range of up to 10 μM.

An interesting result is observed upon addition of PPI. In this particular case, up to one equivalent of PPI induces a decrease (about 1 fold) in the fluorescent intensity of **10.Zn**, and for higher concentrations an increase is observed. This may be explained by the fact that, until one equivalent of concentration is reached, each molecule of PPI coordinates simultaneously with two Zn (II)-DPA groups from two sensor molecules (figure 52).

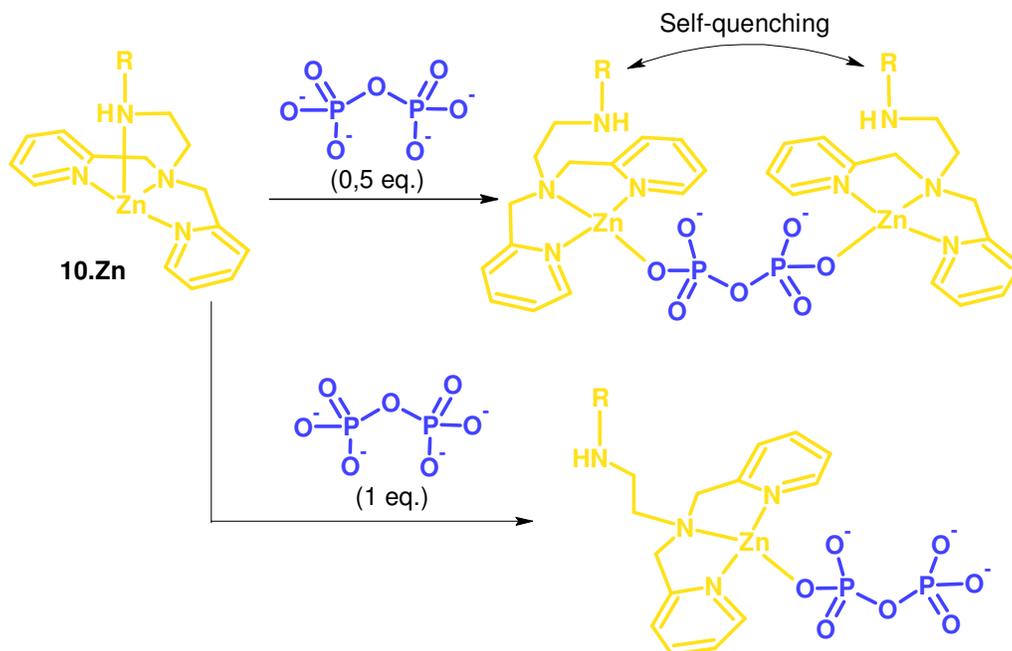


Figure 52. Proposed mechanism for the interaction between **10.Zn** and PPI.

This causes them to be in close vicinity and therefore induces self-quenching of **10.Zn**.⁹⁴ When PPI is present in excess, the coordination of one molecule of PPI per chemosensor molecule is favoured because the electron density of an unbound PPI molecule is stronger than a PPI which is already bound to a Zn (II)-DPA center. However, the fluorescent signal changes with this analyte are much smaller than for ATP and ADP. This is a strong indicator that not only the binding interaction of the pyrophosphate with the Zn (II)-DPA center in these latter molecules is responsible for the response to the analytes. A possibility is that adenine interacts directly with the π -system of the naphthalimide fluorophore in **10.Zn**, leading to an increase in its fluorescence emission or an enhanced complexation.

In order to compare the interaction between ATP and ADP with **10.Zn**, their association rate constants were determined.

The equilibrium of the reaction between **10.Zn** and the three aforementioned analytes (ATP, ADP and PPI) can be described as follows:



in which **S**, **A** and **SA** represent sensor, analyte and the resulting sensor-analyte complex, respectively. The association constant is defined through equation [IV]:

$$K = \frac{[SA]}{[S].c_A} \Leftrightarrow [SA] = K.[S].c_A \quad \text{[IV]}$$

which relates the concentrations of the species involved in the equilibrium.

The reaction coefficient α is defined by the fraction between concentration of the sensor-analyte complex, [SA], and the total concentration of sensor within the sample. This coefficient is directly related to the fluorescence of the sample with the following formula:

$$\alpha = \frac{[SA]}{[S] + [SA]} = \frac{S_X - S_S}{S_{SA} - S_S} \quad \text{[V]}$$

with S_S , S_{SA} corresponding to the fluorescence of pure sensor and sensor-analyte complex respectively, while S_X represents the fluorescence of the sample at a given analyte concentration.

Substituting equation [IV] in equation [V] and rearranging it leads us to equation [VI]:

$$S_X = \frac{K.c_A.S_{SA} + S_S}{1 + K.c_A} \quad \text{[VI]}$$

By plotting the fluorescence intensity against the logarithm of analyte concentration, the experimental points assume the shape of a sigmoidal curve. With the help of a program, *Origin 8.0*[®] (ORIGINLABS), a sigmoidal function was fitted to the experimental points yielding the association constants for both analytes (figure 53). The obtained values are comparable to others found in the literature.⁸⁰ Nevertheless, it must be stressed out that these

values are only “apparent” and not thermodynamic constants, since it is assumed that the fluorescent intensity changes directly corresponds to the response of dye. Furthermore, factors such as diffusion or the microenvironment of the sensor are not taken into account since all samples are highly diluted and in aqueous solution, the molecules present a high degree of “freedom”.

Table 4. Apparent association constants K with **10.Zn**.

Analyte	$K \times 10^5 \text{ (M}^{-1}\text{)}$
ATP	1.86
ADP	3.22
PPi	0.35*

*only increasing trend of the corresponding graph from figure 51 (above 0.5 eqs. PPi) was considered for these calculations.

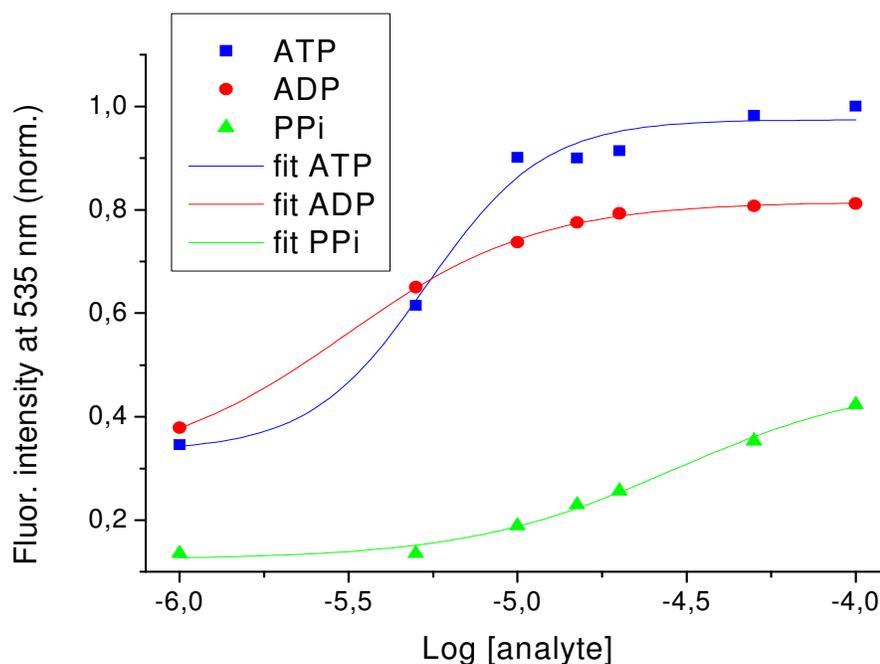


Figure 53. Curves of fluorescence intensity of **10.Zn** versus the logarithm of analyte concentration. The sigmoidal fits were obtained using *Origin 8.0*[®] (R^2 (fit ATP) = 0,973, R^2 (fit ADP) = 0,999, R^2 (fit PPi) = 0,986).

Although K is slightly higher for ADP than ATP, the increase in fluorescence intensity of **10.Zn** is significantly stronger with the latter. We assume the second phosphate group present

in ATP to be responsible for this effect because it may additionally act as a coordinating ligand moiety towards the metal through its third phosphate group. This confers an increased donating strength in the coordination from the tertiary amine of the DPA unit which results in a further decrease of PET. Another hypothesis is that ATP presents more negative charges than ADP, and this may also strengthen the binding of ATP towards the metal centre.

We also compared ATP sensitivity of **10.Zn** specifically against the other triphosphorylated nucleotides, namely GTP, CTP and UTP (figure 54).

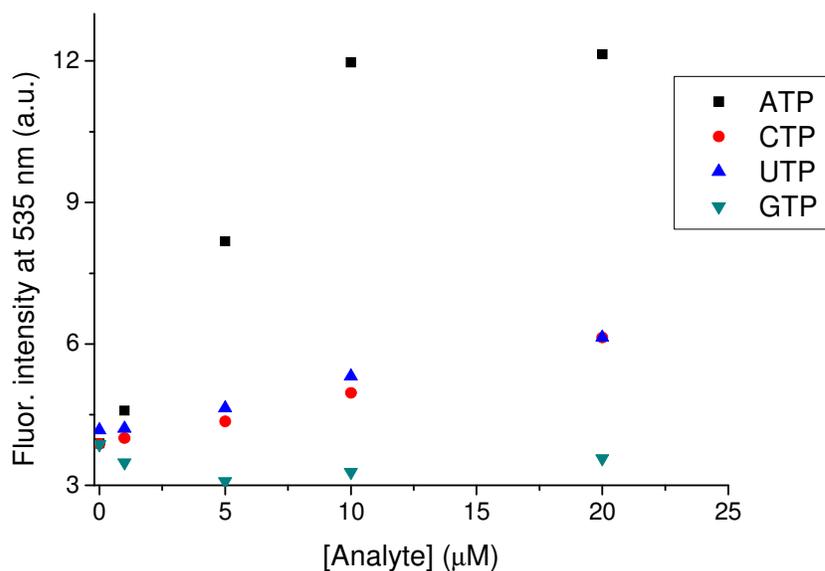


Figure 54. Changes in fluorescence intensity of **10.Zn** (5μM) upon exposure to different concentrations of triphosphorylated nucleotides ($\lambda_{exc}=450\text{nm}$, $\lambda_{em} = 535 \text{ nm}$).

Although these nucleotides present very similar structures, differing only in the base unit, they induce almost no effect on the fluorescence signal of the chemosensor. This preference of ATP over the other nucleotides is probably related to the previously referred additional π - π stacking effect of adenine with the naphthalimide aromatic π system, since all the nucleotides possess three negatively charged phosphate groups. Such effects have been reported for explaining the interaction differences between closely related nucleotides (which differed only in the nucleic base) and acridine with an appended Zn (II)-cyclen unit.^{95, 96} This effect is also consistent with the observed strong binding of ADP. Although these results suggest such a hypothesis, more data are needed to confirm it.

4.6. Fluorescent silica nanoparticles for ATP sensing

4.6.1. Synthesis and characterization of surface functionalized silica nanoparticles – **10.Zn-NPs**

Fluorescent nanoparticles have gained increased interest in the scientific community, as they can be used for continuous monitoring of analytes in living cells and tissues. As mentioned in section 3.3.1, several materials can nowadays be used for the production of such nanosensors and depending on the material, different functionalizations and architectures can be designed depending on the desired application. The immobilization of fluorescent sensors within these nanomaterials is important since plain organic dyes are often toxic to cells. Moreover, many sensor dyes only show changes in fluorescent intensity. This makes them unreliable for ratiometric sensing, since effects such as dye aggregation or fluctuations in the light source intensity may influence their fluorescence. This problem can be overcome if, apart from the sensor dye (indicator), an inert fluorescent dye is also immobilized in the nanoparticles. By relating fluorescence changes in the indicator dye against the reference dye, ratiometric measurements can be achieved.

One of the most attractive materials for the production of fluorescent nanoparticles consists of hybrid or composite silicates. Such silica nanosensors present several advantages over other materials, namely mechanical and photostability, high brightness, biocompatibility and relatively low cytotoxicity.^{97, 98} Furthermore, their chemical versatility allows for multiple and varied functionalization, depending on the desired application. Although silica nanoparticles present a strongly hydrophilic character, the high degree of cross-linking makes it difficult for larger analytes to enter the dense matrix. Therefore, for ATP sensing, attachment of the indicator dye is performed preferably on the outer surface of the nanoparticle to better promote the interactions with the analyte.

In section 4.2.1, the potential of naphthalimides in sensor applications was highlighted due to, not only its advantageous optical properties but also to its chemical versatility. In the specific case of **10**, we added a carboxylic acid group in the structure of the chemosensor molecule since the final objective was to attach the chemosensor **10.Zn** to silica nanoparticles functionalized with amine groups in their outer surface. The amine functionalized silica cores were provided by Dr. Tristan Doussineau, who covalently attached a rhodamine derivative to the silica core of the nanoparticles, to be used as reference dye.⁹⁹

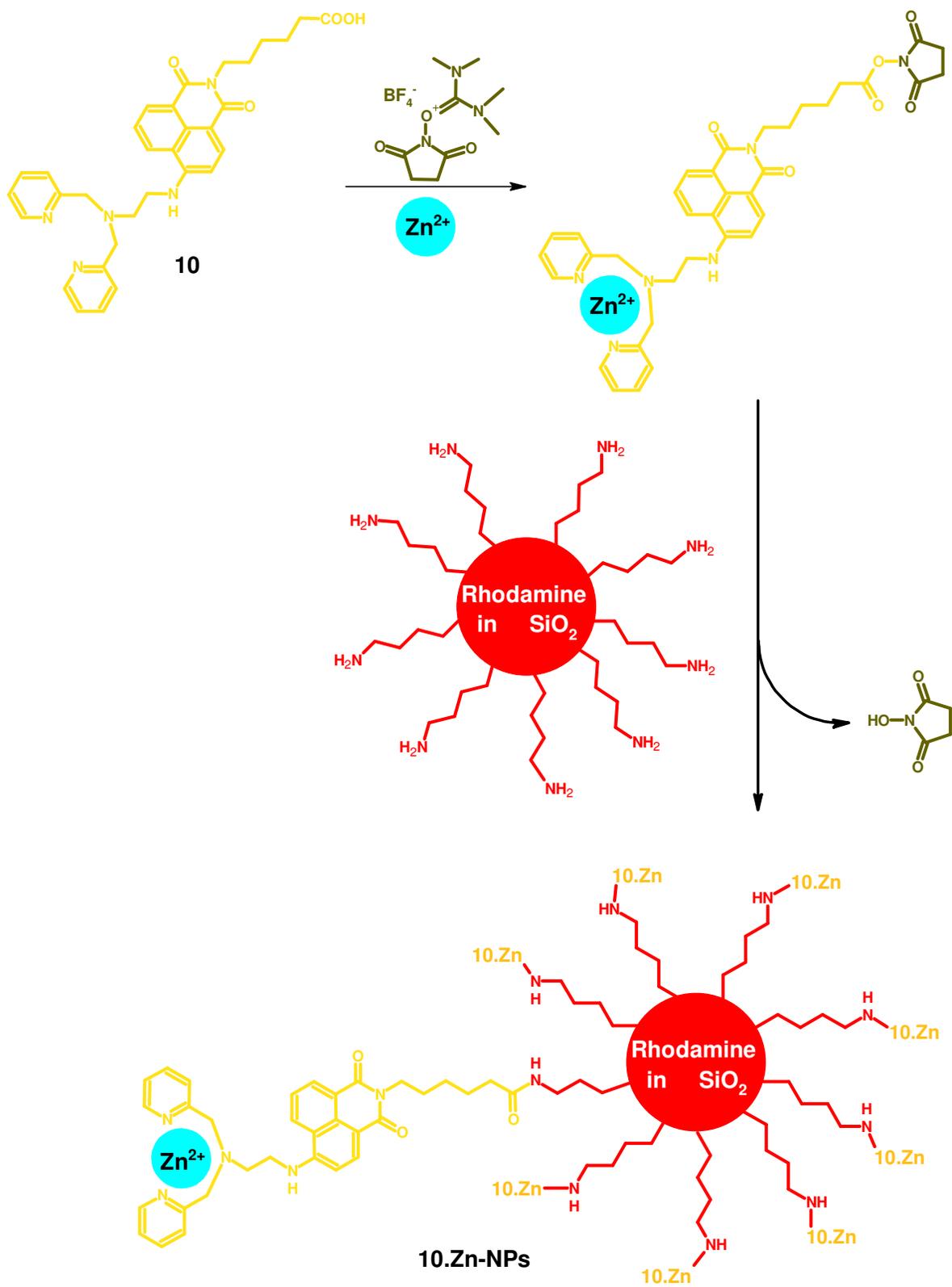


Figure 55. Surface functionalization of rhodamine silica nanoparticles – **10.Zn-NPs**.

For the synthesis of **10.Zn** surface functionalized nanoparticles, the formation of complex **10.Zn** was performed *in-situ*, by adding zinc perchlorate to a solution of **10** in DMF. 2-Succinimido-1,1,3,3-tetramethyluronium-tetrafluoroborate (TSTU) was used to activate the carboxylic group through formation of an NHS-ester. The amine-functionalized nanoparticles were then added to the mixture and subsequent nucleophilic attack yielded nanostructure **10.Zn-NPs** (figure 55). The obtained **10.Zn-NPs** were thoroughly washed by cycles of “centrifugation/resuspension” in methanol, ethanol and water, to ensure that no free **10.Zn** remained in solution. Picture 56 shows suspensions of the nanoparticles in each of the three solvents during the washing steps.

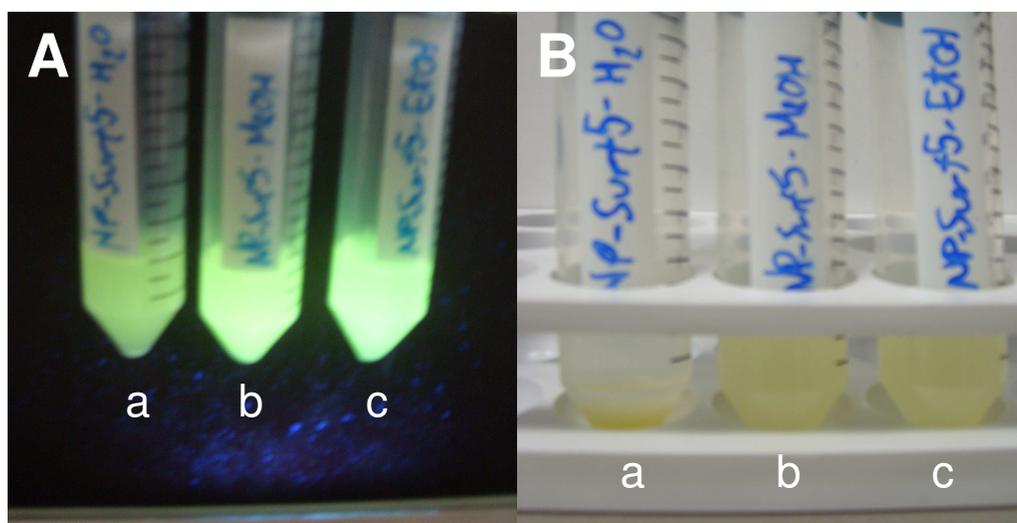


Figure 56. A) **10.Zn-NPs** suspended in (a) water (b) methanol, (c) ethanol and under UV light (366 nm). B) **10.Zn-NPs** suspended in (a) water (b) methanol, (c) ethanol after 1 hour.

Under UV light, the differences between the three nanoparticle suspensions are clearly visible (figure 56A). As expected, nanoparticles suspended in organic solvents present a stronger fluorescence than when they are suspended in water. Apart from that, if the particles were left standing at room temperature for 1 hour, their deposition was clearly visible in the case of water, whereas in ethanol and methanol, such deposition only took place after 48 hours and to a lesser extent (figure 56B). This may indicate that the nanoparticles are more stable in organic solvents, probably due to the presence of the aromatic part of chemosensor which is now at their surface. Nevertheless, and all throughout the fluorescence

measurements, no such sedimentation was observed since the necessary concentration of **10.Zn-NPs** in the sample to achieve a stable fluorescent signal was very low (around 0.03 mg/ml).

To have comparable results, size characterization of the nanoparticles was performed both prior and after functionalization with **10.Zn** (figure 57).

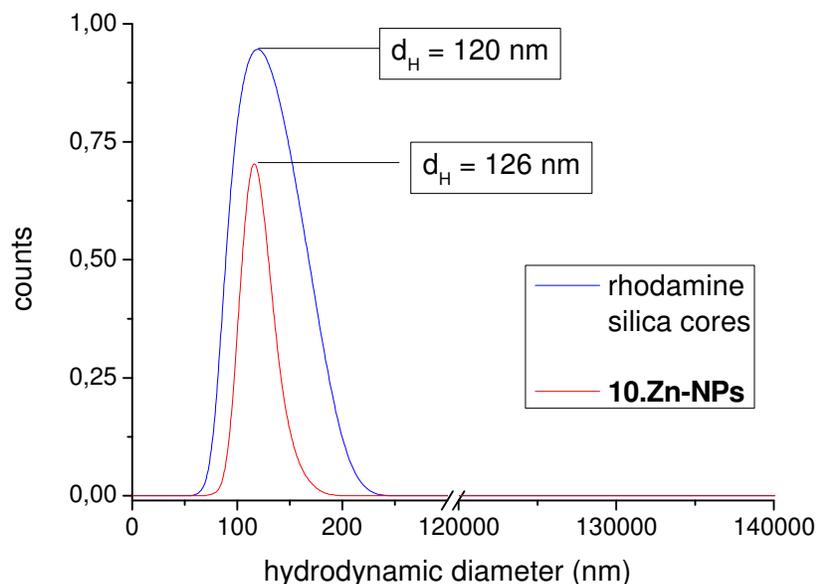


Figure 57. DLS measurements of rhodamine silica cores (blue line) and **10.Zn-NPs** (red line) in ethanol. PDI values were 0.04 and 0.07 (± 0.01), respectively.

The diameter of the nanoparticles was 120 nm for the rhodamine silica core and 126 nm for the **10.Zn-NPs**. This small variation is a good indication that only minor changes occurred at a superficial level of the nanoparticles which was expected since the amine groups used for attachment of the dye should be present only in the surface of the nanoparticles. The PDI values (0.04 and 0.07, for rhodamine cores and **10.Zn-NPs** respectively) were under 0.1 for both cases, indicating that the nanoparticles are monodisperse, with a homogenous size distribution.

4.6.2. Evaluation of **10.Zn-NPs** as ATP fluorescent nanosensors

Fluorescence measurements with **10.Zn-NPs** were carried out in the same manner as for **10.Zn**, by adding a small aliquot of a suspension of nanoparticles in water into a cuvette containing HEPES buffer 0.1 M at pH 7.4. A stable fluorescence signal was observed at 535 nm upon excitation at 450 nm, confirming the successful attachment of the sensor dye **10.Zn**. Excitation of the sample at 530 nm also originated a stable signal corresponding to the reference dye, rhodamine.

The first experiment was to determine if the Zn (II) metal ion was still complexed with the DPA unit from the sensor dye. Thus, the fluorescent response of the nanoparticles was measured upon addition of a strong complexing agent, ethylenediaminetetraacetic acid disodium salt, EDTA (figure 58).

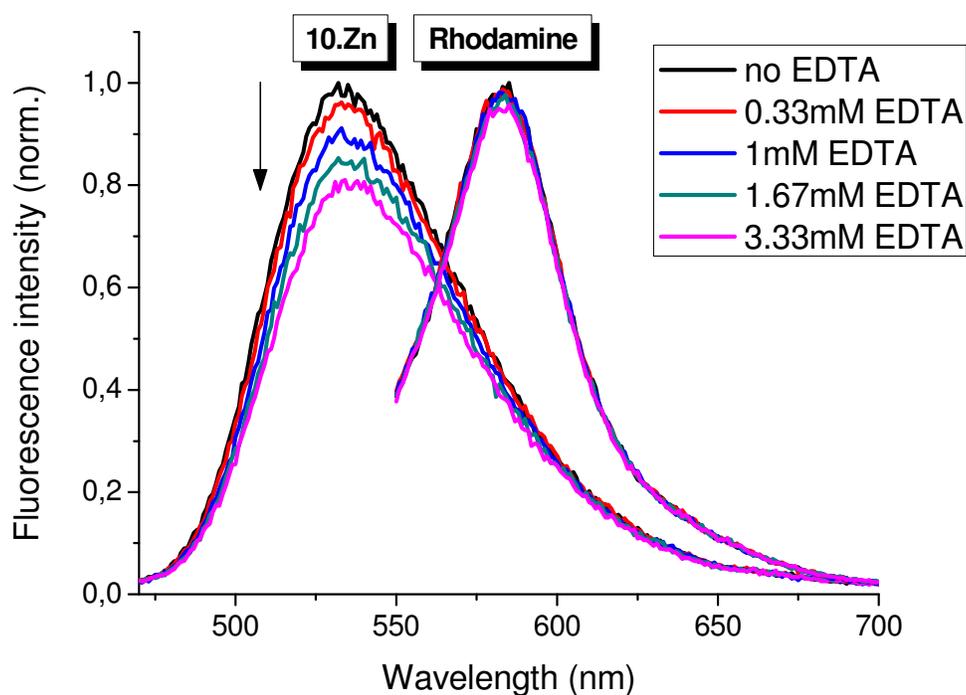


Figure 58. Changes in fluorescence of **10.Zn-NPs** upon addition of EDTA (λ_{exc} (**10.Zn**) = 450 nm, λ_{exc} (Rhod.) = 530 nm).

The fluorescence of the sensor dye was slightly decreased at high concentrations of EDTA, providing a good indication that Zn (II) ions were still present in the nanostructures.

Fluorescent response of **10.Zn-NPs** towards ATP was studied by successively adding small amounts of an ATP aqueous solution (up to 100 μL) to the cuvette containing suspended nanoparticles in HEPES buffer, in analogy to the studies with EDTA. The corresponding fluorescence emission spectra for both reference and indicator dye were recorded. The results are shown in figure 59.

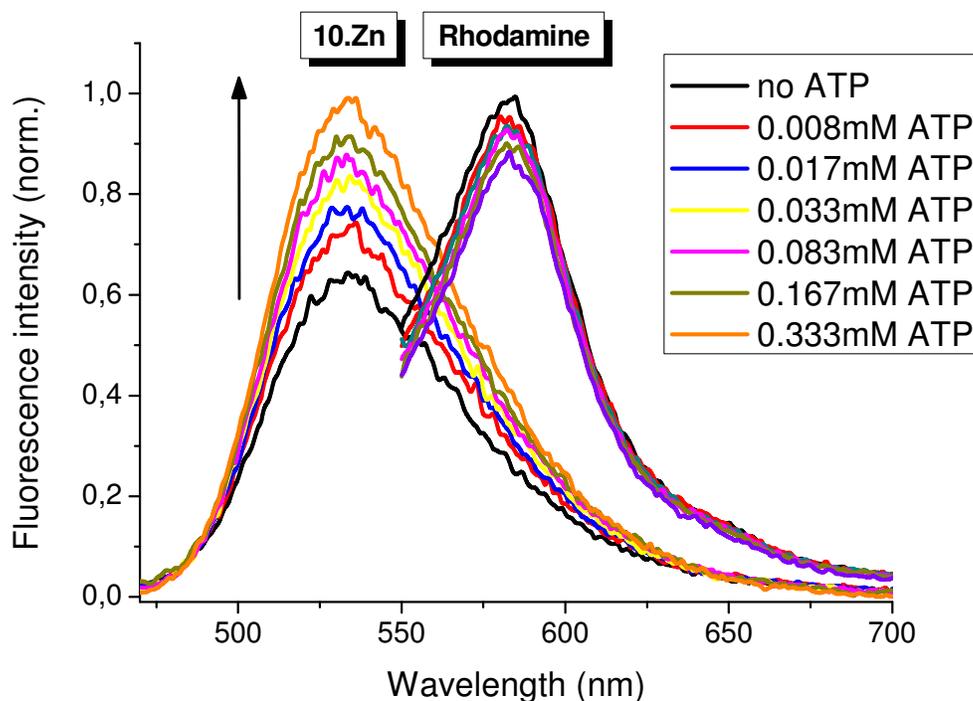


Figure 59. Changes in fluorescence of **10.Zn-NPs** upon addition of ATP (λ_{exc} (**10.Zn**) = 450 nm, λ_{exc} (Rhod.) = 530 nm).

An increase can be observed in the fluorescence of the sensor dye **10.Zn**, while minor changes occur in the fluorescence of the reference dye. However, it is noteworthy that the changes in fluorescence of **10.Zn-NPs** are significantly smaller (around 0.5 fold) than for the chemosensor in solution (2.3 fold). In analogy to the studies performed with **10.Zn** in solution, the apparent association constant for **10.Zn-NPs** with ATP was also estimated by plotting the fluorescence intensity changes (corrected with the signal from the reference dye) against the logarithm of concentration. Sigmoidal fitting to the experimental points using *Origin 8.0*[®] yielded apparent K (figure 60).

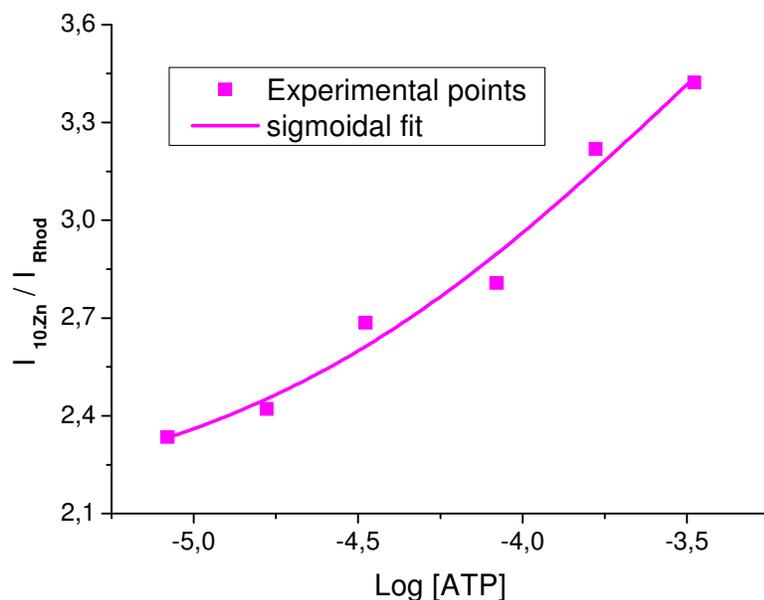


Figure 60. Plot of fluorescence intensity of **10.Zn-NPs** versus the logarithm of ATP concentration. The apparent association constant was found to be $3.3 \times 10^3 \text{ M}^{-1}$ (R^2 (fit ATP) = 0,951).

The loss in sensitivity can be explained by sterical hindrance that prevents ATP molecules to interact freely with the attached sensor dye that is now in a more confined microenvironment. Another factor that can contribute to the loss of signal changes is the presence of non-reacted amine groups at the surface of the nanoparticles, which can induce a constant PET to over the naphthalimide fluorophore.

As a continuation of the previous experiment, an aliquot (50 μL) of a 0.1 M EDTA aqueous solution was added (after the last addition of ATP). The resulting spectra show a significant decrease in the fluorescence of the sensor dye, with no visible changes in the reference dye (figure 61). This result is a confirmation that Zn (II) is still present in the sensor molecules which are attached to the nanoparticles and that, upon removal of Zn (II) from the DPA centre, sensitivity towards ATP is no longer observed.

With these results in mind, the possibility of removal and subsequent rebinding of Zn (II) to the nanoparticles and how this process affects their sensitivity towards ATP was studied. Proven successful, this approach would provide an interesting way of “recycling” the nanoparticles after their use. Therefore, washing them with EDTA and then rebinding the metal to the receptor unit would be a method for screening several samples by using only one

batch of nanoparticles. Furthermore, such an approach would provide a platform for the application of **10.Zn-NPs** in microfluidics^{100, 101} if the nanoparticles were to be physically attached to such a system.

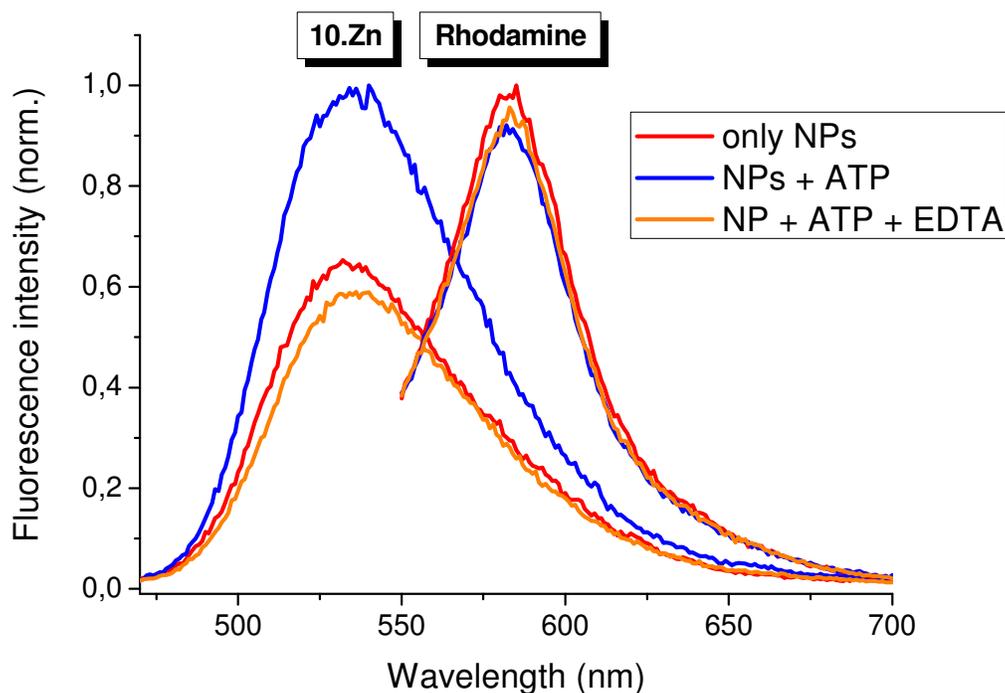


Figure 61. Changes in fluorescence of **10.Zn-NPs** upon successive addition of ATP and EDTA (λ_{exc} (**10.Zn**) = 450 nm, λ_{exc} (Rhod.) = 530 nm). Description: **red lines** – only **10.Zn-NPs**; **blue lines** – **10.Zn-NPs** with 0.333 mM ATP; **orange lines** – **10.Zn-NPs** with 1.667 mM EDTA (after addition of ATP).

Thus, an aliquot of **10.Zn-NPs** was suspended in a vial containing an aqueous solution of EDTA and stirred overnight. Upon three washing cycles with water, fluorescence measurements were processed by first, addition of Zn (II) (100 μL of 0.1 M solution) to the sample and secondly, addition of ATP. For better comprehension, these nanoparticles are referred to as **10-NPs**, since Zn (II) is no longer bound. The resulting spectra are shown in figure 62.

A 0.5 fold increase is observed upon rebinding of ATP, meaning that full recovery of fluorescence enhancement is achieved in the presence of ATP after rebinding of Zn (II), when

compared to the “original” **10.Zn-NPs** sample. As expected, the rhodamine signal remained essentially the same throughout the measurements.

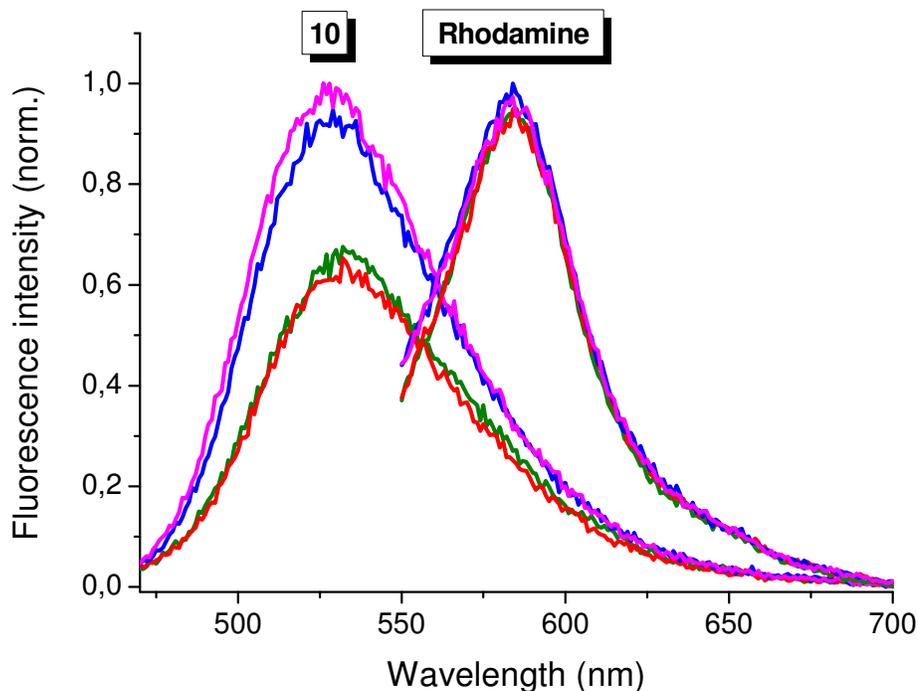


Figure 62. Rebinding of Zn (II) and subsequent addition of ATP to **10-NPs** (λ_{exc} (**10**) = 450 nm, λ_{exc} (Rhod.) = 530 nm). Description: **green lines** – only **10-NPs**; **red lines** – **10-NPs** with 3.33 mM Zn (II); **blue lines** – **10-NPs** with 1.67 mM ATP (after Zn (II) rebinding); **violet lines** – **10-NPs** with 3.33 mM ATP (after Zn (II) rebinding).

It is noteworthy to mention that upon Zn (II) rebinding, the spectrum of the sensor dye did not experience significant changes which raised some doubts whether Zn (II) had actually been completely removed from the DPA complex with EDTA washings. Therefore, a second experiment was made, similar to the one shown in figure 49 for **10.Zn** (see section 4.5.1). The simple test consisted on adding ATP to a sample of **10-NPs**, prior to Zn (II) rebinding (figure 63). The results demonstrated that Zn (II) ion had been indeed completely removed from the nanoparticles, since the expected fluorescence enhancement in the presence of ATP only took place after addition of Zn (II) to the sample.

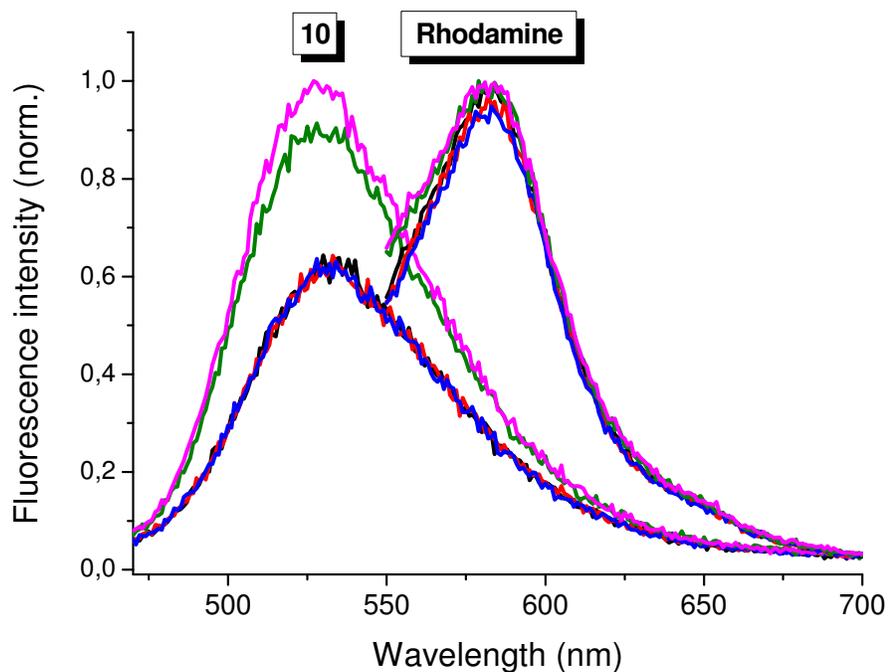


Figure 63. Changes in fluorescence of **10**-NPs upon successive addition of ATP and Zn (II) in HEPES buffer 0.1M at pH 7.4 (λ_{exc} (**10**) = 450 nm, λ_{exc} (Rhod.) = 530 nm). Description: **black lines** – only **10**-NPs; **red line** – **10**-NPs with 0.167mM ATP; **blue line** – **10**-NPs with 0.333 mM ATP; **green line** – **10**-NPs with 1.667 mM Zn (II) (after ATP addition); **violet line** – **10**-NPs with 3.33 mM Zn (II) (after ATP addition).

Finally, an assessment regarding possible interferences was performed. Apart from ATP, the same phosphate derivatives which were studied for the free dye **10.Zn** were also analyzed at two different concentrations: 0.167 mM and 0.333 mM. The results are presented in figure 64.

The graph shows that ATP is the analyte that induces the strongest changes in the ratiometric fluorescent signal of the nanoparticles. Simultaneously, the nanoparticles show the highest sensitivity also towards ATP even when compared to ADP, in opposition to the findings in solution. Moreover, **10.Zn**-NPs present similar sensitivity for ADP and CTP. This may indicate that, in the case of the functionalized nanoparticles, electrostatic interactions between the dye and the analyte are more relevant than stacking effects between the naphthalimide and the nucleobase.

Nevertheless, all the other analytes induce smaller response to the fluorescence of the nanoparticles. This study is therefore, in accordance with the postulated hypothesis for specificity of **10.Zn** towards the adenine nucleotides ATP and ADP.

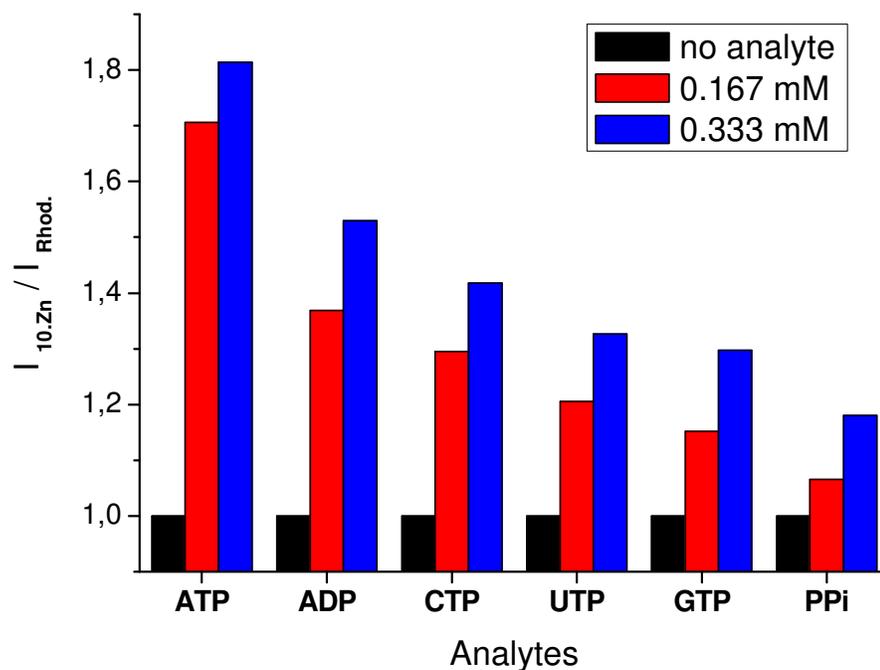


Figure 64. Influence of analytes in the fluorescence properties of **10.Zn-NPs**.

4.7. Conclusions

In conclusion, a fluorescent naphthalimide sensor molecule, structure **10**, was successfully synthesized. The structure possessed a dipicolylamine (DPA) group as a receptor function capable of complexing metal ions. Studies with several metals showed that the Zn (II)-DPA unit was the best complex to interaction with ATP. Therefore, complex **10.Zn** was characterized structurally through mass spectrometry, and optically regarding its sensing properties towards ATP and related derivatives. The sensor presented high sensitivity towards ATP and ADP in the low micromolar range, and good selectivity against a wide variety of other anions. Apparent association constants with **10.Zn** were determined to be 1.86×10^5 , 3.22×10^5 and $3.50 \times 10^4 \text{ M}^{-1}$ for ATP, ADP and PPI, respectively, with a fluorescence enhancement of around 2.3 fold in the case of ATP. The results suggested that, not only the pyrophosphate unit was responsible for binding of the analytes, but probably a π - π stacking effect also occurred between the adenine nucleobases and the naphthalimide fluorophore, which translated into a strong fluorescence enhancement. Other triphosphorylated nucleobases induced only minor fluorescence response from the chemosensor.

By introducing a carboxylic function into the structure of **10.Zn**, it was possible to immobilize the chemosensor onto the surface of amine functionalized silica nanoparticles, through NHS-ester activation. The synthesized nanoparticles, **10.Zn-NPs**, additionally possessed a rhodamine derivative in its core, covalently bound to the silica matrix. This allowed for ratiometric sensing, since rhodamine showed no interaction with the analytes and would only act as a reference dye. The hydrodynamic diameter of the synthesized nanoparticles was found to be 126 nm, with a PDI of 0.07, indicating that the nanoparticles were monodisperse.

Although a strong decrease in sensitivity of **10.Zn-NPs** was observed when compared to the dissolved chemosensor **10.Zn**, the obtained nanoparticles presented a similar behaviour in fluorescence response regarding ATP and ADP, while only minor changes were recorded for other analytes. However, in the case of nanoparticles, the sensitivity towards ATP was greater than ADP. The apparent association constant for **10.Zn-NPs** with ATP was found to be $3.3 \times 10^3 \text{ M}^{-1}$, with a maximum fluorescent enhancement of 0.55 fold (at 0.333 mM ATP). Nevertheless, sensing of concentrations down to the low micromolar range was also proven possible (see figure 59).

5. Summary and outlook

In this work, the design and characterization of two chemosensor dyes, represented by structures **2** and **10**, for two distinct analytes, respectively Naproxen and adenosine triphosphate (ATP) is fully described.

For the first case, the synthesis of **2** consisted of two reaction steps, performed in relatively good yield. The dye presented a styrylpyridinium system as a fluorophore, yielding absorbance and fluorescence properties in the visible range, with maxima at 478 and 610 nm, respectively. The sensing properties of **2** were studied towards a wide range of negatively charge, taking advantage of the positive charge on the structure of the dye. The strongest response was found against Naproxen, a drug from the class of NSAIDs, used as the active substance on the production of anti-pyretic and anti-inflammatory medicaments. The sensing mechanism was based on twisted intramolecular charge transfer (TICT) mechanism, which led to fluorescence enhancement in the presence of Naproxen in buffer solution at neutral pH, with a calculated limit of detection (LOD) of 0.054 mM. Furthermore, the sensor dye presented a methacrylate group in its structure, which enabled its use as a fluorescent functional monomer in the synthesis of polyacrylamide nanoparticles, **PAA-NPs**. The size of the nanoparticles was determined through dynamic light scattering (DLS) and found to be 34 nm, with a polydispersity index of 0.1, indicating homogeneous size distribution. Although covalent attachment to the polymeric matrix decreased the leaching of the dye, the sensitivity of the **PAA-NPs** to Naproxen was decreased when compared to the free dye in solution, with a LOD of 0.50 mM. This fact may be explained by the high cross-linking degree of the nanoparticles which affects, not only the sensing capacity of the dye due to physical constraints, but also because it prevents Naproxen from interacting with the sensor molecules located within the polymeric matrix. Selectivity and competitive assays were performed against other drugs and anions, with cyclic Adenosine monophosphate (cAMP) being the strongest interferent with Naproxen detection. Nevertheless, results indicate that the **PAA-NPs** can be used for rapid diagnosis of Naproxen overdose in plasma samples.

As future perspectives, an additional receptor function should be introduced in the sensor molecule, to ensure a better selectivity with another interaction point towards the analyte, as electrostatic interactions are often proven unselective, due to their non-specificity. Furthermore, for nanoparticles preparation, a co-porogen should also be introduced in the synthetic procedure, as it may lead to a lower degree of cross-linking which would allow for

better penetration of the analyte, as well as decrease the hindrance towards the functional monomer.¹⁰² In this manner, the observed problem with the loss of sensitivity may be reduced or overcome.

In a parallel investigation, naphthalimide dye **10** was synthesized in a converging synthesis between structures **3** and **9**, which were previously synthesized separately in one and three reaction steps, respectively. The newly designed sensor presented a dipicolylamine unit, able to complex with metal ions, which allowed later for the sensing of ATP. Several metal complexes were tested, with **10.Zn** yielding the best response towards the phosphorylated nucleobases. The sensitivity of **10.Zn** was in the low micromolar range of analyte concentration, with apparent association constants of 1.86×10^5 , 3.22×10^5 and $3.50 \times 10^4 \text{ M}^{-1}$ for ATP, ADP and PPI, respectively. Although with a slightly lower K value than ADP, ATP induced the strongest fluorescent enhancement in **10.Zn** (about 2.3 fold). Results against other possible interferents, such as triphosphorylated nucleobases suggested that, not only the pyrophosphate was responsible for binding, but also adenine appeared to present a preference in interaction with the naphthalimide fluorophore, probably through stacking.

The structure of **10** presented a carboxylic group, which enabled its covalent attachment to amine surface-functionalized silica nanoparticles through NHS-ester activation, with the complex **10.Zn** being generated *in-situ*. The nanoparticles, **10.Zn-NPs**, were found to be homogenous in size, with a hydrodynamic diameter of 126 nm and a PDI of 0.07. Sensing properties of **10.Zn-NPs** towards ATP showed a significant decrease in sensitivity when compared to the dye in solution, with an apparent association constant of $3.3 \times 10^{-3} \text{ M}^{-1}$, although sensing of concentrations in the low micromolar range were also found possible. The nanoparticles were also sensitive to ADP, which was in accordance with the results obtained for the free dye. Future improvements to this methodology should include studies on the influence in the length of spacer between the fluorophore and the surface of the nanoparticles in the sensing of ATP and ADP. Furthermore, studies with ATP-enzymes must be performed to determine their application for measurements in biological samples.

6. Zusammenfassung und Ausblick

In der vorliegenden Arbeit wird die Synthese und Charakterisierung zweier Chemosensorfarbstoffe (Verbindungen **2** und **10**) beschrieben, welche zum Nachweis der Analyten Naproxen und Adenosintriphosphat (ATP) dienen.

Eine zweistufige Synthese lieferte das Styrylpyridiniumfluorophor **2** zur Bestimmung von Naproxen in relativ gute Ausbeuten. Der Farbstoff besitzt Absorptions- und Fluoreszenzbanden im sichtbaren spektralen Bereich mit Maxima bei 478 nm und 610 nm. Aufgrund seiner positiven Ladung wurde der Sensorfarbstoff hinsichtlich seines Ansprechverhaltens auf negativ geladene Analyten untersucht, wobei Naproxen die stärksten Signaländerungen zeigte. Die Wechselwirkung des Analyten mit dem Farbstoff beruht auf einem „twisted intramolecular charge transfer“ (TICT) Mechanismus, der zu einem Anstieg der Fluoreszenzintensität in Gegenwart des Analyten führt. Die berechnete Nachweisgrenze für Naproxen in wässriger Pufferlösung bei neutralem pH, lag bei 0,054 mM. Der Farbstoff wurde außerdem mit einer Methacrylatgruppe funktionalisiert, die eine kovalente Bindung an Polyacrylamidnanopartikel ermöglicht. Die dynamische Lichtstreuung der so hergestellten fluoreszierenden Nanopartikel ergab einen hydrodynamischen Durchmesser von 34 nm mit einem Polydispersitätsindex (PDI) von 0,1. Die Copolymerisation des Farbstoffs in die Nanopartikel minimierte das Auswaschen, jedoch zeigten die Nanopartikel im Vergleich zum Sensorfarbstoff in Lösung eine geringe Analytsensitivität (Nachweisgrenze 0,5 mM). Selektivitätsuntersuchungen und kompetitive Tests mit anderen Pharmazeutika und Anionen zeigten, dass zyklisches Adenosinmonophosphat am stärksten mit der Naproxenerkennung konkurriert. Trotzdem lässt sich aus den Ergebnissen schliessen, dass die Sensornanopartikel zur schnellen Detektion von Naproxenüberdosen in Plasma geeignet sind. Eine erhöhte Selektivität des Chemosensors könnte durch eine zusätzliche Rezeptorfunktion erzielt werden, welche nicht auf unspezifischen elektrostatischen Wechselwirkungen mit dem Analyten beruht, sondern vielmehr auf kovalenten Erkennungsmechanismen. Weiterhin könnte ein Co-Porogen bei der Nanopartikelherstellung dazu dienen, die Struktur der Partikel poröser zu gestalten und damit die Diffusion des Analyten in die Nanopartikelmatrix zu erleichtern. Auf diese Weise könnte die Sensitivität der Sensorpartikel gesteigert werden.

Die Synthese des Naphthalimidfarbstoffs **10** erfolgte konvergent aus den Verbindungen **3** und **9**, die vorher separat hergestellt wurden. Der Sensorfarbstoff weist eine Dipicolylamingruppe zur Komplexierung von Metallionen auf, die dann zum Nachweis von ATP dient. Von allen untersuchten Metallkomplexen, zeigte **10.Zn** das beste Ansprechverhalten gegenüber phosphorylierten Nucleobasen. Die Sensitivität von **10.Zn** lag im unteren mikromolaren Bereich und lieferte scheinbare Assoziationskonstanten von 1.86×10^5 , 3.22×10^5 bzw. $3.50 \times 10^4 \text{ M}^{-1}$ mit den Analyten ATP, ADP bzw. PPI. Trotz der etwas geringen Assoziationskonstante im Vergleich zu ADP, wurde mit ATP der größte Anstieg der Fluoreszenzintensität von **10.Zn** gemessen (ca. 2.3-fach). Untersuchungen mit anderen Analyten, wie zum Beispiel triphosphorylierten Nucleobasen, deuteten darauf hin, dass nicht nur die Pyrophosphatgruppe zur Bindung beiträgt sondern auch die Adenineinheit und zwar durch π -Wechselwirkungen mit dem Fluorophor. Der Farbstoff **10** besitzt eine freie Carboxylatgruppe mit welcher er durch NHS-Esteraktivierung kovalent an aminofunktionalisierte Silikananopartikel angebunden wurde. Der Zn-Komplex wurde in situ erzeugt. Die Sensornanopartikel zeigten eine homogene Größenverteilung mit einem hydrodynamischen Durchmesser von 126 nm und einem PDI von 0.07. Auch wenn der Analytnachweis im mikromolaren Bereich möglich war, ist die Sensitivität der Nanopartikel mit einer scheinbaren Assoziationskonstante von $3.3 \times 10^{-3} \text{ M}^{-1}$ signifikant geringer als die des freien Farbstoffs in Lösung. In Übereinstimmung mit dem gelösten Sensorfarbstoff zeigten die Nanopartikel ebenfalls Sensitivität gegenüber ADP. Zukünftige Untersuchungen sollten den Einfluss der Spacerlänge zwischen dem Fluorophor und der Nanopartikeloberfläche auf die Erkennung von ATP und ADP einbeziehen. Weiterhin müssen ATP-Enzyme getestet werden, um die Eignung der Sensorpartikel für biologische Proben zu bestimmen.

7. Experimental Section

7.1. Materials and apparatus

The NMR spectra were recorded on Bruker AC-250 or AC-400 apparatus. The chemical shifts (δ) are given in parts per million (ppm) and the peak assignments are abbreviated as follows: s – singlet; d – doublet; t – triplet; m – multiplet. Mass spectra were recorded either on a MAT SSQ 710 from Finnigan or TRIO 2000 from Fisons. The absorption spectra were obtained using a Lambda 16 spectrometer from Perkin Elmer. The fluorescence spectra for all samples were obtained on a Fluorolog 3 from Jobin Yvon-Spex at a temperature of $(25 \pm 1)^\circ\text{C}$. The value and polydispersity of the hydrodynamic diameter of the PAA-NPs and the silica NPs were determined in aqueous suspension using dynamic light scattering (second order cumulant analysis) using an ALV-NIBS/HPPS system with an external ALV-5000/EPP correlator (ALV-GmbH, Langen, Germany). The fluorescence quantum yields were determined on a LS 50B from Perkin Elmer, using quinine sulfate in a 0.1 N H_2SO_4 solution. All aqueous solutions and buffers were prepared using deionized double distilled water (conductivity $\leq 0.055 \mu\text{S cm}^{-1}$) produced by Seralpur PRO 90 CN system (Seral, Ransbach-Baumbach, Germany). The membranes for ultrafiltration of the PAA-NPs were Whatman Anodisc 47 filters with a pore size of 20 nm. All the referred pH measurements were controlled with a digital pH meter from Hanna Instruments and calibrated at $25 \pm 1^\circ\text{C}$ with standard buffers pH 4.0 and pH 7.0 (Merck).

7.2. Chemicals

All organic solvents were of analytical-reagent grade and were purchased from Roth Chemicals (Karlsruhe, Germany) unless denoted otherwise. No further purifications were performed. All deuterated solvents for NMR characterization were supplied by Aldrich.

7.2.1. Fluorescent monomer **2**

For the full synthesis of monomer **2**, 4-(chloromethyl)benzyl alcohol, methacryloyl chloride, 4-[4-(dimethylamino)-styryl]pyridine and anhydrous sodium sulphate were supplied by Aldrich (St. Louis, USA). Tetrahydrofuran, triethylamine and acetonitrile were obtained from Fluka.

For fluorescence measurements, citric acid monohydrate and the buffer components disodium hydrogen phosphate dihydrate and sodium dihydrogen phosphate monohydrate were obtained from Fluka. Perchlorate, pyrophosphate, ibuprofen, naproxen, tolmetin, salicylate, metamizole, adenosine 3':5'-cyclic monophosphate (cAMP) and guanosine 3':5'-cyclic monophosphate (cGMP) stock solutions were prepared in water from sodium salts purchased from Sigma-Aldrich. L-Glutamic acid, L-aspartic acid, acetylsalicylic acid, and acetaminophen were supplied by Aldrich (Sigma-Aldrich). The chemicals were used as received. A 0.5 M phosphate buffer solution (pH 7.2) was prepared from sodium dihydrogen phosphate monohydrate and sodium hydroxide supplied by Sigma (Sigma-Aldrich) until the desired pH was achieved. The pH was controlled with a digital pH meter.

The response of **2** in solution was evaluated by adding 100 μL of the test solution with the analyte or interfering species to a 1x1 cm cubic quartz cuvette (Hellma, Müllheim, Germany) containing a solution of **2** (final concentration of $1 \times 10^{-5} \text{M}$) in 0.5 M phosphate buffer (pH 7.2). The excitation wavelength was 478 nm in all measurements, with a slit width set to 5 nm bandpass.

7.2.2. Polyacrylamide nanoparticles (**PAA-NPs**)

For preparing the PAA-NPs, sodium bis(2-ethylhexyl)sulfosuccinate (AOT), polyoxyethylene-4-lauryl ether (Brij®30), *N,N,N',N'*-tetramethyl ethylenediamine (TEMED), acrylamide and ammonium peroxydisulfate (APS) were obtained from Fluka. *N,N'*-Methylenebisacrylamide was purchased from Sigma-Aldrich. The fluorescent monomer, (E)-4-[4-(dimethylamino)styryl]-1-[4-(methacryloyloxymethyl)benzyl]pyridinium chloride (**2**) was synthesized according to the procedure described below (see section 6.3).

For fluorescence measurements, the sensor nanoparticles were used in a concentration of $6 \text{ mg}\cdot\text{mL}^{-1}$, equilibrated for 5 min with each standard solution of analyte and using the same

buffer as for the free monomer. The excitation wavelength for all PAA-NPs samples was 460 nm, with a slit width set to 5 nm bandpass.

7.2.3. Fluorescent chemosensor **10**

For the synthesis of the cyclen derivatives (see figure 34, section 4.3), 1,4,7,10-tetraazacyclododecane (cyclen) was obtained from ABCR (Karlsruhe, Germany), di-*tert*-butyldicarbonate (di-Boc) and bromoacetonitrile were purchased from Aldrich, and sodium borohydride was from Fluka.

For the total synthetic procedure of fluorescence chemosensor **10**, di-*tert*-butyldicarbonate (di-Boc), potassium iodide, 2-chloromethylpyridine hydrochloride, trifluoroacetic acid, 4-bromo-1,8-naphthalic anhydride and 6-aminohexanoic acid were purchased from Aldrich. Methoxyethanol, triethylamine, sodium hydroxide, sodium chloride, diisopropylethylamine, acetonitrile, hydrochloric acid and ethylenediamine were obtained from Fluka.

All fluorescence and absorbance measurements were performed in 0.1 M HEPES buffer (HEPES - 2-(4-(2-hydroxyethyl)-1-piperazine)ethanesulfonic acid sodium salt, purchased from Aldrich), with pH adjusted to 7.4 using a 6N solution of hydrochloric acid (Fluka). The excitation and emission wavelengths of fluorescence spectra were 450 and 530 nm, respectively, with a slit width of 2 nm bandpass for both excitation and emission spectra. For pH studies on **10** (see section 4.4.1), 67 mM phosphate buffer solutions were prepared by mixing 67mM solutions of sodium dihydrogen phosphate hydrate and disodium hydrogen phosphate dihydrate until the desired pH was reached. For pH buffers under 4 and above 9, the pH was reached by adding 1 M solutions of hydrochloric acid or sodium hydroxide, respectively.

All studied metal ions were obtained from Aldrich in the form of hydrated perchlorate salts. All anions were supplied by Aldrich (except for sodium pyrophosphate which was from Fluka) in the form of hydrated sodium salts.

General procedure for absorbance measurements: 50 μ L of a 0.3 mM **10** solution in methanol were added to a 10 mm wide absorbance quartz cuvette containing 2950 μ L of a 0.1 M HEPES buffer solution with pH previously adjusted to 7.4. The absorbance spectrum was then collected. Afterwards, small aliquots of a 0.6 mM solution of the metal ion in water were added and the absorbance spectrum was registered between each addition. The total volume

of the added metal ion solution was 50 μL . Afterwards, 50 μL of a 0.6 mM ATP solution (freshly prepared) were added and the final spectrum was acquired.

The procedure for fluorescence measurements was identical to the absorbance measurements, apart from the used cuvette (in this case, a fluorescence cuvette was used), except for Zn^{2+} .

For fluorescent measurements of compound **10** complexed with Zn^{2+} , a previously prepared solution of compound **10** (1.65mg, 3 μmol) and 2 equivalents of zinc perchlorate hexahydrate (2.23mg, 6 μmol) in methanol (10mL) was used. An aliquot (50 μL) of this solution was dissolved in 2950 μL of HEPES buffer 0.1M at pH 7.4 in a quartz cuvette, resulting in a final concentration of 5 μM for **10.Zn**. To the cuvette, small aliquots of the anionic analyte (up to a total volume of 100 μL) were added and fluorescence spectra were acquired between each addition.

7.2.4. **10.Zn** surface functionalized nanoparticles (**10.Zn-NPs**)

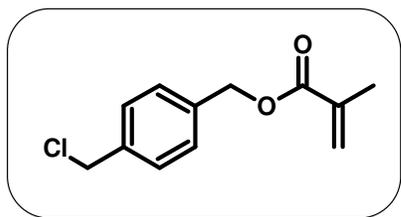
For the synthesis of the surface functionalized nanoparticles, amine-surface-functionalized silica-core nanoparticles bearing a covalently bound rhodamine derivative were used. These cores were supplied by Dr. Tristan Doussineau. Details for their preparation can be found in reference 99.

For further functionalization with **10.Zn**, 2-succinimido-1,1,3,3-tetramethyluronium-tetrafluoroborate (TSTU) was purchased from IRIS BIOTECH GmbH (Marktredwitz, Germany) and *N,N*-diisopropylethylamine (Hünig base) was obtained from Fluka.

For fluorescence measurements with **10.Zn-NPs**, the procedure was made as follows: to a fluorescence quartz cuvette (10 mm) containing 2900 μL of HEPES 0.1M with pH previously adjusted to 7.4, 100 μL of a suspension of nanoparticles with a concentration of 1 (\pm 0.2) mg/mL were added. The emission spectra for both indicator dye ($\lambda_{\text{Exc}} = 450$ nm) and Rhodamine ($\lambda_{\text{Exc}} = 530$ nm) were acquired separately. Then, aliquots of an aqueous solution of 10 mM of anionic analyte were successively added (up to 100 μL of total added volume), with the emission spectra of both indicator and reference dyes being registered between each addition. For the studies with ethylenediamine tetraacetate sodium salt (purchased from Aldrich), an aqueous solution of 0.1 M EDTA was used. The excitation wavelengths for all **10.Zn-NPs** samples were 450 nm (for **10.Zn**) and 530nm (for rhodamine), with a slit width set to 2 nm bandpass.

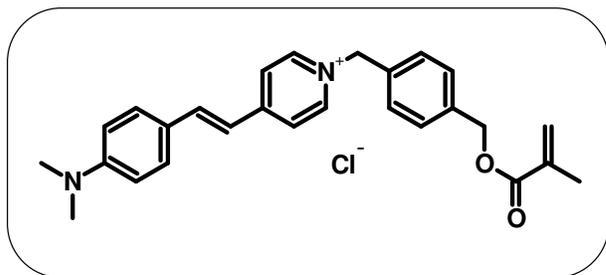
7.3. Synthetic Procedures

Synthesis of **1**



A solution of 2.16 g of methacryloyl chloride in 5 mL of dry tetrahydrofuran (THF) was added dropwise to a mixture of 1 g of 4-(chloromethyl)benzyl alcohol (6.4 mmol), 5 mL of triethylamine, 60 mg of hydroquinone and 60 mL of dry THF cooled to 0°C and stirred under nitrogen. The reaction mixture was then heated at 45°C overnight. After evaporation of the solvent, the residue was dissolved in dichloromethane, washed once with a saturated solution of sodium bicarbonate and twice with water. The organic solution was dried with anhydrous sodium sulphate, filtered and the solvent was removed under reduced pressure. Chromatography using dichloromethane as the eluent yielded 1.4 g of a brown oil. Although mass spectra still revealed a significant amount of methacrylic acid, this product was used as such in the following step.

Synthesis of **2**



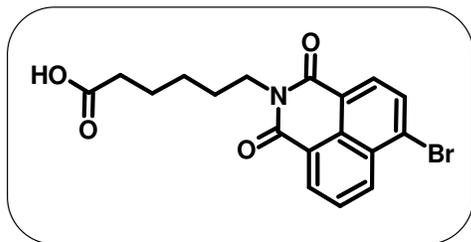
The product from the first step **1** (0.60 g, 2.68 mmol) was added dropwise to a solution of 4-[4-(dimethylamino)-styryl]pyridine (0.35 g, 1.56 mmol) in 25 mL of dry acetonitrile under

argon. Upon addition, the reaction mixture immediately changed its colour from yellow to orange. The solution was then refluxed for 24 h, presenting at the end of the reaction a deep red colour. The solvent was evaporated under reduced pressure and the residue was purified on silica-gel with a mixture of *n*-hexane/ethyl acetate (2:1) as the eluent, and then increasing polarity with methanol to recover compound **1**. Yield: 36% (230 mg). ¹H NMR (CDCl₃, δ in ppm): 9.14 (d, 2H); 7.74 (d, 2H); 7.62-7.59 (m, 2H); 7.49 (d, 2H, J=8.9 Hz); 7.38-7.35 (m, 2H); 7.26 (s, 2H); 6.81-6.75 (m, 1H); 6.67 (d, 2H, J=8.9 Hz); 6.03 (s, 2H); 5.19-5.09 (m, 3H); 3.07 (s, 6H); 1.94 (s, 3H). Mass spectrometry (Micro-ESI in methanol), m/z: 413 [M-Cl]⁺.

Synthesis of polyacrylamide nanoparticles (PAA-NPs)

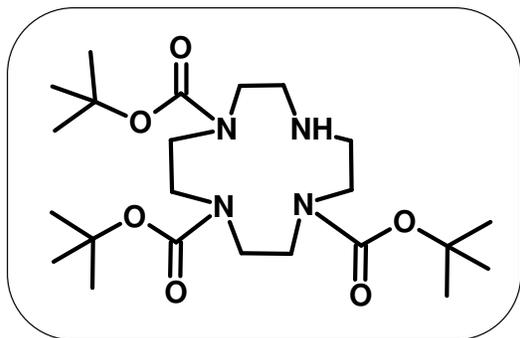
A solution of 3.08 g of Brij 30 and 1.59 g (3.6 mmol) of AOT in 43 mL of hexane was purged with argon for 30 min. Phosphate buffer solutions (pH 7.2) were prepared by mixing 105 mg of sodium dihydrogen phosphate hydrate and 180 mg of disodium hydrogen phosphate dehydrate in 150 mL of H₂O. In a separate flask, 1.5 mL of a solution of 1 mM of **2** in water was added to a solution of 0.40 g (2.6 mmol) of *N-N'*-methylenebisacrylamide and 1.85 g (26 mmol) of acrylamide in 3 mL of phosphate buffer (pH 7.2). 2 mL of the resulting mixture was then added to the prepared solution of surfactant in hexane under argon with intensive stirring (500 rpm). Afterwards, the polymerization was started by adding 24 μL of an aqueous APS solution (15%) and 10 μL of TEMED. The polymeric sensor nanoparticles were formed by dispersing the polymers in the oil solution of the surfactants. To finish the polymerization process, the emulsion was stirred (1000 r.p.m.) at room temperature for 3 h. Then hexane was removed by evaporation, resulting in a cloudy residue of nanoparticles, which was suspended in 100 mL of ethanol and kept overnight under rotation at 20 r.p.m. Afterwards, the nanoparticles suspended in ethanol were purified via filtration by a Millipore system using filter membranes with a pore size of 20 nm to remove unreacted monomers, the fluorescent monomer and the surfactants. Then, the nanoparticles were washed with 200 mL of ethanol until the filtrate was colourless. Finally, the obtained solid nanoparticles were dried under vacuum.

Synthesis of 3



In a 250 mL round bottom flask, 3 g of 4-bromo-1,8-naphthalic anhydride (10.8 mmol) and 1.43 g of 6-aminohexanoic acid (10.9 mmol) were refluxed in 100 mL of ethanol. The reaction is complete when the initially milky suspension becomes a brown clear solution. Upon cooling, crystals of the product are formed. The gathered crystals were purified through recrystallization in ethanol. In the end, 2.12 g of **3** were obtained ($\eta = 50\%$). ^1H NMR (250 MHz, MeOD) δ (ppm): 8.34 (d, 1 H, H-Aryl-); 8.10 (d, 1 H, H-Aryl-); 7.89 - 7.57 (m, 3 H, H-Aryl-); 4.10 (t, 2 H, -N-CH₂-); 2.32 (t, 2H, -CH₂-C=O); 1.71 (m, 4 H, -CH₂-); 1.45 (m, 2 H, -CH₂-). ^{13}C -NMR (60 MHz, CDCl₃) δ (ppm): 178.5, 163.60, 163.58, 133.23, 132.04, 131.23, 131.09, 130.65, 130.22, 129.01, 128.06, 123.11, 122.25, 40.24, 33.68, 27.64, 26.48, 24.33. Mass spectrometry (DEI), m/z : 389.2 [M-H]⁺.

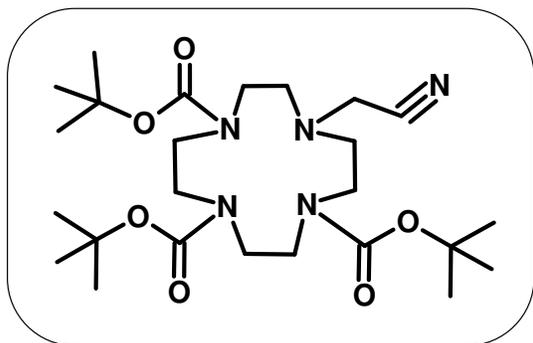
Synthesis of 4



To a solution of 1.50 g of 1,4,7,10-tetraazacyclododecane (cyclen, 8.7 mmol) in 10 mL of chloroform, 3.40 mL of triethylamine (23.5 mmol) were slowly added. A previously prepared solution of 4.95 g of di-*tert*-butyl dicarbonate (di-Boc, 22.6 mmol) in 5 mL of chloroform was added dropwise to the reaction mixture and the solution was left under stirring overnight. The

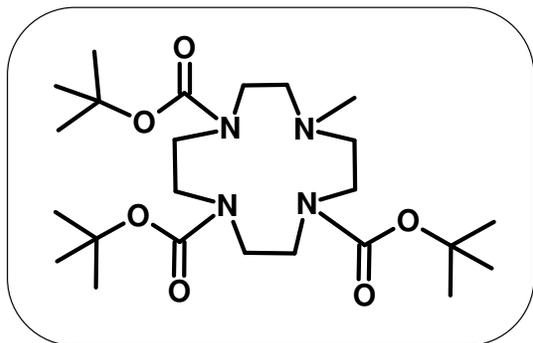
reaction mixture was then washed with brine and the aqueous phases were further extracted with chloroform. The organic phases were gathered, dried with magnesium sulphate, filtered and evaporated to dryness. Column chromatography with ethyl acetate yielded 2.77 g of pure **4** as a white foam ($\eta = 69\%$). ^1H NMR (250 MHz, CDCl_3) δ (ppm): 3.68-3.56 (m, 4H); 3.42-3.20 (m, 8H); 2.89-2.78 (m, 4H); 1.46 (s, 9H, *t*-butyl); 1.43 (s, 18H, *t*-butyl).

Synthesis of **5**



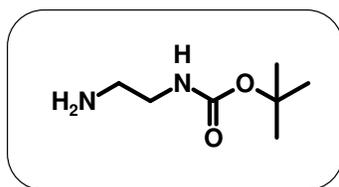
To a round bottom flask containing 2.77 g of **4** (5.9 mmol) in 20 mL of acetonitrile were added 0.98 g of potassium carbonate (7.1 mmol) and 0.45 mL of bromoacetonitrile (0.78 g, 6.5 mmol). The suspension was heated at 50°C for 6 hours. Afterwards, the reaction was cooled to room temperature and a further 0.45 mL of bromoacetonitrile was added. The reaction was again heated and kept stirring at 50°C overnight. After cooling to room temperature, the solid was filtered off and the solvent was removed in a rotavapor under reduced pressure. The viscous crude product was purified through column chromatography using ethyl acetate as eluent, yielding 2.74 g of pure **5** as a white foam ($\eta = 96\%$). ^1H NMR (400 MHz, CDCl_3) δ (ppm): 3.81 (m, 2H, $\text{CH}_2\text{-CN}$); 3.48 (m, 4H); 3.40-3.30 (m, 8H); 2.88-2.76 (m, 4H); 1.47 (s, 9H, *t*-butyl); 1.45 (s, 18H, *t*-butyl). ^{13}C -NMR (100 MHz, CDCl_3) δ (ppm): 155.8, 155.1, 114.4, 80.1, 79.5, 54.5, 53.9, 49.8, 47.3, 46.5, 38.9, 28.7, 28.5, 28.4.

Synthesis of 6



In a round bottom flask equipped with an Argon inlet, 2.70 g of **5** (5.3 mmol) and a catalytic amount of nickel boride were mixed in 30 mL of dry methanol. Afterwards, 0.73 g of sodium borohydride (3 equivalents) were carefully added under vigorous stirring. The reaction was kept under Argon. The mixture was left to react overnight at room temperature. The suspension was then filtered through a celite pad, which was then washed three times with methanol. The filtrates were diluted with water and extracted with ethyl acetate. The organic extracts were dried over magnesium sulphate, filtered and evaporated. Column chromatography yielded 0.17 g of **6** ($\eta = 7\%$). ^1H NMR (400 MHz, CDCl_3) δ (ppm): 3.56-3.32 (m, 12H); 3.12-2.88 (m, 4H); 2.71-2.64 (m, 3H); 1.44 (s, 27H, *t*-butyl). ^{13}C -NMR (100 MHz, CDCl_3) δ (ppm): 156.5, 155.6, 155.4, 80.3, 79.6, 57.1, 55.1, 43.3, 36.8, 29.6, 28.6, 28.5. Mass spectrometry (DEI), m/z : 485 $[\text{M-H}]^+$.

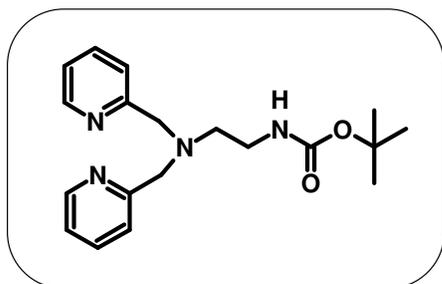
Synthesis of 7



In a 500 ml round bottom flask, 50 mL of ethylenediamine and 6 mL of triethylamine were dissolved in 100 mL of ethanol. The mixture was cooled in an ice bath and a solution of 13 g of di-*tert*-butyldicarbonate in 15 mL of ethanol was then added dropwise. The reaction mixture was stirred at room temperature for 3 hours and the solvents were removed under

reduced pressure in the rotavapor. The remaining residue was redissolved in 150 mL of dichloromethane, washed 3 times with 50 mL of a 1 M hydrochloric acid solution. The aqueous phases were gathered and neutralized with 50 mL of a 2 M sodium hydroxide solution, and then extracted with dichloromethane (1x100 mL and 2x50 mL). The organic phases were collected, dried over anhydrous sodium sulphate, filtered and the solvent was evaporated. In the end, 6,43 g ($\eta = 67\%$) of a pale yellow oil was obtained. ^1H NMR (CDCl_3 , δ in ppm): 5.21 (s, 1H, NH amide); 3.12 (m, 2H, CH_2); 2.77 (m, 2H, CH_2); 2.27 (m, 2H, NH_2); 1.38 (s, 9H, CCH_3). ^{13}C NMR (CDCl_3 , δ in ppm): 156.3, 79.2, 43.0, 41.6, 28.3.

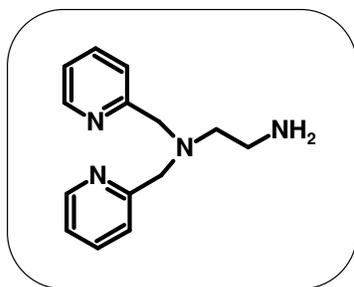
Synthesis of 8



In a 500 mL round bottom flask, 3.26 g of **7** (20,4 mmol) and 1,3 g of potassium iodide (7,8 mmol) were dissolved in 130 mL of acetonitrile. Afterwards, 7,52 g of 2-chloromethylpyridine hydrochloride were added to the mixture. After 30 minutes of stirring at room temperature, 60 mL of *N,N*-diisopropylethylamine (Hünig Base) were slowly dropped into the solution and the reaction mixture was refluxed overnight. TLC (dichloromethane/methanol 10:1, $R_f = 0.46$) revealed the completion of the reaction. Upon cooling down to room temperature, the solution was concentrated in the rotavapor under reduced pressure until only an oily residue was left. The residue was redissolved in 100mL of brine and extracted 3 times with 100 mL of dichloromethane. The organic extracts were collected, dried over anhydrous sodium sulphate, filtered and the solvent was removed, yielding a dark brown oil. Column chromatography using a dichloromethane/methanol mixture of 10:1 recovered the pure product with a yield of 54% (3.73 g, 10.9 mmol). ^1H NMR (CDCl_3 , δ in ppm): 8.50 (m, 2H, Ar – H); 7.61 (m, 2H, Ar – H); 7.39 (m, 2H, Ar – H); 7.13 (m, (m, 2H, Ar – H); 5.82 (s, 1H, NH amide); 3.83 (s, 4H, Ar – CH_2 – N tert.); 3.19 (m, 2H, CH_2); 2.67 (m, 2H, CH_2); 1.41 (s, 9H, CCH_3). ^{13}C NMR (CDCl_3 , δ in ppm): 159.2, 156.2,

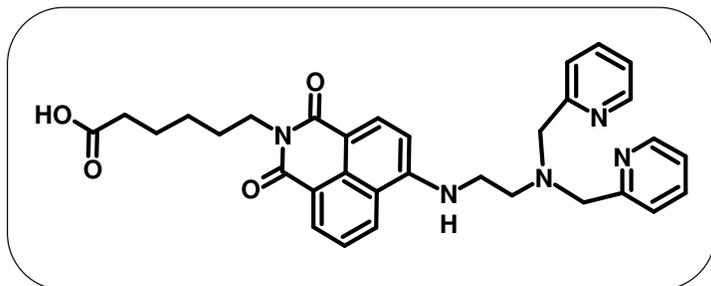
149.0, 136.6, 124.9, 122.2, 78.7, 60.2, 53.6, 38.5, 28.4. Mass spectrometry (DEI), m/z: 342.2 [M]⁺.

Synthesis of **9**



Compound **8** (3.73 g, 10.9 mmol) was dissolved in 60 mL of dichloromethane and the solution was cooled to 0°C in an ice bath. To the flask, 30 mL of trifluoroacetic acid were added dropwise during 30 minutes. Afterwards, the reaction was allowed to warm up to room temperature and it was stirred for 3 hours. Then, the solvents were evaporated under reduced pressure in the rotavapor and the resulting residue was redissolved in a 2 N sodium hydroxide solution. The aqueous mixture was extracted with dichloromethane, the organic extracts were collected and dried over anhydrous sodium sulphate, filtered and the dichloromethane was evaporated, yielding **9** of the pure product ($\eta = 67\%$). ¹H NMR (CDCl₃, δ in ppm): 8.51 (m, 2H, Ar – H); 7.62 (dt, 2H, Ar – H, ³J = 7,7); 7.45 (dd, 2H, Ar – H, ³J = 7,8); 7.13 (m, 2H, Ar – H); 3.82 (s, 4H, Ar – CH₂ – N tert.); 2.79 (t, 2H, CH₂, ³J = 5,7); 2.66 (t, 2H, CH₂, ³J = 5,7); 2.34 (s, 2H, NH₂). ¹³C NMR (CDCl₃, δ in ppm): 159.5, 149.0, 136.4, 123.0, 122.0, 60.6, 57.1, 39.4. Mass spectrometry (DEI), m/z: 242.1 [M]⁺.

Synthesis of **10**



In a 50 mL round bottom flask, 0.11 g of **3** (0.28mmol), 0.25 g of *N*-bis-pyridin-2-ylmethylethane-1,2-diamine **9** (1mmol) and 1 mL of triethylamine were refluxed in 15 mL of methoxyethanol. The reaction was monitored through TLC (Eluent: dichloromethane/methanol 5:1). When the reaction was completed, the solvent was removed by heating. The crude product was then purified through column chromatography, with increasing solvent polarity using a dichloromethane/methanol mixture (from 5:1 until 3:1). In the end, 80 mg (η = 52%) of pure **10** were obtained. ^1H NMR (400 MHz, DMSO- d_6) δ (ppm): 8.68 (d, 1H, $^3J=8.4\text{Hz}$); 8.49 (d, 2H, $^3J=4.3\text{Hz}$); 8.42 (d, 1H, $^3J=7.3\text{Hz}$); 8.15 (d, 1H, $^3J=8.5\text{Hz}$); 7.85 (m, 1H); 7.70-7.63 (m, 2H); 7.50 (d, 2H, $^3J=7.8\text{Hz}$); 7.22 (m, 2H); 6.64 (d, 1H, $^3J=8.6\text{Hz}$); 3.98 (t, 2H); 3.89 (s, 4H); 3.51 (m, 1H, Ar-NH); 2.85 (t, 2H); 2.12 (t, 2H); 1.56 (m, 4H); 1.32-1.23 (m, 4H). ^{13}C NMR (100 MHz, DMSO- d_6) δ (ppm): 164.2, 163.3, 159.6, 150.9, 149.3, 136.9, 134.5, 131.1, 129.9, 128.7, 124.8, 123.3, 122.6, 122.4, 122.3, 120.6, 108.1, 104.3, 60.1, 51.5, 41.1, 35.4, 28.0, 26.8, 25.3. MS (Micro-ESI): 550.5 (M-H).

Synthesis of **10.Zn-NPs**

In a plastic vial, 2.2 mg of **10**, 9.0 mg of zinc perchlorate and 4.2 mg of TSTU were dissolved in 5 mL of DMF. The mixture was then submitted to a sonication bath for 1 minute and left another 15 minutes for stirring. To the reaction mixture, 2.5 mL of an ethanolic solution of amine surface-functionalized silica nanoparticles (20 mg/mL) were added (this solution was sonicated just before addition, to ensure the homogeneity upon volume transferring) and the reaction mixture was left to stir for 48 hours at room temperature. Afterwards, the vial was centrifuged (20 minutes at 9000 r.p.m.), the supernatant was removed and the solids were resuspended in 10 mL of methanol. Cycles of

centrifugation/resuspension were repeated 4 times with methanol and 4 times with ethanol. The supernatants were monitored under UV light until there was no visible fluorescence left (which happened after the third methanol washing step). Then, the solvent was changed gradually to water by removing half of the supernatant and replenishing the volume with water up to 10 mL. This procedure for solvent exchange was performed in 3 times, with cycles of centrifugation/resuspension in between. Finally, the resulting nanoparticles were stored suspended in water. Prior to every fluorescent measurement, the nanoparticles were resuspended 5 minutes in sonication bath.

8. Bibliography

- ¹ Valeur B., *Molecular Fluorescence-Principles and Applications*, Wiley-VCH, Weinheim, **2002**.
- ² Kang C.-C., Chen C.-T., Cho C.-C., Lin Y.-C., Chang C.-C., Chang T.-C., *Chem. Med. Chem.* **2008**, 3, 725.
- ³ Lakowicz J.R., *Principles of fluorescence spectroscopy*, 3rd ed., Springer, Heidelberg, **2006**.
- ⁴ DiCesare N., Lakowicz J.R., *J. Phys. Chem. A* **2001**, 105, 6834.
- ⁵ Wetzl B.K., Yarmoluk S.M., Craig D.B., Wolfbeis O.S., *Angew. Chem.* **2004**, 116, 5515.
- ⁶ Höfelschweiger B.K., Dürkop A., Wolfbeis O.S., *Anal. Biochem.* **2005**, 344, 122.
- ⁷ Mohr G.J., Demuth C., Spichiger U.E., *Anal. Chem.* **1998**, 70, 3868.
- ⁸ Mohr G.J., Tirelli N., Spichiger U.E., *Anal. Chem.* **1999**, 71, 1534.
- ⁹ Gräfe A., Haupt K., Mohr G., *Anal. Chim. Acta* **2006**, 565, 42.
- ¹⁰ Mohr G.J., Lehmann F., Grummt U.-W., Spichiger U.E., *Anal. Chim. Acta* **1997**, 344, 215.
- ¹¹ Mohr G.J., Spichiger U.E., *Anal. Chim. Acta* **1997**, 351, 189.
- ¹² Mohr G.J., Citterio D., Spichiger U.E., *Sens. Actuators B* **1998**, 49, 226.
- ¹³ Létard J.-F., Lapouyade R., Rettig W., *J. Am. Chem. Soc.* **1993**, 115, 2441.
- ¹⁴ Trupp S., Schweitzer A., Mohr G.J., *Microchim. Acta* **2006**, 153, 127.
- ¹⁵ Turkewitsch P., Wandelt B., Ganju R.R., Darling G.D., Powell W.S., *Chem. Phys. Lett.* **1996**, 260, 142.
- ¹⁶ Turkewitsch P., Wandelt B., Ganju R.R., Darling G.D., Powell W.S., *Anal. Chem.* **1998**, 70, 2025.
- ¹⁷ Chen Y.L., Wu S.M., *Anal. Bioanal. Chem.* **2005**, 381, 907.
- ¹⁸ Gros M., Petrovic M., Barceló D., *Anal. Bioanal. Chem.* **2006**, 386, 941.
- ¹⁹ Suenami K., Lim L., Takeuchi T., Sasajima Y., Sato K., Takekoshi Y., Kanno S., *Anal. Bioanal. Chem.* **2006**, 384, 1501.
- ²⁰ Kot-Wasik A., D-Öbska J., Wasik A., Namieñnik J., *Chromatographia* **2006**, 64, 13.
- ²¹ Galliard-Grigioni K.S., Fehr M., Reinhart W.H., *Eur. J. Pharmacol.* **2008**, 595, 65.
- ²² Pharmacological information on Naproxen available at: <http://www.rxlist.com/naprelan-drug.htm#>.
- ²³ Valcárcel M., Simonet B., Cárdenas S., *Anal. Bioanal. Chem.* **2008**, 391, 1881.
- ²⁴ Nath N., Chilkoti A., *Anal. Chem.* **2002**, 74, 504.

-
-
- ²⁵ Guo M., Yan Y., Zhang H., Yan H., Cao Y., Liu K., Wan S., Huang J., Yue W. *J. Mat. Chem.* **2008**, *18*, 5104.
- ²⁶ Gräfe A., Stanca S.E., Nietzsche S., Kubicova L., Beckert R., Biskup C., Mohr G.J. *Anal. Chem.* **2008**, *80*, 6526.
- ²⁷ Ruedas-Rama M.J., Hall E.A.H. *The Analyst* **2008**, *133*, 1556.
- ²⁸ Mohr G.J., Standardization and Quality Assurance in Fluorescence Measurements I, Springer Berlin, Heidelberg, **2008**.
- ²⁹ Hornig S., Biskup C., Gräfe A., Wotschadlo J., Liebert T., Mohr G.J., Heinze T., *Soft. Matter* **2008**, *4*, 1169.
- ³⁰ Costa-Fernández J., *Anal. Bioanal. Chem.* **2006**, *384*, 37.
- ³¹ Cywinski P.J., Moro A.J., Stanca S.E., Biskup C., Mohr G.J., *Sensor. Actuat. B – Chem.* **2009**, *135*, 472.
- ³² Landfester R.M., *Adv. Mater.* **2002**, *14*, 651.
- ³³ Liu Z., Xiao H., Wiseman N., Zheng A., *Colloid Polym. Sci.* **2003**, *281*, 815.
- ³⁴ Lieberzeit P., Afzal A., Glanzing G., Dickert F., *Anal. Bioanal. Chem.* **2007**, *389*, 441.
- ³⁵ Schulz A., Hornig S., Liebert T., Birckner E., Heinze T., Mohr G.J., *Org. Biomol. Chem.* **2008**, *7*, 1884.
- ³⁶ Sun J., Zhuang J., Guan S., Yang W., *J. Nanopart. Res.* **2008**, *10*, 653.
- ³⁷ Peng J., He X., Wang K., Tan W., Wang Y., Liu Y., *Anal. Bioanal. Chem.* **2007**, *388*, 645.
- ³⁸ Patil Y.B., Toti U.S., Khdaïr A., Ma L., Panyam J., *Biomaterials* **2009**, *30*, 859.
- ³⁹ Ishizu K., Park J., Tanimura K., Uchida S., Tamura T., *J. Mater. Sci.* **2004**, *39*, 4353.
- ⁴⁰ Du Y., Qiao Y., Zou C., Dai J., Yang P., *Colloid Polym. Sci.* **2007**, *285*, 553.
- ⁴¹ Allard E., Larpent C., *Journal of Polymer Science Part A: Polymer Chemistry* **2008**, *46*, 6206.
- ⁴² Doussineau T., Smaïhi M., Mohr G.J. *Adv. Funct. Mater.* **2009**, *19*, 117.
- ⁴³ Abramson S., Srithammavanh L., Siaugue J.M., Horner O., Xu X., Cabuil V., *J. Nanopart. Res.* **2009**, *11*, 459.
- ⁴⁴ Nagao D., Yokoyama M., Saeki S., Kobayashi Y., Konno M., *Colloid Polym. Sci.* **2008**, *286*, 959.
- ⁴⁵ Chen Z.G. and Tang D.Y., *Bioprocess and Biosystems Engineering* **2007**, *30*, 243.
- ⁴⁶ Roca A.G., Morales M.P., O'Grady K., and Serna C.J., *Nanotechnology* **2006**, *17*, 2783.
- ⁴⁷ Pankhurst Q., *BT Technology Journal* **2006**, *24*, 33.
- ⁴⁸ Gao H., Zhao Y., Fu S., Li B., Li M., *Colloid Polym. Sci.* **2002**, *280*, 653.
- ⁴⁹ Mohr G.J., *Optical Chemical Sensors*, Springer Netherlands **2006**.

-
-
- ⁵⁰ Clark H.A., Hoyer M., Philbert M.A., Kopelman R., *Anal. Chem.* **1999**, *71*, 4831.
- ⁵¹ Analytical Chemistry Division, *Pure Appl. Chem.* **1995**, *67*, 1669.
- ⁵² Palma A., Lapresta-Fernández A., Ortigosa-Moreno J., Fernández-Ramos M., Carvajal M., Capitán-Vallvey L., *Anal. Bioanal. Chem.* **2006**, *386*, 1215.
- ⁵³ Cocks R.A., Rainer T.H., Chan T.Y.F., Maycock P.F., Lam N.Y.L., *Resuscitation* **2000**, *45*, 105.
- ⁵⁴ Packer J.L., Werner J.J., Latch D.E., McNeill K., Arnold W.A., *Aquatic Sciences - Research Across Boundaries* **2003**, *65*, 342.
- ⁵⁵ Langford K.H., Thomas K.V., *Environment International* **2009**, *35*, 766.
- ⁵⁶ De Silva A.P., Rupasinghe R.A.D.D., *Chem. Comm.* **1985**, 1669.
- ⁵⁷ Walkup, G.K., Burdette, S.C., Lippard, S.J., Tsien R.Y., *J. Am. Chem. Soc.* **2000**, *122*, 5644.
- ⁵⁸ Zhang X., Hayes D., Smith S.J., Friedle S., Lippard S.J., *J. Am. Chem. Soc.*, **2008**, *130*, 15788.
- ⁵⁹ Loudet A., Burgess K., *Chem. Rev.* **2007**, *107*, 4891.
- ⁶⁰ Gabe S.Y., Urano Y., Kikuchi K., Kojima H., Nagano, T., *J. Am. Chem. Soc.* **2004**, *126*, 3357.
- ⁶¹ Urano Y., Asanuma D., Hama Y., Koyama Y., Barrett T., Kamiya M., Nagano T., Watanabe T., Hasegawa A., Choyke P.L., Kobayashi H., *Nat. Med.* **2009**, *15*, 104.
- ⁶² Loudet A., Burgess K., *Chem. Rev.* **2007**, *107*, 4891 and references cited therein.
- ⁶³ Trupp, S., "Synthese, Charakterisierung und Immobilisierung von fluoreszierenden Sensorfarbstoffen zur pH- und Saccharidbestimmung", PhD. Thesis, FSU Jena, **2009**.
- ⁶⁴ De Silva A. P., Gunaratne H. Q. N., Gunnlaugsson T., Huxley A. J. M., McCoy C. P., Rademacher J. T., Rice T. E., *Chem. Rev.* **1997**, *97*, 1515.
- ⁶⁵ He H., Mortellaro M.A., Leiner M.J.P., Fraatz R.J., Tusa J.K., *J. Am. Chem. Soc.* **2003**, *125*, 1468.
- ⁶⁶ He H., Mortellaro M.A., Leiner M.J.P., Young S.T., Fraatz R.J., Tusa J.K., *Anal. Chem.* **2003**, *75*, 549.
- ⁶⁷ Guo X., Qian X., Jia L., *J. Am. Chem. Soc.* **2004**, *126*, 2272.
- ⁶⁸ Bianchi A., Bowman-James K., Gracia-Espana E., *Supramolecular Chemistry of Anions*, Wiley-VCH, New York, **1997**.
- ⁶⁹ Takeda E., Yamamoto H., Nashiki K., Sato T., Arai H., Taketani Y., *J. Cell. Mol. Med.* **2004**, *8*, 191.
- ⁷⁰ Beer P.D., Gale P.A., *Angew. Chem. Int. Ed.* **2001**, *40*, 486.

-
-
- ⁷¹ Spangler C., Schaeferling M., Wolfbeis O.S., *Microchim Acta* **2008**, *161*, 1.
- ⁷² Eguchi Y., Shimizu S., Tsujimoto Y., *Cancer Res.*, **1997**, *57*, 1835.
- ⁷³ Schaeferling M., Wolfbeis O.S., *Chem. Eur. J.* **2007**, *13*, 4342.
- ⁷⁴ Miao Y., Liu J., Hou F., Jiang C., *J. Luminesc.* **2006**, *116*, 67.
- ⁷⁵ Yin C., Gao F., Hu F., Yang P., *Chem. Comm.* **2004**, 934.
- ⁷⁶ Alexiou M., Tychopoulos V., Ghorbanian S., Tyman J. H. P., Brown R.G., Brittain P.I., *J. Chem. Soc., Perkin Trans. 2* **1990**, 837.
- ⁷⁷ Gunnlaugsson T., Ali H.D.P., Glynn M., Kruger P.E., Hussey G.M., Pfeffer F.M., Dos Santos C.M.G., Tierney J., *J. Fluorescence* **2005**, *15*, 287.
- ⁷⁸ Gunnlaugsson T., Kruger P.E., Lee T.C., Parkesh R., Pfeffer F.M., Hussey G.M., *Tetrahedron Lett.* **2003**, *44*, 6575.
- ⁷⁹ Sun Y., Zhong C., Gong R., Fu E., *Org. Biomol. Chem.* **2008**, *6*, 3044.
- ⁸⁰ Mizukami S., Nagano T., Urano Y., Odani A., Kikuchi K., *J. Am. Chem. Soc.* **2002**, *124*, 3920.
- ⁸¹ Kikuchi K., Hashimoto S., Mizukami S., Nagano T., *Org. Lett.* **2009**, *11*, 2732.
- ⁸² Ojida A., Mito-oka Y., Inoue M., Hamachi I., *J. Am. Chem. Soc.* **2002**, *124*, 6256.
- ⁸³ Sakamoto T., Ojida A., Hamachi I., *Chem. Commun.* **2009**, 141.
- ⁸⁴ Lee D.H., Kim S.Y., Hong J.-I., *Angew. Chem. Int. Ed.* **2004**, *43*, 4777.
- ⁸⁵ Huang X., Guo Z., Zhu W., Xie Y., Tian H., *Chem. Commun.* **2008**, 5143.
- ⁸⁶ Jose D.A., Mishra S., Ghosh A., Shrivastav A., Mishra S.K., Das A., *Org. Lett.* **2007**, *9*, 1979.
- ⁸⁷ Ghosh A., Shrivastav A., Jose D.A., Mishra S.K., Mishra S., Chandrakanth C.K., Das A., *Anal. Chem.* **2008**, *80*, 5312.
- ⁸⁸ Caddick S., Haynes A. K. de K., Judd D.B., Williams M.R.V., *Tetrahedron Lett.* **2000**, *41*, 3513.
- ⁸⁹ Khurana J.M., Kukreja G., *Synt. Commun.* **2002**, *32*, 1265.
- ⁹⁰ Kiyose K., Kojima H., Urano Y., Nagano T., *J. Am. Chem. Soc.* **2006**, *128*, 6548.
- ⁹¹ Wang J., Xiao Y., Zhang Z., Qian X., Yang Y., Xu Q., *J. Mater. Chem.* **2005**, *15*, 2836.
- ⁹² Jiang W., Fu Q., Fanb H., Wang W., *Chem. Commun.* **2008**, 259.
- ⁹³ Jiangli F., Peng X., Wu Y., Lu E., Hou J., Zhang H., Zhang R., Ru X., *J. Luminesc.* **2005**, *114*, 125.
- ⁹⁴ Lakowicz J.R., *Principles of fluorescence spectroscopy*, 3rd ed., Springer, Heidelberg, **2006**.
- ⁹⁵ Hosseini M.W., Blacker A.J., Lehn J.-M., *J. Am. Chem. Soc.* **1990**, *112*, 3896.

-
-
- ⁹⁶ Shionoya M., Ikeda T., Kimura E., Shire M., *J. Am. Chem. Soc.* **1994**, *116*, 3848.
- ⁹⁷ Jin Y., Kannan S., Wu M., Zhao X., *Chem. Res. Toxicol.* **2007**, *20*, 1126.
- ⁹⁸ Dahm A., Eriksson H., *J. Biotechnol.* **2004**, *111*, 279.
- ⁹⁹ Doussineau T., Trupp S., Mohr G.J., *J. Colloid Int. Sci.* **2009**, *339*, 266.
- ¹⁰⁰ Ackermann K.R., Henkel T., Popp J., *Chem. Phys. Chem.* **2007**, *8*, 2665.
- ¹⁰¹ Funfak A., Cao J., Wolfbeis O.S., Martin K., Köhler J.M., *Microchim. Acta* **2009**, *164*, 279.
- ¹⁰² Schmidt, R.H., Haupt K.O., *Chem. Mat.* **2005**, *17*, 1007.

List of publications

Book chapters:

1. Cywinski P.J., Moro A.J., Kutner W., Mohr G.J. – “*Sensors in Molecular Imprinting of Polymers*” book chapter in *Topics in Current Chemistry*, submitted to an editor.

Peer-reviewed papers:

1. Carreira R.J., Cordeiro F.M., Moro A.J., Rivas M.G., Rial-Otero R., Gaspar E.M., Moura I., Capelo J.L. – “New Findings for In-Gel Digestion Accelerated by High-Intensity Focused Ultrasound for Protein Identification by Matrix-Assisted Laser Desorption/Ionization Time-of-Flight Mass Spectrometry” – *J. Chromatogr. A* **2007**, *1153*, 291.
2. Rial-Otero R., Carreira R.J., Cordeiro F.M., Moro A.J., Fernandes L., Moura I., Capelo J.L. – “Sonoreactor-based Technology for Fast Hightthroughput Proteolytic Digestion of Proteins” – *J. Proteome Res.* **2007**, *6*, 909.
3. Rial-Otero R., Carreira R.J., Cordeiro F.M., Moro A.J., Santos H.M., Vale G., Moura I., Capelo J.L. – “Ultrasonic Assisted Protein Enzymatic Digestion for Fast Protein Identification by Matrix-Assisted Laser Desorption/Ionization Time-of-Flight Mass Spectrometry: Sonoreactor versus Ultrasonic Probe” - *J. Chromatogr. A* **2007**, *1166*, 101.
4. Cywinski P.J., Moro A.J., Stanca S.E., Biskup C., Mohr G.J. – “Ratiometric porphyrin-based layers and nanoparticles for measuring oxygen in biosamples” – *Sens. Actuator B-Chem.* **2008**,
5. Lapresta-Fernández A., Cywinski P.J., Moro A.J., Mohr G.J. – “Fluorescent polyacrylamide nanoparticles for naproxen recognition“, *Anal. Bioanal. Chem.* **2009**, *395*, 1821.
6. Moro A.J., Cywinski P.J., Körsten S., Mohr G.J. – “ An ATP Fluorescent Chemosensor Based on a Zn(II)-Complexed Dipicolylamine Receptor Coupled with a Naphthalimide Chromophore“, *Chem, Commun.* **2010**, DOI: 10.1039/b919661g.

-
-
7. Moro A.J., Doussineau T., Mohr G.J. – “Surface-functionalized fluorescent silica nanoparticles for ATP sensing”, *manuscript in preparation*.

Conferences:

1. Talk: “Synthesis of Polymerisable Fluorophores for Use in Molecular Imprinting”. International Workshop on “Sensor Nanoparticles for Medical Research 2007”, 22 – 23rd June 2007, Jena, Germany.
2. Talk: “Synthesis of polymerisable fluorophores for use in Molecular Imprinting”. International Meeting of the European Project NASCENT, 9 – 12th September 2007, London, UK.
3. Poster: “Design of Optical Sensors for Molecularly Imprinted Nanomaterials”. Marie Curie Conference 2008, 17 – 18th July 2008, Barcelona, Spain.
4. Talk: “Synthesis of fluorescent monomers and preparation of MIPs based on ionic, covalent and hydrogen bonding”. International Meeting of the European Project NASCENT, 29 – 30th July 2008, Paris, France.
5. Talk: “Combining Fluorescence with Intelligent Nanomaterials: the Future of Highly Selective Sensor Devices”. 1st Portuguese Young Chemists Meeting, 15 – 17th October 2008, Lisbon, Portugal.
6. Talk: “Fluorescent sensor nanoparticles for Naproxen detection”. International Meeting of the European Project NASCENT, 26 – 29th July 2009, Budapest, Hungary.
7. Poster: “Fluorescent nanosensors for ions”. 3rd European Conference on Chemistry for Life Sciences, 2 – 5th September 2009, Frankfurt am Main, Germany.

Curriculum vitæ

PERSONAL DATA:

Full Name: Artur Jorge Carneiro Moro

Family status: married

Birthdate/Birthplace: 09-05-1982, Cascais, Portugal

Nationality: Portuguese

EDUCATION:

Nov. 2006 – Jan. 2010 – PhD. student in Jena, Germany, within a European Union project, “Nanomaterials for Applications in Sensors, Catalysis and Emerging Technologies - NASCENT” (www.nascent.qmul.ac.uk), as part of the 6th Framework Program from the European Union Marie Curie Actions. Supervisor: Dr. Gerhard Mohr (www2.uni-jena.de/~c1moge/).

Mar. 2006 – Jul. 2006 – Internship within the group of Dr. J.L. Capelo, with the title “NOVAS METODOLOGIAS PARA A SEPARAÇÃO E IDENTIFICAÇÃO DE PROTEÍNAS – Estudo da influência do volume, temperatura e da concentração mínima de proteínas no tratamento de amostras por High Intensity Focused Ultrasound”, in the field of Proteomics. Final mark: **20/20**.

Sep. 2000 – Jul. 2006 – College Degree in Applied Chemistry, with an Organic Chemistry Specialization (equivalent to Diploma) from the Faculty of Sciences of the New University of Lisbon (“Universidade Nova de Lisboa”). Final mark: **16/20**.

Sep. 1994 – Jun. 2000 – High school student at “Escola Secundária de Carcavelos”, Carcavelos, Portugal.

Sep. 1992 – Jun. 1994 – Preparatory school student at “Escola Preparatória Santo António”, Parede, Portugal.

Sep. 1988 – Jun. 1992 – Elementary school student at “Escola Cartaxeira”, Carcavelos, Portugal.

Acknowledgements

This German adventure would not have been possible without the support of a significant amount of people which I will try to mention accordingly.

First of all, I would like to thank the AG Mohr for all the help and without whose support I would have surely been completely “lost in translation”.

Dr. Mohr (a.k.a. “the Big Boss”), thanks for all the advices, helping me to settle in and for giving me the opportunity to meet all the following people which I will certainly never forget.

Anja Gräfe (a.k.a. “Frau Dr. Schulz”), thank you for handling with the very nice people from the Bürgeramt, for choosing the worst hotel in London (sorry, but I’m still traumatized) and for always helping me when I needed, both in and out of the lab.

Suzie Reinert (a.k.a. “Frau Dr. Körsten”), thank you for all the help in bureaucracy stuff and also for all the wonderful cakes which sometimes filled the lab with their scent and our bellies with joy.

Frau Dr. Trupp (a.k.a. Sabine, “the German shotgun championess”), thank you for showing me the rebel side of Germany in the first person, but also for teaching me to work with naphthalimides, my Sensei.

Dr. Doussineau (a.k.a. Tristan, “l’Enfant Terrible”), thanks for all the wonderful discussions about beer, football, rugby, tennis, etc., and also for the many festival occasions in which I had the pleasure of your company. Ah, and also thanks for the silica nanoparticles.

Dr. Lapresta (a.k.a. Alex, “the crazy Spanish”, o mejor, “el loco Granadense”), thanks for all the good times laughing about our misadventures in this foreign land.

To the other groupies, Dr. Beate Bussemer and Heidrun Müller, I also thank for their valuable help, both in technical/professional and work-related issues, as well as garden party-related issues.

Also, my very special thanks to Dr. Cywinski (a.k.a. Piotr, “the Polish exciter”) and his wonderful family, for all the drinking, eating and football playing and watching, and whose friendship I hope will remain alive for at least 50 more years or so.

Regarding people who are not directly connected to the Institute, I would like to thank Dr. Martin Schulz (a.k.a. Schulzi) for providing me with nickel boride for my experiments, as well as for other non-work-related matters, such as the art of brewing beer and making home made liquors (and drinking them, of course).

I would like to also say that it was a pleasure working with Nicole Kirshner, Petra Lüders and Anuj Sharma, even though only for a short period of time.

I thank the people at the Institute of Physical Chemistry for technical and professional support, namely Dr. Dorothea Berg (mass spectrometry), Frau Preusse and Frau Schmidt for the order of chemicals, and Frau Zeise and Frau Krause for help in bureaucratic issues.

I also leave my utmost gratitude to Prof. Dr. Rainer Beckert from the Institute of Organic and Supramolecular Chemistry, for accepting to be my second reviewer in such a short notice, and for his readiness in reviewing this dissertation.

Not to forget, I also thank gratefully the Portuguese community in Jena, namely Luís Figueiredo, Luís Ramos, Hélder Alves and Filipa Viola, and the new additions Anne-Marie Fischer and Christoph Mathes, for all the laughter, parties, discussions, addiction to German “geek” board games (e.g. Siedlers), movies, more parties, football (VIVÓ BENFAS!!!!) and everything else that I forgot to mention.

Unforgettable are also the people from the NASCENT project scattered throughout Europe. Thank you, Rita (Margem-Sul power!), Ania (oye loca, ven pa ca!), Ana (un poquito de jamón, maestro?), Giorgio (Mini-MIPE master), Gita (Praha guide), Yevgen (paparazzo!), Silvia (italian hebrew), Kevin (Red Devils 4ever!), Pinar (who told you??!?!), Davide (sardinean C3PO), Natalyia (bielorussian MIPartner), and PIs Marina, Karsten, Levi, Maria, Stephanie, Andrea, Wlodek, Andrea, Sylvie, George guys, for all the times we shared together and for giving the privilege to work and have fun with such an interesting and joyful group of people. I also thank the European Union for the financial support.

Last but not least, I want to thank my family, my mother Deolinda, my father Jorge, my brother Sérgio, for always encouraging me, with no exception in facing this adventure as the great opportunity that it actually was.

Finally, I thank the one person who stood by me all along the way, for good or bad, in happiness and sadness, in sickness and in health, and to who I owe the meaning of me being here, alive today, my beautiful wife Ana. I love you and I always will, babes.

Some words in my mother tongue:

Este trabalho é dedicado ao meu avô, Abel Augusto Carneiro (1924-2008) e à minha avó Maria da Conceição Martins, que trabalharam a vida inteira pelo bem da família deles. Os mais sinceros agradecimentos a estas pessoas extraordinárias como já não há iguais nos dias que correm.

Selbständigkeitserklärung

Ich erkläre, dass ich die vorliegende Arbeit selbständig und unter Verwendung der angegeben Hilfsmittel, persönlichen Mitteilungen und Quellen angefertigt habe.

Jena, den